SYNTHESIS OF MAGNETIC CATALYST FROM PALM OIL FRONDS FOR BIODIESEL PRODUCTION

LEONG WENG FAI

UNIVERSITI TUNKU ABDUL RAHMAN

SYNTHESIS OF MAGNETIC CATALYST FROM PALM OIL FRONDS FOR BIODIESEL PRODUCTION

LEONG WENG FAI

A project report submitted in partial fulfilment of the requirements for the award of Bachelor of Engineering (Hons.) Chemical Engineering

Lee Kong Chian Faculty of Engineering and Science
Universiti Tunku Abdul Rahman

September 2017

DECLARATION

I hereby declare that this project report is based on my original work except for citations and quotations which have been duly acknowledged. I also declare that it has not been previously and concurrently submitted for any other degree or award at UTAR or other institutions.

Signature : _____

Name : LEONG WENG FAI

ID No. : 1301043

Date : 15/9/17

APPROVAL FOR SUBMISSION

I certify that this project report entitled **"SYNTHESIS OF MAGNETIC CATALYST FROM PALM OIL FRONDS FOR BIODIESEL PRODUCTION"** was prepared by **LEONG WENG FAI** has met the required standard for submission in partial fulfilment of the requirements for the award of Bachelor of Engineering (Hons.) Chemical Engineering at Universiti Tunku Abdul Rahman.

Approved by,

Signature : _____

Supervisor : _____

Date : _____

ACKNOWLEDGEMENTS

I would like to thank everyone who had contributed to the successful completion of this project. I would like to express my gratitude to my research supervisor, Dr. Steven Lim for his invaluable advice, guidance and his enormous patience throughout the development of the research.

I would also like to thank Miss Tang Zo Ee and Mr Ong Ching Yeh from Postgraduate Studies for their advice and support given throughout the research. They have given me many encouragements which kept me going througout the research,

Lastly, my deepest thanks to UTAR for providing the opportunity and platform to complete my final year project.

SYNTHESIS OF MAGNETIC CATALYST FROM PALM OIL FRONDS FOR BIODIESEL PRODUCTION

ABSTRACT

Biodiesel has been produced by many countries using homogenous catalyst. However, tedious separation and expensive post treatment are required when using conventional homogeneous catalyst. Heterogeneous catalyst on the other hand does solve the separation problem. However it has a much lower yield as compared to the homogeneous counterpart. The catalyst used in this research was ensured to have magnetic properties as an alternative separation method. Acid based magnetic carbon based catalyst was successfully produced with the highest conversion of 87.56 %. Palm oil fronds was used as a natural carbon source of support to synthesis magnetic solid catalyst by undergoing reaction with $FeCl_3$, calcination and subsequent sulphonation. Sulphonation at 50 °C with 10 M for 3 hours gave the highest catalyst acid density at 3.1636 mmol/g. The catalysts were characterized using TGA, SEM, EDX, XRD, BET and FTIR. XRD result showed that the presence of Fe_3O_4 in the catalyst which provided the magnetic properties. TGA result reported that the catalyst was thermally stable up to a temperature of 400˚C. FTIR analysis showed the presence of $–SO_3H$ and Fe-O at 1041.72 and 561.18 cm^{-1} respectively which indicated the successful attachment of $-SO_3H$ and Fe-O which provided the active site and magnetic properties respectively. For the synthesis of biodiesel, it was tested using GC. The optimum esterification condition was at 75 °C, 3 hours, 10 wt % catalyst loading with 20:1 methanol to oil ratio.

TABLE OF CONTENTS

LIST OF TABLES

LIST OF FIGURES

LIST OF SYMBOLS / ABBREVIATIONS

BET	Brunauer–Emmett–Teller
CNG	compressed natural gas
DLCR	Downflow Liquid Contactor Reactor
EDX	Energy-dispersive X-ray spectroscopy
EMA	Engine Manufacturers Association
FAME	fatty acid methyl esters
FFA	free fatty acids
FSP	flame spray pyrolysis
FTIR	Fourier transform infrared spectroscopy
GC	Gas chromatography
LPG	liquefied petroleum gas
OECD	Organisation for Economic Co-operation and Development
OPEC	Organization of the Petroleum Exporting Countries
PFAD	palm fatty acid distillate
SEM	scanning electron microscope
TEM	transmission electron microscopy
XRD	X-ray powder diffraction

LIST OF APPENDICES

CHAPTER 1

INTRODUCTION

1.1 Background

Diesel is an important fuel for our everyday life, from trucks, locomotive to cars. It is relatively important for logistics and transportation service. Despite overproduction of petroleum in OPEC countries and the discovery of shale oil in USA contributing to the lowest crude oil price since 2008, OPEC along with other oil producing countries decided to cut production to firm up prices in the first 6 months of 2017 (Amaro, 2016).

In the long term, oil price is guaranteed to increase as it is getting scarcer. Inevitably, biofuel will replace conventional fuel while biorefineries will replace oil refineries. Another challenge faced by biofuel is the replacement of existing light vehicles by electric models such as Tesla car. It is believed that cargo and aviation sectors will be using biofuels for a long time. In many OECD countries, biodiesel is blended with conventional diesel fuel from 5% in France and 20% in the US. Some of the trucks in Germany use 100% biodiesel (Iea, 2004). Vehicle engine does not need to undergo major modification in order to use biofuel. Besides, the limited range of electric vehicles travelling in a single charge is not helping it either. Logistics and transportation service usually require to travel a long range with minimum stoppage time in order to reduce expenses.

There are many types of biofuel, biodiesel is the one that this research is focused on. Distinct from vegetable or waste cooking oils, biodiesel is meant to be used by existing diesel engine with little to no modification made to it. Other alternatives such as compressed natural gas (CNG), liquefied petroleum gas (LPG) and electricity in electric vehicle all require expensive modifications to the fuel distribution and vehicle refuelling infrastructure (Iea, 2004). A typical example of biodiesel production is by reacting lipids with alcohol to produce fatty acid esters.

1.2 Biodiesel

Biodiesel is defined as methyl or ethyl esters of vegetables oils or animal fats; fermentation butanol, micro-emulsions of alcohols and water into vegetable oils; diesel-vegetable oil blends; pyrolysis products (Borgelt et al., 1994). It is believed to be a promising alternative fuel for diesel engines (Knothe, 2001). Initially, vegetable

oils with similar calorific value as diesel were used to replace diesel (Dalai et al., 2012). However, the viability is being questioned by early researchers. Knothe (2001) reported that glycerides in vegetable oil have no fuel value and may cause coking problem. It is necessary to separate triglycerides from residual fatty acid (Knothe, 2001). According to Dunn (2005), the high viscosity in vegetable oils and animal fats will cause problems in the diesel engine such as plugging especially during cold weather due to deposits.

1.3 Advantage and Drawbacks

Biodiesel has many advantages, particularly on the low emission of carbon dioxide. However, most companies do not use biodiesel because it does not save operating cost. Due to its lower energy value, biodiesel increases fuel consumption of up to 6%. Biodiesel's cost is almost equivalent to diesel with biodiesel generally cost 2% less than the latter (Duncan, 2003). The low price of diesel today does not help either, reducing the justification of most companies to use biodiesel. Most benefits can be obtained from the carbon tax cut. However, it is varied from countries to countries. Based on the analysis by Duncan (2003), biodiesel will require more than combined assistance of carbon tax credits before it can compete with conventional diesel. Either the price of crude oil can increase, or the production cost can be further reduced. Another disadvantage is that the raw material for the production of biodiesel is made of edible oil. This raises the debate of the food vs fuel. The production of biodiesel is believed to eventually lead to the shortage of food and increase in food price.

1.4 Synthesis

There are four major methods to reduce the viscosity of the unprocessed vegetables oils in order for them to replace diesel without damaging the engine. They are blending with petrodiesel, pyrolysis, microemulsification and transesterification.

1.4.1 Dilution with Petrodiesel

Mixing or diluting vegetables oils with diesel is the most straightforward method to produce a biodiesel blend. For short term, it shows promising result with one of the reports showing that the blend passed 200-h Engine Manufacturers Association (EMA) engine durability test with no measurable increase in deposits or contamination of lubrication oil. However, injector coking, carbon and lacquer build-up was displayed

after the engine tear-downs which were significant enough to conclude that the end result is similar to using 100% vegetables oils. It is concluded that this method is not suitable for long-term fuelling for conventional diesel engine as rapid failure may occurred (Dunn, 2005).

1.4.2 Pyrolysis

Pyrolysis involves breaking the chemical bonds of vegetable oils, animal fats, natural fatty acids and methyl esters of fatty acids to form smaller molecules. Although, the product is chemically similar to conventional gasoline or diesel, the pyrolysis process removes much of the oxygen in the oils which eliminates any environmental benefits of using oxygenated fuel. Besides, the equipment requires for pyrolysis or thermal processing is not affordable for modest throughputs (Ma and Hanna, 1999).

1.4.3 Microemulsions or Co-Solvent Blends

Mixing vegetable oils with low-molecular-weight alcohols is one of the approaches to reduce the viscosity of the oil. However, certain alcohols have limited solubility in nonpolar vegetable oils. In order to increase the solubility, amphiphilic compounds are added. The process is known as microemulsification where its function is to formulate a hybrid diesel fuels which is thermodynamically stable while still remains in a single-phase without requiring any agitation at normal condition. Another similar method which can be employed is by adding co-solvent to solubilize the alcohol-oil mixture. Co-solvent blends involve high concentration of solvents which lead to a relatively dilute solution. This method is relatively inexpensive as compared to transesterification as it only required mixing of multiple components at ambient temperature. However, most studies are against long-term use of vegetable oil based hybrid diesel fuels due to durability issues (Dunn, 2005).

1.4.4 Transesterification

Transesterification is the most common way to produce biodiesel today. It occurs when fat or oil react with alcohol to form esters and glycerol as shown is Figure 1.1. The reaction is reversible, therefore excess alcohol is usually used to shift the equilibrium to increase the conversion of biodiesel. A catalyst is also used to increase the production rate and yield (Ma and Hanna, 1999).

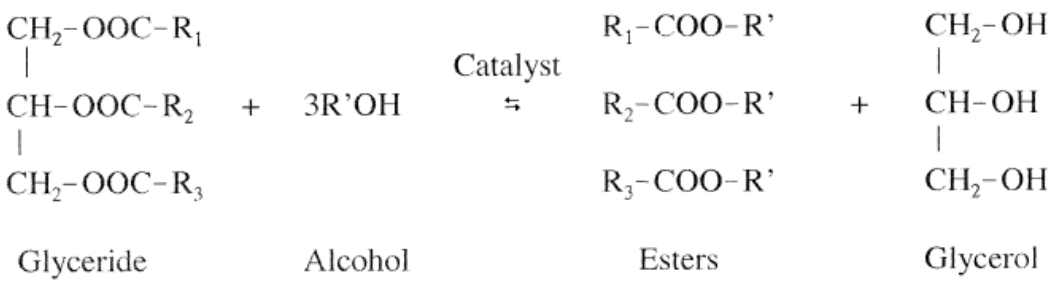

Figure 1.1: Transesterification Reaction to Produce Biodiesel (Esters)

1.5 Raw Materials for Transesterification

1.5.1 Feedstock

The oils used as feedstock for the production of biodiesel are depended on the regional climate (Dalai et al., 2012). Table 1.1 shows the main feedstock produced by different region.

Table 1.1: Oil in Different Regions

Type of Oil	Region
Rapeseed oil	European countries and Canada
Soybean oil	United States
Palm oil	Indonesia and Malaysia
Coconut oil	Coastal area in tropical countries

The usage of the edible oil as feedstock is controversial as it raises the debates regarding food vs fuel.

1.5.2 Palm Oil Fatty Acid Distillate (PFAD)

Palm Oil Fatty Acid Distillate or PFAD in short is a by-product in the refining of crude palm oil product. Currently PFAD is used in animal feeds industries and as a raw material for oleochemical industries. It is also used as a source of vitamin E, squalene and phytosterols. As can be seen in Table 1.2, the high concentration of Free Fatty Acids (FFA) and glycerides makes it a good feedstock for transesterification and esterification process. Besides, Malaysia being one of the biggest producers of palm oil is one of the reasons that PFAD is a suitable choice as a feedstock in this research (Gapor Md Top, 2010).

Table 1.2: Composition of PFAD

Component	Composition (%wt)
Free Fatty acids	81.7
Glycerides	14.4
Vitamin E	0.5
Squalene	0.8
Sterols	0.4
Others	2.2

1.5.3 Alcohol

Methanol, ethanol, propanol, butanol and amyl alcohol are examples of alcohol that can be used in transesterification process. Among these, methanol is used most frequently, due to its affordability and its polarity and short chain which provide chemical and physical benefits (Ma and Hanna, 1999). In Brazil, ethanol is used instead due to its lower cost (Dunn, 2005).

1.5.4 Catalyst

There are three classifications of catalyst, acid, alkali and enzyme. Acid and alkali catalyst are most commonly used in industry due to its higher rate of conversion and lower production cost as compared to enzyme (Talha and Sulaiman, 2016). They can be further divided into homogeneous and heterogeneous catalysts.

1.5.4.1 Homogeneous Alkali Catalyst

Potassium hydroxide (KOH), Potassium methoxide ($KOCH_3$), sodium hydroxide (NaOH), sodium methoxide ($NaOCH_3$) and sodium ethoxide ($NaOCH_2CH_3$) are some of the common basic catalysts for transesterification process. Several of the advantages include, able to catalyse reaction at low reaction temperature and atmospheric pressure, high conversion, high rate of reaction and economically available. As compared to its acid counterparts, alkali-catalysed transesterification is much faster, making it the preferable choice in industry (Ma and Hanna, 1999). However, oils with high content of free fatty acids (FFA) may form soaps, an undesired product as shown in Figure 1.2.

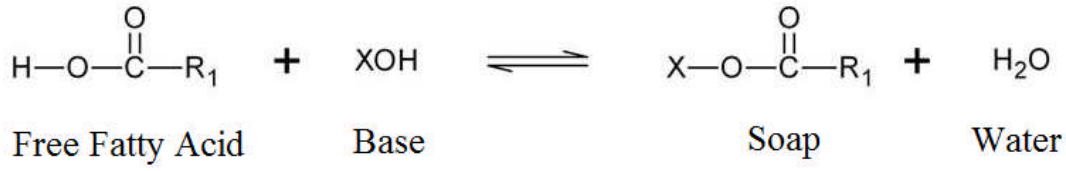

Figure 1.2: Saponification of FFA When Base is Used as Catalyst

1.5.4.2 Homogeneous Acid Catalyst

Several oils such as waste cooking oils contain free fatty acids (FFA) which produce the by-product soap during the transesterification process. The soap in turn will inhibit the separation of ester and glycerine thereby reducing its conversion and yield. This problem can be averted using acid catalyst such as sulphuric acid, sulphonic acid, hydrochloric acid and ferric sulphate. Aside from transesterification of glycerides, sulphuric acid also allows the esterification of fatty acid to form alkyl esters as shown in Figure 1.3. As mentioned previously, the acid catalyst has a slow reaction rate compared to alkali counterpart. In order to speed up the reaction rate, the alcohol to oil molar ratio will be increased to favour the biodiesel production (Dalai et al., 2012).

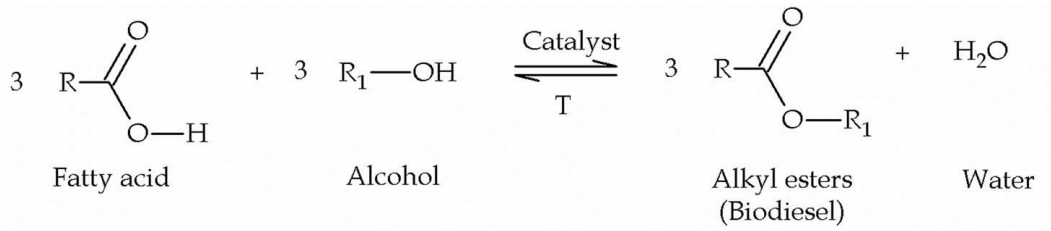

Figure 1.3: Esterification of Fatty Acids to Produce Biodiesel

1.5.4.3 Magnetic Catalyst

There are two forms of catalyst for transesterification process homogeneous and heterogeneous catalyst. Homogeneous catalyst produces a very high yield under mild conditions. However, post treatments which include the process of separation and removal of catalyst from product are usually costly and tedious. Aside from that, homogeneous catalyst also produces large amounts of wastewater and pollution (Guo et al., 2012). Heterogeneous catalysts are usually preferred due to easier separation of catalyst and reusing of the catalyst. Usually, filtration or centrifugation methods are used to recover heterogeneous catalyst which are both time-consuming and low energy efficient (Zhang et al., 2017). Magnetic catalyst on the other hand has an advantage in

easier catalyst-product separation. In an operating condition where there is an absence of magnetic field, the catalyst will disperse homogeneously within the reactant. After the reaction has completed, a magnet would be used to isolate the catalyst from the product. For continuous reactor, magnetic catalyst can be used as pseudo-fixed bed reactors. The catalyst can be fixed artificially within a reactor using permanent magnets. Another concept for magnetic catalyst is inductive heating. Instead of heating a reactant or solution, microwave can be used to heat the catalyst instead. However, the catalyst life may be shortened due to deactivation (Vaccaro, 2017).

1.5.5 Palm oil Fronds

Palm oil frond is a by-product from the harvesting of ripe fruit bunches. During cultivation, palm fronds may be cut or pruned. Pruning provide better visual assessment of fruit ripeness and easier access for pollination aside from easier harvesting (Lim et al., 2000). However, the fact that palm fronds are being underutilised, leading to disposal problem (Abdullah and Sulaiman, 2013). It is suitable as a carbon support for catalyst due to it high cellulose content (Khalil et al., 2006). Figure 1.4 shows the palm fronds with its leaflets removed.

Figure 1.4: Palm Oil Fronds with its Leaflets Removed

1.6 Problem Statement

Oil reserve is depleting at a high rate and there must be a solution or alternative to this problem. There is a need to be prepared for the day where fossil fuel is completely

depleted. Alternative fuels such as biodiesel will come into play in this situation. As mentioned previously, the main reason biodiesel does not become mainstream in many countries is due to the higher cost as compared to conventional diesel.

Production of biodiesel is dependent on the types of catalyst and the raw material and it is crucial that the synthesis process is able to produce a high conversion while maintaining a low cost of production.

The raw material of the biodiesel is relatively cheap as it can be taken from waste produced by palm oil. The expensive part is the catalyst. Homogeneous strong acid and alkali catalyst are usually used in the production of biodiesel owning to their high conversion. However, homogeneous catalysts exhibit low reusability and high difficulty in purification and catalyst separation which encourage new development. Over the years, researchers have been experimenting with heterogeneous catalyst where the catalyst can be separated from the product easily. Many types of materials are being experimented with carbon based materials ranked as the most ideal replacement mainly due to its low cost of materials, high surface area and thermal stability.

In heterogeneous catalysts, separation of catalyst and reusing the catalyst are important. However, separation process is usually costly and tedious. Therefore, the catalyst used in this research is ensured to have magnetic properties as an alternative separation method. This would provide a huge advantage in easier and cheaper separation process. In this research, magnetic solid acid catalyst would be used to test their characteristic and performance such as conversion and reusability.

1.7 Aims and Objectives

The aim of the research is to study the performance of catalyst in term of conversion and reusability. The objectives are as followed.

1. To synthesis carbon-based magnetic solid acid catalyst from palm oil fronds.
2. To characterize the catalyst produced using SEM, EDX, BET surface analyser, TGA, FTIR and XRD.
3. To determine the optimum condition for the synthesis of catalyst for biodiesel production.
4. To determine the reusability of the catalyst.

1.8 Scope of Study

The research will focus on the synthesis of magnetic solid acid catalyst from palm oil fronds. The mass of $FeCl_3$ and calcination temperature during the preparation of magnetic core will be varied. The research will investigate the sulphonation process using sulphuric acid where the effects of duration, concentration and temperature during the sulphonation will be investigated. After the catalysts were prepared, different equipment such as SEM, EDX, BET, TGA, FTIR and XRD were used to characterize the catalyst. Subsequently, the best catalyst will be selected to be tested for their esterification performance using palm fatty acid distillate and methanol as raw material. At the same time, the optimum operating condition for the process will be determined. Lastly, the biodiesel will be characterized with acid value test and GC.

1.9 Outline of the Report

Chapter 1 gives an introduction of the research. It started by giving a brief background on diesel and its potential biodiesel replacement. Next, the various methods for the synthesis of biodiesel is explained. One particular method, transesterification is explained in detail regarding the types of catalysts available and its advantages and drawbacks. Lastly, it is concluded with problem statement, objective and scope of study of the research.

Chapter 2 is about the literature reviews regarding the detailed explanation of different types of heterogeneous catalyst used in transesterification. The various methods used to prepare magnetic core are also explained in this section. Next, the parameter for the catalyst preparation are compared and discussed followed by the analysis of optimal condition for biodiesel production. Lastly, the equipment used to analyse the catalyst are investigated.

Chapter 3 describes the methodology of the research. All of the materials and equipment are listed in the first part of the section. The details in catalyst synthesis are described in the subsequent section, followed by a list of catalysts with different preparation condition. Next, the steps for characterization of both feedstock and catalyst are explained. Lastly, the section contains the synthesis and the characterization of biodiesel.

Chapter 4 provides the result, discussion and explanation of the research findings. There are 4 parts: (a) Preliminary Stage Observation (b) Preparation of Magnetic Support (c) Sulphonation Optimization (d) Characterization of catalyst (e) Biodiesel Optimization (f) Characterization of biodiesel and (g) Catalyst reusability test.

Chapter 5 includes the conclusion along with the recommendation suggested in order to improve the research in the future.

CHAPTER 2

LITERATURE REVIEW

2.1 Background

Conventional biodiesel production is based on transesterification of triglycerides and alcohols. It is used due to its simplicity and low cost of production. Biodiesel production economy depends mainly on the feedstock and the catalyst. Biodiesel plants such as soybean, rapeseed and cottonseed are relatively expensive, comprising almost 80% of the overall biodiesel production cost. Despite the fact that using homogeneous catalyst provides a fast process and produce low quantity by-product, it has plenty of disadvantages. Firstly, the catalyst cannot be recovered easily and have to be neutralised with either acid or base after the reaction is completed, which in turn produces unwanted salts. Besides, the process requires high quality feedstock due to its sensitivity towards water and FFA (Kaushik et al., 2007). In order to improve the cost efficiency, manufacturers nowadays focus on heterogeneous catalysis and low-cost feedstock such as waste cooking oil and non-edible oil.

2.2 Heterogeneous Catalysis

2.2.1 Carbon as catalyst

Activated carbon is defined by its extremely porous and high surface area for both adsorption and chemical reactions purposes. It is usually produced using high carbon content material such as coal, wood and petroleum residues (Konwar et al., 2014). The properties of the catalyst are depended on the active site of the carbon material. It is crucial to ensure the dispersion of the active phase to be as high as possible on the carbon material (Jüntgen, 1986).

2.2.2 Acid Catalyst

Direct sulphonation has been extensively studied due to its simple synthesis route. In conventional process, high carbon content sources such as sugars, activated carbon and cellulose are heated for a specified time at approximate 300 °C. The sample undergoes pyrolysis which produced a brown-black solid. The colour is due to the incomplete carbonisation of the aromatic carbon (Okamura et al., 2006). The solid is then grounded into powder and mixed with concentrated H_2SO_4 for sulphonation process.

As shown in Figure 2.1, hydroxyl (-OH), carboxyl (-COOH) and sulphonic (-SO_3H) functional group will bind with the carbon support during the process (Toda et al., 2005). Finally, the catalyst is rinsed multiple times with water at elevated temperature (> 80 °C) until the washed water is at neutral pH without any presence of sulphate ions impurity (Lou et al., 2008).

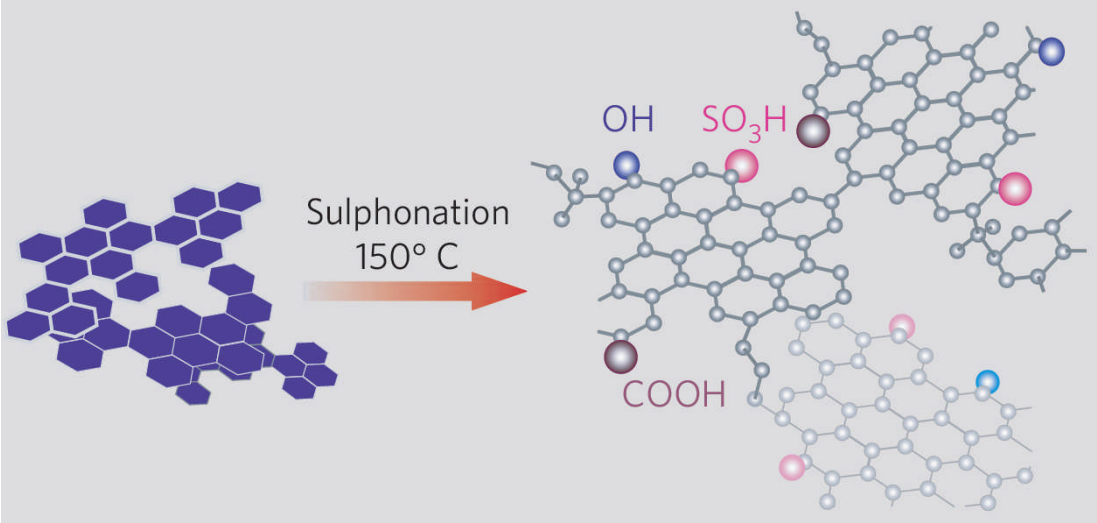

Figure 2.1: Formation of –OH, -COOH and –SO_3H Groups After Sulphonation

Similar to its homogeneous counterpart, heterogeneous acid functionalized catalyst is able to perform simultaneous esterification and transesterification of waste oils. This is particularly useful when converting high FFA-containing waste oil to biodiesel. According to Lou et al. (2008) research, it was found that carbohydrate-derived catalyst particularly starch based catalyst was highly effective in producing biodiesel from high FFA-containing waste oil. It was able to achieve 92 % yield after 8 hours when 27.8 wt% FFAs was used. The reaction mechanism for transesterification of triglycerides using acid as catalyst can be seen in Figure 2.2.

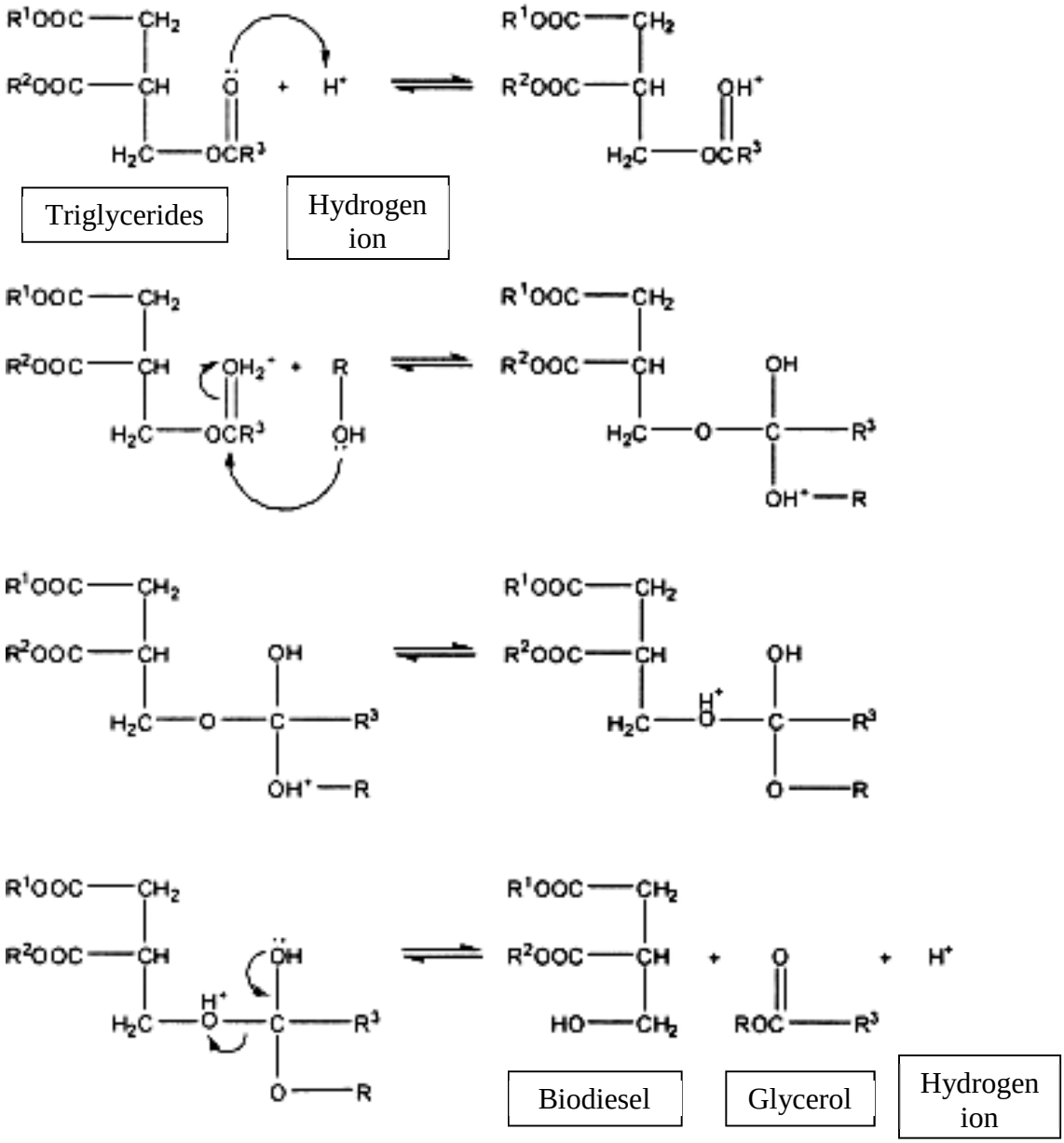

Figure 2.2: Reaction Mechanism of Transesterification of Triglycerides with Acid as Catalyst (Sivasamy et al., 2009)

2.2.3 Base catalyst

The more well-known heterogeneous base catalyst is metal oxides such as CaO or MgO (Guo and Fang, 2011). In order to increase the basic strength of the catalyst, a combination of two metal oxides is synthesized. Kawashima et al. (2008) was able to achieve 90 % yield when using the CaO-CeO_2 sample. However, according to Lee et al. (2016) results, mixed metal oxides did not guarantee an improvement in yield. Aside from CaO-ZnO which obtained a yield of 94 %, CaO-MgO produced yield of 90 % respectively which was slightly lower compared to the 91 % yield of CaO,

despite the fact that the basic strength for mixed oxide was doubled to that of the single metal oxide. The reusability of mixed oxide CaO-MgO on the other hand, was much better compared to CaO which decreased from a yield of 91 % to 58 %. In other words, mixed oxide is more resistant to leaching.

The other notable alkali catalyst is supported base catalyst. Typically, an alkali metal such as Na, K, Ba, Ca, Mg are supported in alumina or silica. Xie and Li (2006) prepared the catalyst by mixing the alumina with a solution of potassium iodide before drying it in rotary evaporator at 80 °C. The solid was then dried overnight in an oven at 120 °C. The KI/Al_2O_3 catalyst was able to reach the highest conversion of 96 % with a high methanol to oil ratio of 15:1 after 8 hours. Al_2O_3 is the most popular support due to its high thermal resistant, high surface area, porosity, low density and transition crystalline phase existed in a wide temperature range (Guo and Fang, 2011). In terms of reusability, supported alkali is at a disadvantage as compared to metal oxides. According to Liu et al. (2008), supported alkali $K_2CO_3/\gamma\text{-}Al_2O_3$ and $KF/\gamma\text{-}Al_2O_3$ showed a decrease of yields from 81.1 % to 30.6 % and 79.9 % to 17.8 % respectively after 4 runs. Meanwhile, CaO remained 86 % with approximately 2 % drop in yield after 20 repetitions.

For base functionalized activated carbon, Yuan et al. (2012), prepared amino-grafted graphene by mixing reduced graphene oxide (r-GO) with n-butyl lithium under the N_2 atmosphere for 10 hours at room temperature. 2-(diethylamino)ethyl bromide hydrobromide was vacuum dried before adding it to the solution and stirred for another 12 hours. The amino-grafted graphene precipitate was filtrated and washed with methanol to ensure there was no unreacted amine present. Based on Figure 2.3, the binding of amine functional group, $-NH_2$ to the carbon was similar to the binding of sulphonic ($-SO_3H$) functional group in acid functionalised carbon. The catalyst had good thermal stability. Reusability of the catalyst showed strong deactivation on the catalyst surface. More tests on the production of biodiesel is still required. The mechanism of transesterification of triglycerides using base as catalyst can be seen as in Figure 2.4.

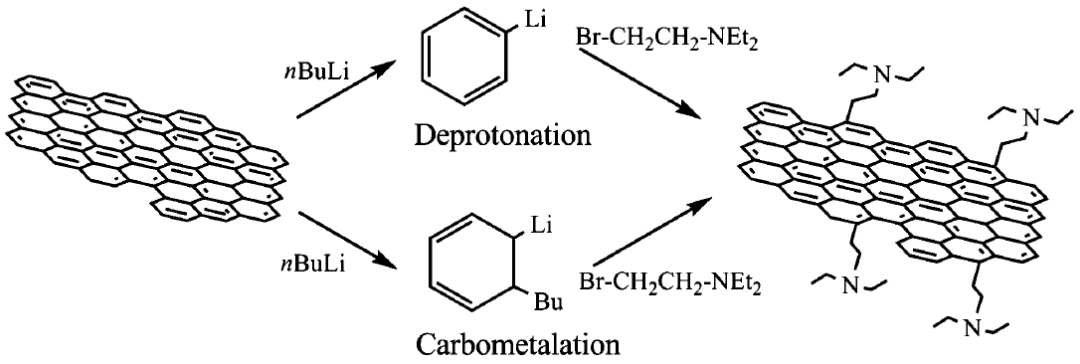

Figure 2.3: Binding of -NH_2 on the Graphene After Amino-grafting of Graphene (Sivasamy et al., 2009)

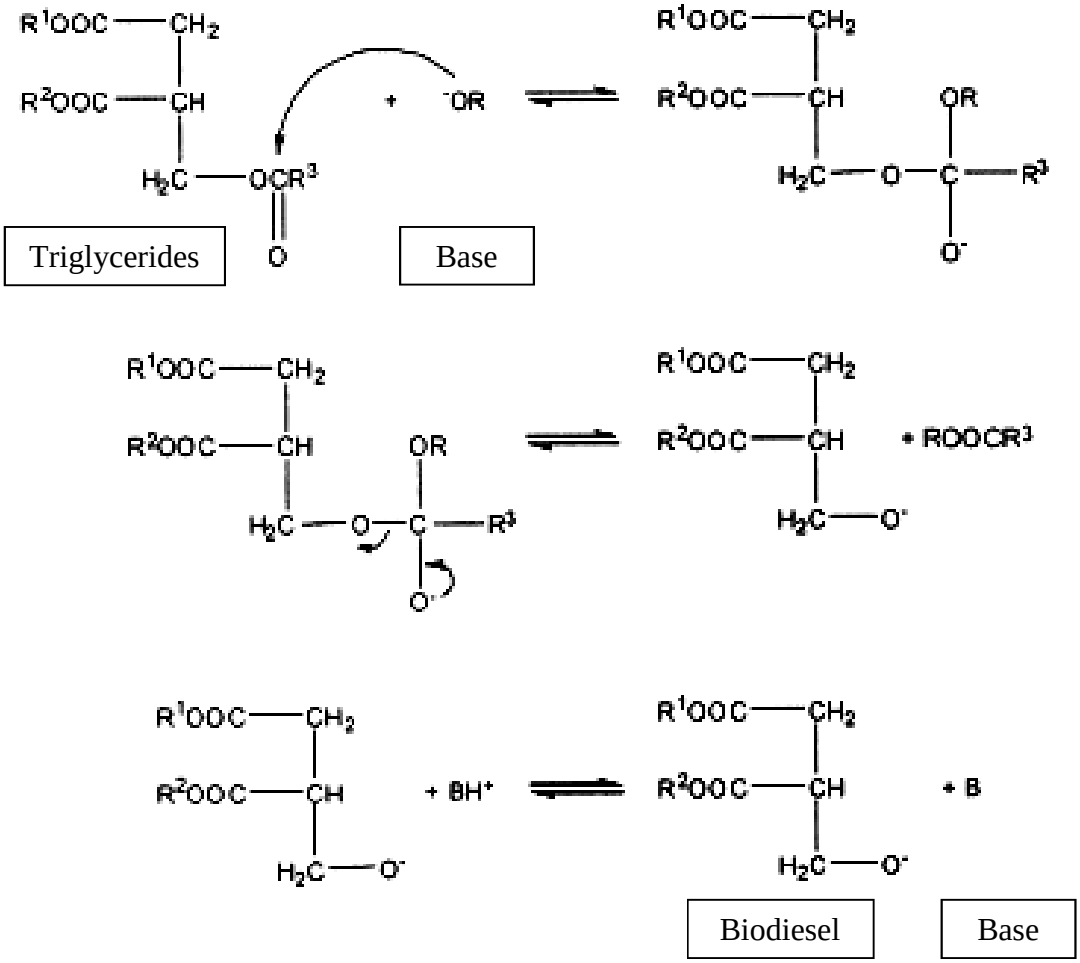

Figure 2.4: Reaction Mechanism of Transesterification of Triglycerides with Base as Catalyst (Sivasamy et al., 2009)

2.3 Magnetic Catalyst

2.3.1 Types of Preparation

The major preparation methods are coprecipitation, thermal decomposition, microemulsion and flame spray synthesis. The various synthesis methods are discussed below.

2.3.1.1 Coprecipitation method

The most conventional method was mixing ferric and ferrous ions with a base solution at room or elevated temperature, producing Fe_3O_4 magnetic particles (Wu et al., 2015a). It was noted that the size and shape of the iron oxide particles depended on the type of salt used ranging from chlorides, sulphates, nitrates to perchlorates. Other factors such as the ferric and ferrous ions ratio, reaction temperature, pH value, ionic strength of the media, stirring rate and the dropping speed of the basic solution were the parameters that affect the iron oxide morphology, structure and magnetic properties (Wu et al., 2008).

A study done by Li and Liang (2016) dissolved a combination of $FeCl_3 \cdot 6H_2O$ and $FeSO_4 \cdot 7H_2O$ in deionized water followed by addition of ammonia solution. Iron oxide (Fe_3O_4) was collected as precipitate and washed with water to ensure that the precipitate was in neutral pH. The Fe_3O_4 was later embedded in a silica shell which acted as a catalyst support before allowed mixing with H_2SO_4 to allow the formation of active sites. Based on the result from TEM analyser, it was found that the Fe_3O_4 was encapsulated in the silica shell. This would prevent the corrosion of the metal oxide by H_2SO_4. The biodiesel obtained reached a maximum of 98.9 % yield at 70 °C after 9 hours when using waste oil. Besides, the catalyst had a good recyclability with an impressive yield of 98 % after six runs.

Similarly, Liu et al. (2010) dissolved $FeSO_4 \cdot 7H_2O$ and $Fe_2(SO_4)_3 \cdot 7H_2O$ in distilled water with a 1:2 iron salt to water ratio before adding 20% of ammonia into the mixture. The black precipitate also known as the magnetic core formed was collected after several times of washing to ensure the pH was neutral. The magnetic core was later added to $CaCl_2$ solution before being titrated with NaOH. The mixture was aged for 18 hours to allow the active Ca^{2+} catalyst to bind with the magnetic core. The precipitate collected was again washed multiple times to ensure neutral pH and dried. The mixture of multiple oxides precipitate was calcined in order to produce nanometre structure of magnetic catalyst. Surprisingly, the non-magnetic pure CaO

catalyst yielded below 80 % conversion which was lower compared to magnetic catalyst. In others word, there was an optimum proportion of CaO to Fe_3O_4 proportion. This was because at high proportion of Ca^{2+}, excess CaO may blocked the active sites of CaO-Fe_3O_4 while low proportion of Ca^{2+} formed less active sites in CaO-Fe_3O_4.

Tang et al. (2012) utilised a much straight forward method where Fe_3O_4 nanoparticles was directly combined with the mixture of NaOH and $Ca(OH)_2$. In this research, it was found that the FAME yield increased with the increment of Ca to Fe proportion and reached the maximum at 5:1 ratio before decreasing. This result was consistent with Liu et al. (2010) where pure CaO did not have the best yield.

For acid catalyst, Liu et al. (2013) used relatively different method. $FeCl_3$ solution was mixed with dry carbon based biomass at constant temperature while stirred. The solid precipitate was dried and sieved. It was then undergone carbonisation before being mixed with concentrated sulphuric acid for sulphonation process. Lastly, the solid catalyst was rinsed with deionised water until there were no $–SO_3H$ ion being detected in the washed water.

2.3.1.2 Thermal decomposition

It can be said that co-precipitation method is one of the successful and classical techniques for synthesizing particles with good magnetic properties. However, one of the disadvantages of the methods is the broad particle size distribution of the product due to fast particle formation rates. Thermal decomposition method is able to control the size distribution and produce highly crystalline magnetic particles (Wu et al. 2015b).

Lin et al. (2013) had reported the production of CaO/α-Fe fibres from organic gel-thermal decomposition method. Firstly, metal salts and citric acid were mixed and dissolved in deionized water while stirring with a continuous magnetic stirring at room temperature. After 20-24 hours, the aqueous solutions were evaporated in a rotary evaporator at 60-65 °C to remove excess water, producing a viscous liquid. Using a spinning machine, the gels fibres were drawn from the liquid and dried in a vacuum oven at 80 °C for 24 hours. Lastly, the dried gel fibres were calcined from 600 to 1000 °C in air atmosphere for 2 hours to produce the final magnetic catalyst. The magnetic catalyst successfully yielded 97.5 % of biodiesel and achieved 85.2% yield after 20 runs.

2.3.1.3 Microemulsion

When there are two immiscible phases, a surfactant can be added to disperse the phases forming a thermodynamically stable isotropic single phase layer called microemulsion. The surfactant molecules will dissolve in both oil and aqueous phase, self-assembled into different structures from spherical and cylindrical micelles to lamellar phases and bicontinuous microemulsions. Using these properties, different shapes and sizes of iron oxide particles can be obtained (Wu et al. 2008).

In Vidal-Vidal et al. (2006) two types of magnetic core were synthesized namely coated and uncoated maghemite nanoparticles. In both preparations, microemulsion of cyclohexane/Brij-97/aqueous phase was used but with different organic bases as precipitant agents: cyclohexylamine and oleylamine. Firstly, the aqueous phase which contained 1 M Fe(III), 0.5 M Fe(II) and 0.1 M in HCl was prepared. Next, 250ml of microemulsion was produced by mixing cyclohexane/Brij-97 and aqueous phase at a volume ratio of 90:7:3. The samples produced where placed in a thermostatic bath and was stirred with a magnetic stirrer at 50 °C. After microemulsion was formed, it was waited for 5 mins before injection of the base was carried out. The function of the injection was to precipitate the particles.

In order to produce uncoated particles, 4 ml of cyclohexylamine diluted in 10 ml of cyclohexane at 50 °C was injected. After 15 min, magnetite particles and their aggregation were formed. They were cooled to room temperature and washed with large amount of acetone. Lastly, the precipitate was washed with 0.5 % tetrametylammonium hydroxide to remove surfactants from particle surface. Then, they were dried at 65 °C for at least 24 hours.

Similarly, oleylamine or oleic acid coated particles was synthesized injecting 13.8 ml of oleylamine diluted in 10 ml of cyclohexane at 50 °C. After 15 mins, 150 ml of synthesis product was separated. 2.40 g of oleic acid and 3.24 g of oleylamine diluted in cyclohexane was added stirred at 50 °C for 30 mins. The particles obtained were flocculated with ethanol before separating with heptane. Finally, particles were dried under vacuum at 30 °C.

2.3.1.4 Flame Spray Synthesis

Another method is the spray pyrolysis synthesis where fine IONPs are produced after the evaporation of ferric salts, drying, and pyrolysis reaction of liquid drops (Wu et al., 2015b). A typical flame spray synthesis can be seen in the synthesis of Strobel and

Pratsinis (2009) research where magnetic core was produced. The study prepared two types of precursors. The first precursor was $Fe(III)(NO_3)_3 \cdot 9H_2O$ dissolved in a 2:2:1 2-ethylhexanoic acid-tetrahydrofuran'-ethanol ratio with 0.65 M of Fe concentration. The second precursor on the other hand was diluted with tetrahydrofuran using 1:1 ratio yielding the final solution with 0.9 M Fe concentration. The setup which consisted of flame spray pyrolysis (FSP) nozzle with an Inconel tube is shown in Figure 2.5. Another internal mixing spray was located above FSP at the 45° angle facing downwards. This function as a rapidly cooling system where deionized water and nitrogen were used to prevent the reignition of hot unburnt gases upon contact with air when exiting the tube nozzle.

The precursors were fed into the FSP nozzle and dispersed by oxygen before ignited by a premixed methane/oxygen flame. The oxidizing rate can be adjusted by controlling the oxygen to fuel ratio. After exiting the tube, the particles were collected on the glass fibre filter.

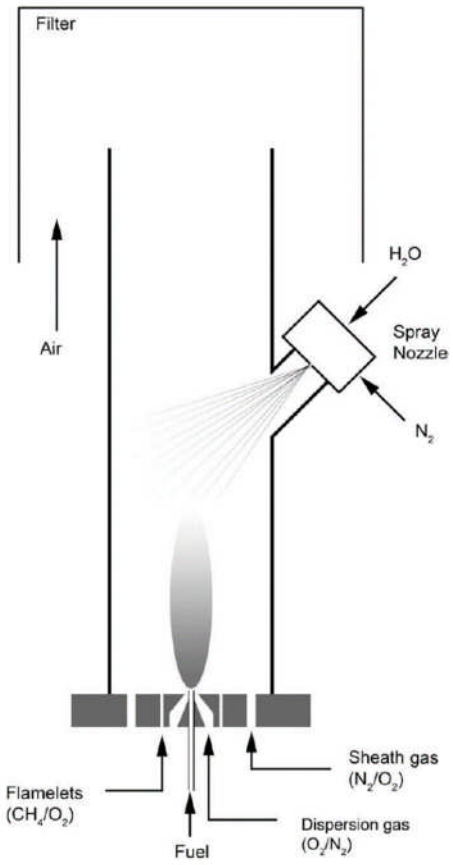

Figure 2.5: The Setup for Flame Spray Synthesis

2.3.2 Catalyst Parameters Study

In this study, the effects of different parameters during the preparation of catalyst are compared and studied. The parameters are mass of $FeCl_3$ added, catalyst size, calcination temperature, sulphuric acid concentration, sulphonation duration and temperature.

2.3.2.1 Mass of Iron (III) chloride

During the precipitation of carbon support with magnetic catalyst, mass of iron (III) chloride or any other precipitator is important as it may affect the composition of Fe/C in the catalyst. According to Feyzi et al. (2013), Fe was optimum at 7 % where the yield of biodiesel was maximum. The precipitation time is also an important parameter. During the hydrothermal precipitation process, the carbonaceous surface areas of the magnetic cores will grow via continuous deposition of bulk carbon derived from the hydrolysates, increasing the loading capacity for sulphonic ($-SO_3H$) group. However, it is important not to overload the carbonaceous coat, as the relative content of magnetic Fe_3O_4 which provide the magnetic properties will be reduced. In contrast, short precipitation time will lead to defective carbonaceous layer. Therefore, the magnetic cores will be more susceptible to corrosion by sulphuric acid, H_2SO_4 during sulphonation process (Zhang et al., 2017).

2.3.2.2 Calcination Temperature

Calcination or more precisely, carbonisation of carbon support is important to evaporate any volatile component, during the conversion of an organic substance into carbon (Zhang et al., 2017). Low carbonisation temperature will lead to the formation of carbide materials and increase water solubility affecting the stability of magnetic acid carbon based catalyst. This will significantly reduce the efficiency of sulphonation due to the loss of active bonding sites for the formation of layers of aromatic carbon in the catalyst (Zhang, Tian, et al., 2017). Aside from the catalytic activity, the carbonisation temperature will affect the magnetic properties of the catalyst. At high temperature, the magnetic strength of the catalyst will be inhibited. Therefore, it is crucial to balance between the total acid content and the magnetic strength of the catalyst (Zhang, Tian, et al., 2017).

High temperature of calcination treatment is favourable for interaction between support and active ingredient, in this case, sulphonic group ($-SO_3H$). During

calcination, new active sites are generated. Therefore, the process is crucial in order to increase the catalytic activity (Hu et al., 2011). According to Hu et al. (2011) research, it was found that the optimum calcination temperature for the magnetic catalyst before sulphonation CaO-Fe_3O_4 was within the range of the decomposition temperature of $Ca(OH)_2$. Therefore, it was expected that the precursor will experience minor weight loss after calcination.

At very high calcination temperature, fine magnetic catalyst will experience sintering as the cluster agglomerate, result in reduction of active sites (Feyzi et al., 2013). Wu et al. (2014) magnetic catalyst also experienced drastic reduction in BET surface area with increasing calcination temperature above 650 °C. The acidity and the yield were also severely decreased. It was because of the loss of sulphate groups in the form of SO_2 on the catalyst surface. Worst still, the high temperature could cause the promotion of crystallization of metal oxides. This destroyed the structure of the solid acid as the $S_2O_8^{2-}$ group which was also the active ingredient of the catalyst did not readily adsorption on the crystalline metal oxide.

2.3.2.3 Calcination Duration

According to Guo et al. (2012), calcination duration was the most important parameter which influenced the FAME yield. As the calcination time increased, the BET specific surface area increased, which in turn increased the catalytic activity of the catalyst (Feyzi et al., 2013).

In Zhang et al. (2016) research, it was found that as the carbonisation time increased, the total acid on the catalyst increased, causing the activity to be higher. When the carbonisation time was short, the H and O content of the calcined product was higher, causing instability on the catalyst support. Therefore, during the sulphonation process, the sulphonic acid will not be able to attach to the carbon support, decreasing its catalytic performance. A long carbonisation time on the other hand will result in lower H and O content, reducing the synergy between hydroxyl and carboxyl groups, reducing the affinity for hydrolysis reaction (Zhang et al., 2016).

2.3.2.4 Sulphonation concentration

In Zillillah et al. (2014), different concentrations of different reagents, phosphoric acid (H_3PO_4), trisodium phosphate (Na_3PO_4) and monosodium phosphate (NaH_2PO_4) were tested for phosphonation process. Phosphonation with H_3PO_4 provided high P content

but low Fe content and magnetic properties. This was due to the corrosion of magnetic core during the phosphonation process. As the concentration of the phosphonation reagent increased, the P content in the resulting catalyst increased.

Similarly, in a study done by Hu et al. (2011), a series of catalysts were prepared with different potassium fluoride (KF) loadings. In this preparation of magnetic base catalyst, as the KF loading increased from 15 wt % to 25 wt %, the biodiesel yield increased from 78 to 95 %. It was said that this was because the KF loading affected the active sites of catalyst surface. However, the loading must not exceed 25 wt % as it may decrease the yield of biodiesel to 81.1 % at 45 wt % KF loading. Excessive KF loading will lead to the covering of active sites of catalyst surface, reducing its effectiveness. It should be noted that different catalyst supports required different concentrations of KF in order to achieve maximum yield or biodiesel.

For the preparation of magnetic sulphonated acid catalyst, it would be safe to assume that the concentration of sulphuric acid does affect the active sites and effectiveness of the catalyst.

2.3.2.5 Sulphonation duration

Other than concentration, the P content or active sites can be increased by extending the phosphonation time (Zillillah et al., 2014). Meanwhile in Zhang et al. (2016) magnetic carbon based solid acid, the yield increased as the sulphonation time increased from 5 to 9 hours. This is because the total amount of acid attached to the surface of catalyst increasing, leading to higher yield of sugar. At above 9 hours, the xylose yield decreased drastically. Catalytic activity depended heavily on the total acid of the catalyst. If the magnetic support was sulphonated for too long, the removal of hydroxyl and carboxyl groups may occur which ultimately lead to decreased catalytic efficiency.

2.3.2.6 Sulphonation Temperature

Zhang et al. (2016) showed that the yield of xylose and the total amount of acid for magnetic solid acid catalyst increased as the temperature increased from 70 to 90 °C. At low temperature, inadequate sulphonation led to lower number of bonding between the sulphonic acid group and aromatic carbon ring, leading to lower yield. However, when the temperature increased from 90 to 150 °C, the total acid reduced by 33.8 %. At high temperature of sulphonation, fracture of the condensed structure may occur,

damaging the structure of the catalyst, reducing the catalyst effectiveness. Besides, the high temperature may promote the carbonisation of carbon support which counteracts the sulphonation reaction. The optimum sulphonating temperature in Zhang et al. (2016) research was 90 °C.

2.4 Optimization of biodiesel synthesis

The main parameters that affect the biodiesel yield during transesterification and esterification process are catalyst loading, methanol to oil molar ratio, reaction temperature, reaction time and the stirring speed. The optimal condition for magnetic solid catalyst are summarised from different literatures as in Table 2.1.

2.4.1 Catalyst Loading

For catalyst loading, it is generally accepted that between 4 to 7 wt % is the optimum. However, $S_2O_8^{2-}/ZrO_2$-TiO_2-Fe_3O_4 from Wu et al. (2014) required a high loading of catalyst at 21.3 wt %. This was probably due to the solid cottonseeds used for feedstock. Aside from that, methyl acetate was used instead of methanol as the reactant for transesterification process.

2.4.2 Methanol to Oil Ratio

Methanol to oil ratio is one of the most important factors affecting the conversion efficiency and yield of biodiesel. Due to the reversible reaction of transesterification, high methanol to oil ratio is required to increase the miscibility in order to promote the contact between the methanol molecules and the triglycerides following Le Chatelier's principle. Excess amount of methanol will shift the equilibrium to the right, increasing the biodiesel conversion (Feyzi et al., 2013). The stoichiometric methanol to oil ratio for transesterification of triglycerides is 3:1. In general, molar ratio higher than 3:1 or in other words excess methanol is used as seen in Table 2.1. This is to break the glycerine-fatty acid linkages during the reaction shifting the reaction to the right (Musa, 2016). Besides, low methanol to oil ratio may cause insufficient alcohol for transesterification process as seen in Zhang et al. (2017) experiment.

2.4.3 Reaction Temperature

According to Guo et al. (2012), the reaction temperature was the most important parameter in determining the FAME yield of the reaction. As can be seen from Table

2.1, the optimal temperature is within 50 to 70 °C with the exception of Zillillah et al. (2014), HPW–PGMA–MNPs reaction. This was because in the reaction, grease was used as a feedstock which have low miscibility with methanol, forming two layer at lower temperature. Therefore, higher temperature was required to enhance the reaction rate (Zillillah et al., 2014). In general, the optimal temperature for reaction depended on the feedstock viscosity, melting point and miscibility.

2.4.4 Reaction Time

Reaction time is heavily depended on the different stirring rates. According to Alenezi et al. (2013), a Downflow Liquid Contactor Reactor (DLCR) could provide extreme mixing intensity due to the high velocity of the liquid jet stream. It could provide a large interfacial area for reaction and high mass transfer between the reactant, which enabled the reaction time to decrease to 2.5 min from the typical 60 to 90 mins while achieving 99.0 % FAME yield. Although there are insufficient information regarding the stirring speed on the reaction time required for magnetic catalyst, it can be assumed that they followed the same principle as non-magnetic catalyst in Alenezi et al. (2013) research.

2.4.5 Reusability

The recovery or reusability of the magnetic catalyst depended on mainly the stability of the catalyst (Li and Liang, 2016). Stable catalyst will have firm attachment of active sites on the magnetic core, which prevents the leakage of active components such as acids, basic sites to the organic phase (Zillillah et al., 2014; Hu et al., 2011; Zhang et al., 2016; Wu et al., 2014). In Wu et al. (2014), the decrease in yield in 8th run was due to the leakage of sulphur while in Guo et al. (2012), large amounts of Na_2SiO_3 were leached into the methanol. There are other factor such as loss of contact sites due to catalyst aggregation during the reaction as seen in Wang et al. (2015) research. Another factor is the binding of crude glycerol or other residuals from the oil to the active sites of the catalyst may cause catalyst deactivation as shown in Zhang et al. (2017) magnetic catalyst.

Table 2.1: Comparison of Optimum Condition for Biodiesel Production

Catalyst	Feedstock used	Optimum Condition					FAME yield (%)	Reusability	Reference
		Catalyst Loading (wt %)	Methanol/Oil Molar Ratio	Temperature (°C)	Time (hours)	Stirring (rpm)			
Cs/Al/Fe_3O_4	Used sunflower oil		14:1	58	2.0	300	96.2	88 % @ 4th runs	Feyzi et al. (2013)
Na_2SiO_3/Fe_3O_4	Refined cottonseed oil	5.0	6:1	60	1.67	400	99.6	90 % @ 7th runs	Guo et al. (2012)
KF/CaO-Fe_3O_4	Stillingia Oil	4.0	12:1	65	3.0	-	95.0	90% @ 14th runs	Hu et al. (2011)
Magnetic solid Acid Catalyst	Frying Cooking Oil	0.63	15:1	70	8.67	-	98.9	98 % @ 6th runs	Li and Liang (2016)
Sulfamic acid-functionalized MNPs[a]	Oleic acid	-	-	70	4.0	-	100.0	95% @ 5th runs	Wang et al. (2015)

Table 2.1: Continued

$S_2O_8^{2-}/ZrO_2$-TiO_2-Fe_3O_4	Cottonseeds	21.3	13.8 ml/g (methyl acetate to oil ratio)	50	10.8	300	98.5	87.4 % @ 8th runs	Wu et al. (2014)
Na_2SiO_3@Ni/JRC[b]	Pre-treated crude Jatropha oil[d]	7.0	9:1	65	2.0	750	96.7	96.5 % @ 3rd runs	Zhang et al. (2017)
HPW–PGMA–MNPs[c]	Waste Grease	4.0	33:1	122	60.0	-	98.9	95 % @ 10th runs	Zillillah et al. (2014)
CaO@ ($Sr_2Fe_2O_5$-Fe_2O_3)	Soybean oil	0.5	12:1	70	2.0	-	94.9	86.0 % @ 4 runs	Zhang et al. (2016)

[a] Magnetic nanoparticles.

[b] JRC: Jatropha residue carbon supporter.

[c] Stands for Phosphotungstic acid, $H_3PW_{12}O_{40}$, poly(glycidyl methacrylate) layer, magnetic nanoparticles.

[d] Pre-treated with esterification of crude oil using CSO_3H@Fe/JHC as catalyst.

2.5 Catalyst Characterization

2.5.1 Thermogravimetric Analysis (TGA)

TGA is used to measure the thermal stability of the catalyst. It is also used to estimate the pyrolysis temperature range for the catalyst. It is important to select the suitable sample atmosphere (PerkinElmer, 2010). In short, running the test under inert gas atmosphere such as nitrogen or helium gas is to detect the thermal stability, while using air is meant for testing the oxidative stability (Dean, 2015).

Non-magnetic acid carbon based catalyst has a high stability at 100 – 240 °C range. Drastic weight loss only occurred at 460 °C (Mo et al., 2008). In contrast, the magnetic catalyst of Zhang et al. (2015) experienced negligible weight loss at 25 – 200 °C with slight weight loss at 200 – 400 °C. From 400 °C to 800 °C, the weight loss was still minimal with only 5.6 % wt loss. However, both characterization methods were different by the fact that Zhang et al. (2015) performed the analysis in He while Mo et al. (2008) performed the test in air. In short, it can be concluded that both catalysts were relatively stable as the temperature for biodiesel synthesis was far below the limit.

2.5.2 Scanning Electron Microscope (SEM) & EDX

SEM is used to study the morphology while TEM is used to study the morphology and crystallization of the catalyst. Both SEM and TEM revealed a rough surface morphology in the magnetic catalyst surface as seen in Figure 2.6. The porous and wire-like structure on the magnetic catalyst can also be observed from TEM. On the other hand, non-magnetic carbonaceous acid showed a much smoother surface with much lesser pores (Liu et al., 2013). This structure was confirmed by Zhang et al. (2015) which showed similar rough structure. In addition, it was discovered in the test that as the temperature of pyrolysis increased, the particle size increased. This was because higher pyrolysis temperature provided higher stability to the structure, making it more resistant to corrosion by H_2SO_4 during the sulphonation process.

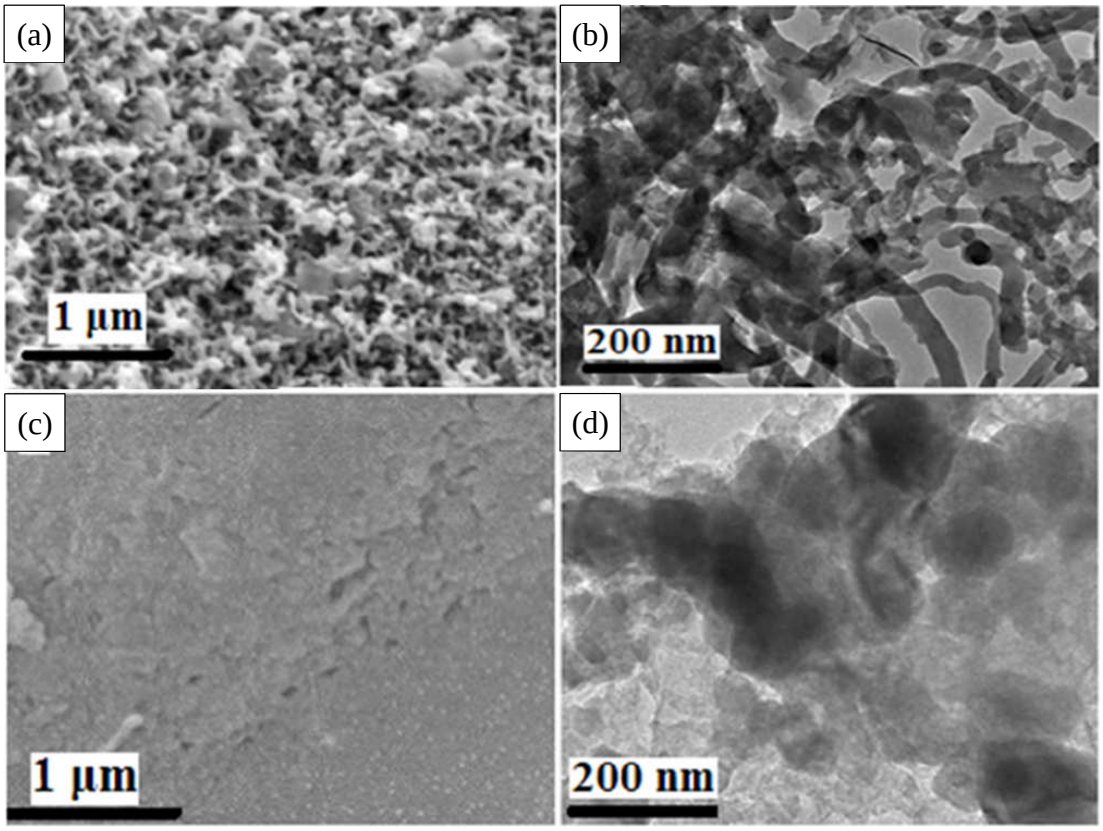

Figure 2.6: SEM and TEM Image of the Magnetic (a) & (b) and Non-magnetic Catalyst (c) & (d) (Liu et al., 2013)

2.5.3 Surface Analysis (BET)

Surface area of magnetic catalyst was 391.7 m^2 g^{-1} which was much higher as compared to the one without magnetic properties at 14.0 m^2 g^{-1} as can be seen in Figure 2.7 (Liu et al., 2013). Magnetic catalyst contained Fe which catalysed the formation of pores during the dehydration and decomposition of $FeCl_3$. This led to increase in pores volume and surface area. However, with an increase in surface area, it can be assumed that the number of active sites also increased. In Liu et al. (2008) test, magnetic catalyst achieved 93 % yield while non-magnetic catalyst with a much smaller specific surface area only achieved 63 % which further validated the assumption.

According Zhang et al. (2015) test which compared the effect of catalyst at different pyrolysis temperatures, as the pyrolysis temperature increased, the surface area increased. This was due to the removal of hydrogen and oxygen during the heating process, creating more porous structures. After sulphonation, the catalyst with the lower pyrolysis temperature had the highest specific surface area. The unstable structure due to incomplete carbonisation enabled the aromatic carbon to easily

corrode and dehydrate by H_2SO_4 in the sulphonation process. Similar to Liu et al. (2013), the higher surface area of sulphonated magnetic catalyst achieved higher yield at 92.7 % which further confirmed the assumption that higher surface area can contain higher number of active sites.

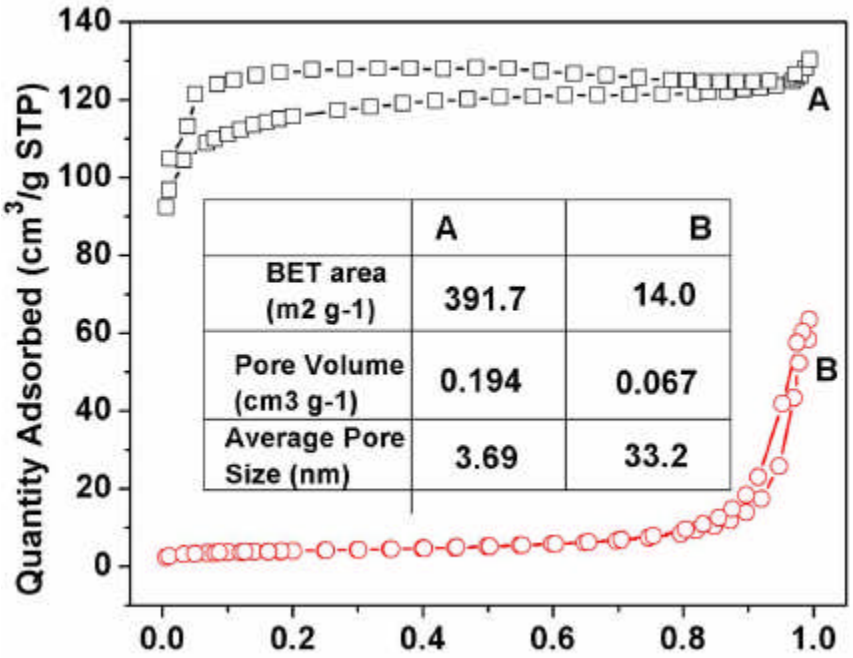

Figure 2.7: BET of Magnetic Catalyst, A and Non-magnetic Catalyst, B (Liu et al., 2013)

2.5.4 X-Ray Diffraction (XRD) Analysis

In order to determine the strain, orientation, crystallographic structure or grain size of the materials, XRD can be used. Li and Liang, (2016) compared the XRD of solid acid with magnetic core. It was found that the diffraction peaks at 30.1°, 35.6°, 43.2°, 51.4°, 57.3° and 62.7° represented the formation of Fe_3O_4. Liu et al. (2013) obtained the same peaks for Fe_2O_3 which confirmed the result. Amorphous carbon which composed of randomly arranged aromatic carbon sheets were detected at a diffraction peak at 23°.

Zhang et al. (2015) compared the metallic core before and after pyrolysis and after sulphonation. The Fe_3O_4 before sulphonation had crystallized structure and symmetric reflection. Aromatic carbon sheet had a weak peak due to its outer coating with glucose previously to prevent the leaching of Fe_3O_4. After pyrolysis, the peaks of Fe_3O_4 disappeared as temperature increased as shown in Figure 2.8. This was because Fe_3C and Fe was formed from Fe_3O_4. After sulphonation, Fe_3O_4 and Fe were dissolved

in the H_2SO_4 solution forming Fe_2O_3. In other words, it showed that the magnetic properties of the catalyst decreased drastically after sulphonation as the amount of Fe_3O_4 and Fe decreased.

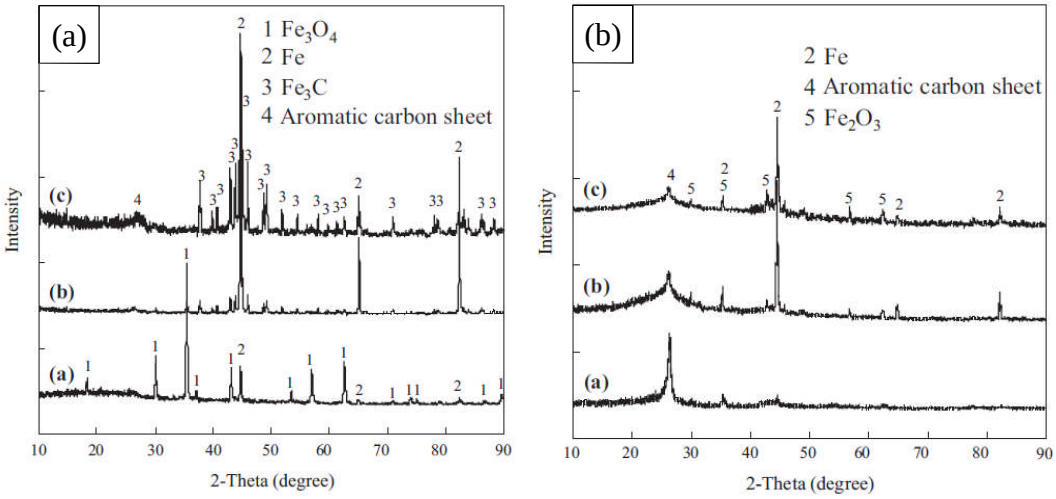

Figure 2.8: XRD of Acid Magnetic Catalyst Before (a) and After Sulphonation (b)

2.5.5 Fourier Transform-Infrared Spectroscopy (FTIR)

FTIR is particularly useful in the determination of functional groups. Since the catalyst studied are acid functionalized carbon, the functional groups are crucial in determining the performance of the catalyst. The catalyst is mainly associated with SO_3H groups which is an important acid sites. Aside from -SO_3H group, -OH group and -COOH group also formed during the sulphonation process (Liu et al., 2013). It was also confirmed by the XPS results with the high S content in the catalyst.

2.5.6 Acid Density

The total acid sites are determined by the titration of NaOH solution. The acid sites includes -SO_3H, -OH and -COOH group though only –SO_3H group is the major active sites (Liu et al., 2013). It was discovered that magnetic catalyst in Liu et al. (2013) had higher number of acid sites as compared to the non-magnetic one. This was due to the higher surface area of magnetic catalyst as mentioned previously. Zhang et al. (2015) also obtained a higher acid density as pyrolysis temperature increased on the magnetic catalyst.

CHAPTER 3

METHODOLOGY

3.1 Material and Equipment

The list of material and equipment required for the synthesis and characterization of both magnetic catalyst and biodiesel was tabulated in Table 3.1 and Table 3.2 respectively.

Table 3.1: List of Material

Material	Brand	Function
2-propanol, C_3H_8O	Friendemann Schmidt	To be used as solvent during the fatty acid characterization
Concentrated Sulphuric acid, H_2SO_4	Duksan Reagent	To be used during sulphonation to introduce the active group
Hydrochloric acid, HCl	-	To be used in testing of acidity of catalyst
Iron (III) Chloride, $FeCl_3$	Friendemann Schmidt	To be used to magnetise the catalyst
Methanol, CH_3OH	Friendemann Schmidt	To be used as one of the reactants for production of biodiesel
Palm Distillate – Fatty Acid	-	To be used as one of the reactants for production of biodiesel
Palm Oil Fronds	Taken from UPM	To be used as the catalyst support
Phenolphthalein	R&M Chemical	To be used in testing of acidity of catalyst and acid value of biodiesel
Potassium hydroxide, KOH	R&M Chemical	To be used in testing of acid value of biodiesel
Sodium hydroxide, NaOH	R&M Chemical	To be used in testing of acidity of catalyst
n-hexane, C_6H_{14}	Friendemann Schmidt	To be used to remove biodiesel and fatty acid from catalyst

Table 3.2: List of Equipment

Equipment	Brand	Function
Brunauer, Emmett and Teller (BET)	ThermoFinnigan Sorptomatic 1990	To determine the specific surface area and pore volume of the catalyst.
Energy Dispersive X-ray Spectroscopy (EDX)	Hitachi BS 340 TESLA6	To determine the weight percentage of element present.
Fourier Transform-infrared (FTIR)	Nicholet IS10	To characterize the surface functional group of the magnetic catalyst.
Furnace	Wise Therm	To carbonise the catalyst support.
Gas Chromatography (GC)	Perkin Elmer Clarus 500	To determine the composition of FAME.
Grinder	Berjaya BJY-CB2LN	To grind the palm oil fronds into powder.
Scanning Electron Microscope (SEM)	Hitachi BS 340 TESLA6	To characterize the pore size and surface morphology of the catalyst.
Thermogravimetric Analysis (TGA)	STA 2500 Regulus	To determine the decomposition temperature of catalyst.
X-ray powder diffraction (XRD)	Shimadzu XRD-600	To characterize the presence of crystalline phases of Fe_3O_4
pH meter	-	To measure the pH value of the washed water.

3.2 Catalyst Preparation

3.2.1 Preparation of Support

Palm oil tree fronds was collected and dried under the sun for at least 24 hours. It was then cut into smaller pieces before being grinded with a blender as shown in Figure 3.1. The powder was then sieved using a 250 μm sieve.

Figure 3.1: The Blender Used in the Preparation of Frond Dust.

3.2.2 Producing Magnetic Support

The support material was prepared by mixing 20.0 g dry frond powder with 5.0 g of $FeCl_3$ in a beaker along with 250 ml of water. The beaker was then placed onto the hot plate at 200 °C while stirring at 200 rpm using a magnetic stirrer to dry the mixture as shown in Figure 3.2. The catalyst support was calcinated in the furnace for 3 hours at 300 °C under air atmosphere as shown in Figure 3.3. The procedure was repeated with different weights of $FeCl_3$ and pyrolysis temperature at 10.0, 15.0, 20.0 g and 400, 500, 600, 700 °C respectively. The conditions which produced the highest magnetic strength and BET specific surface area was selected to continue with the sulphonation step.

Figure 3.2: Apparatus Setup for the Addition of $FeCl_3$.

Figure 3.3: Calcination of Magnetic Support in the Furnace

3.2.3 Producing Catalyst

Sulphuric acid of 40 ml with a concentration of 0.05 M and 2 g magnetic carbonaceous solid were mixed and stirred for 0.5 h at 50 °C temperature. The mixture was washed several times with deionised water until the washed water was at neutral pH. The washed water was tested with pH paper. Then, the mixture solid was dried at 80 °C in the oven to obtain the solid magnetic acid catalyst. The procedure was repeated using different sulphonation duration and temperature at 1, 2, 3 h and 100, 150, 200 °C respectively. The catalyst with the highest acid density will be used for the synthesis of biodiesel. The preparation of catalyst with different variable was summarised as in Table 3.3.

3.3 Synthesis of Biodiesel

10 g Palm Oil Fatty Acid (PFAD) was poured into a 500 ml round bottom flask. Methanol to oil ratio of 15:1 and a catalyst loading of 0.5 wt% were added. The reflux condenser was attached onto it to prevent methanol from vaporizing and escape out of the flask. The round bottom flask was then placed on the heating mantle as shown in Figure 3.4. The temperature and agitation speed were set to 75 °C and 200 rpm respectively and it was left for 0.5 h. The steps were repeated using a different temperature, esterification duration, methanol to oil ratio and catalyst loading at 100, 125, 150 °C, 1, 2, 3 h, 20:1, 25:1, 30:1, 35:1 and 1.0, 5.0, 7.5, 10.0 wt % respectively. The esterification condition were summarised as in Table 3.4.

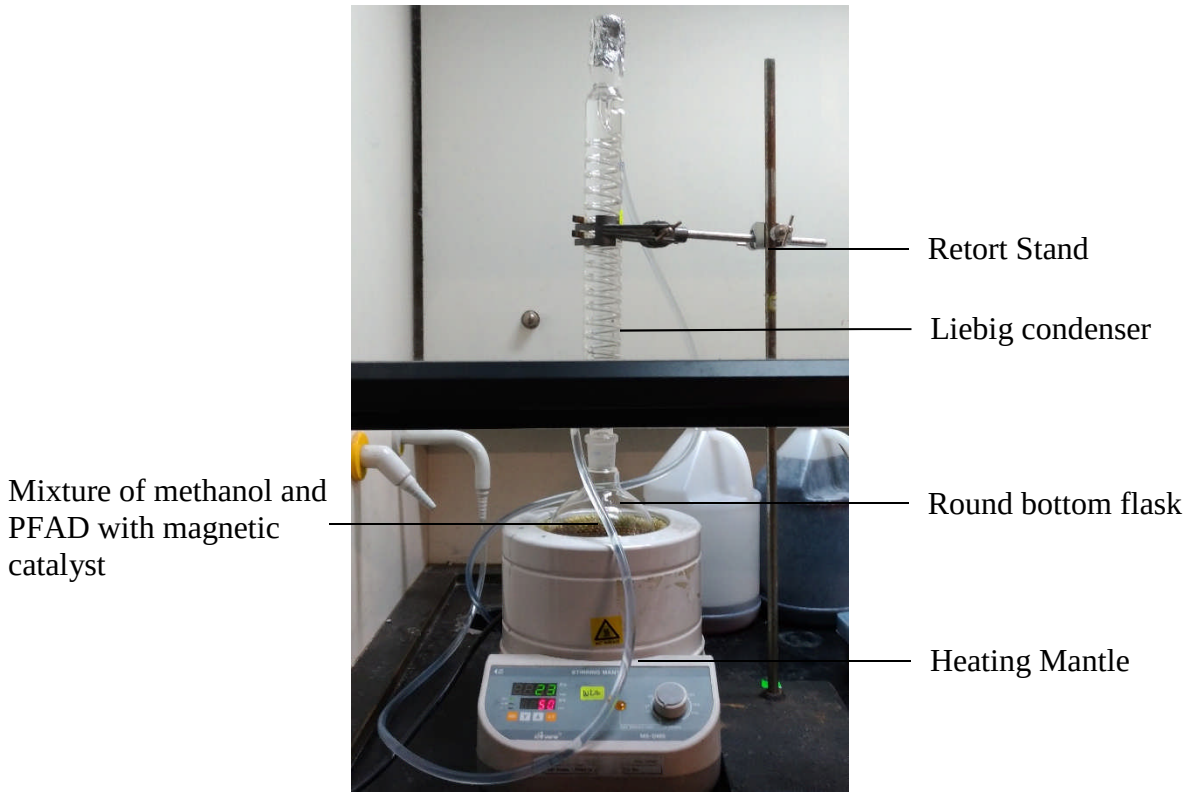

Figure 3.4: Apparatus Setup for the Synthesis of Biodiesel

After esterification, the catalyst was separated using a magnet while the product was poured into a beaker for further distillation. The catalyst removed was then rinsed with water and dry in an oven at 80 °C. After it has been dried, the catalyst was rinsed with hexane in order to remove the remaining fatty acid and biodiesel on the catalyst. The excess methanol in the liquid was removed by simple distillation on a hotplate at 80 °C as shown in Figure 3.5 before pouring the product into a centrifuge tube for storage.

Figure 3.5: Distillation of the Excess Methanol.

Table 3.3: List of Catalyst Preparation

Sample	Sulphonation Condition		
	Temperature (°C)	Duration (h)	Concentration (M)
C1	50	2	5
C2	100	2	5
C3	150	2	5
C4	200	2	5
C5	50	0.5	5
C6	50	1	5
C7	50	3	5
C8	50	3	0.5
C9	50	3	1
C10	50	3	10

Table 3.4: List of Esterification Condition

	Duration (h)	Catalyst Loading (wt%)	Methanol to Oil Ratio	Temperature (°C)
B1	0.5	5	20:1	100
B2	1	5	20:1	100
B3	2	5	20:1	100
B4	3	5	20:1	100
B5	3	0.5	20:1	100
B6	3	1	20:1	100
B7	3	7.5	20:1	100
B8	3	10	20:1	100
B9	3	10	15:1	100
B10	3	10	25:1	100
B11	3	10	30:1	100
B12	3	10	35:1	100
B13	3	10	20:1	50
B14	3	10	20:1	75
B15	3	10	20:1	125

3.4 Characterization of Feedstock

3.4.1 Acidic Value

Potassium Hydroxide, KOH of 0.1 M was diluted before it was poured into the burette which was clamped with a retort stand.

On another beaker, 2.5 ml of PFAD was prepared with 0.5 ml of phenolphthalein and 50 ml of 2-propanol. The PFAD mixture was then titrated with the KOH slowly until the mixture turned light magenta for at least 10 seconds as shown in Figure 3.6. The FFA and Acid number of PFAD can be calculated using Equation 3.1 and 3.2 respectively.

$$FFA(\%) = \frac{M \times N \times V}{Mass\,of\,PFAD\,sample} \tag{3.1}$$

$$Acid\ \ Number\ \ = 1.99\,FFA, \% \tag{3.2}$$

where

M = Molecular Weight of the KOH, 56.11 g/mol

N = Normality of the KOH solution, 0.1 N

V = Titration volume, ml

FFA = Free Fatty Acid, %

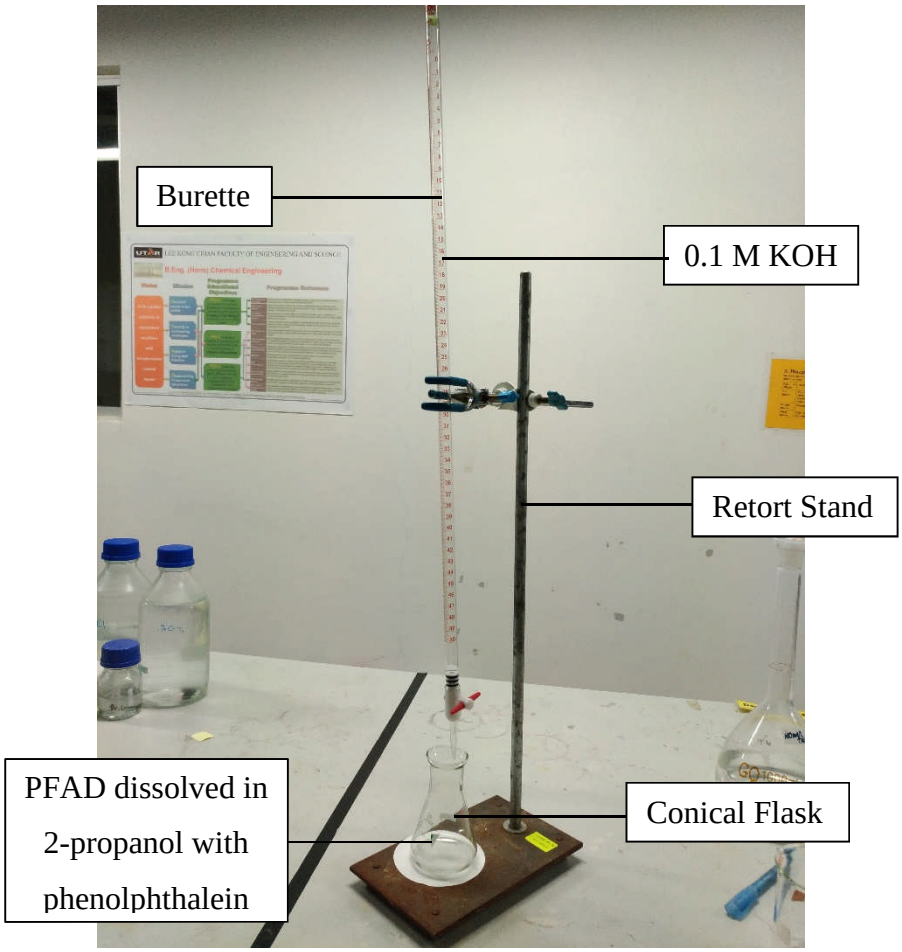

Figure 3.6: Apparatus Setup for the Titration of PFAD with KOH Solution

3.5 Catalyst Characterization

3.5.1 Acid Density Test

The magnetic catalyst of 0.04 g was mixed with 20 ml of NaOH in a beaker for 30 min. The solution was then separated from the catalyst and it was titrated with 0.01 M HCl along with a few drops of phenolphthalein as indicator until the solution turned colourless. The volume of HCl required to neutralise the solution was recorded and the acid density was calculated.

3.5.2 Thermogravimetric Analysis (TGA)

Thermogravimetric analysis (TGA) was the analysis of physical and chemical properties of materials at elevated temperature particularly on the thermal stability. TGA was used to determine the decomposition pattern and the oxidation process of the magnetic support. By obtaining the temperature for decomposition and oxidative mass losses of the catalyst, the pyrolysis temperature of the magnetic support range

can be estimated. Also, the final catalyst stability was also tested to determine the suitable range for esterification temperature. Figure 3.7 shows the TGA used to study the properties of the catalyst.

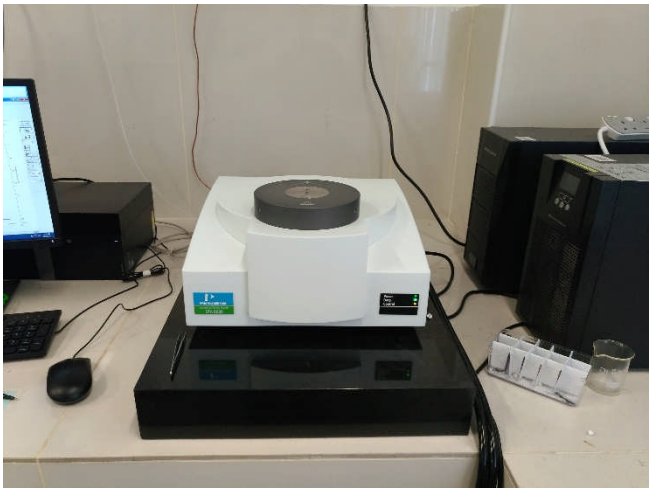

Figure 3.7: Thermogravimetric Analysis (TGA) Used to Study the Stability of the Catalyst.

3.5.3 Scanning Electron Microscope (SEM)

Scanning electron microscope (SEM) was used to produce surface topography image and composition by focusing a beam of electrons into the samples. SEM Model BS 340 TESLA6 was used to analyse the surface morphology of the metallic catalyst as shown in Figure 3.8. The catalysts were then compared by their morphology, structure, surface texturing and pore size at magnification of 500x and 3000x.

3.5.4 Electron Dispersive X-ray (EDX)

Electron Dispersive X-ray (EDX) were usually built-in together with Scanning Electron Microscope (SEM) as shown in Figure 3.8. It was used to find the elemental composition or chemical characterization of the magnetic catalyst. Similarly to SEM, high energy beam was focused into the sample. The X-rays energy emitted from the sample was then measured by energy-dispersive spectrometer. It was used to analyse the pyrolysis and sulphonation effect on the elemental composition of the catalyst during catalyst preparation.

Figure 3.8: Scanning Electron Microscope Together with Electron Dispersive X-rays for the Study of Topography, Morphology and Composition of the Catalyst.

3.5.5 X-Ray Powder Diffraction (XRD)

X-ray Powder Diffraction beams the electrons towards the catalyst, the X-ray spectra received by the X-ray detector provides characteristic information. XRD analysis was carried out using XRD-600 produced by Shimadzu. The catalyst was analysed based on the present of crystalline or amorphous phases. The effect of $FeCl_3$, pyrolysis and sulphonation effect on the catalyst were compared based on their crystallinity. The formation of Fe_2O_3 and Fe_3O_4 was also compared between the sample before and after sulphonation. Continuous scan mode was used with a scanning range between 10 to 80° using a scan speed of 2 °/min.

3.5.6 Brunauer–Emmett–Teller (BET)

Branauer-Emmett-Teller or BET was used to analyse the specific surface area of the magnetic support. The effect of calcination temperature to the specific surface area was compared. BET used the principle of physical adsorption of nitrogen gas on a solid surface at the temperature of 77 K, the boiling point of liquid nitrogen. According to BET theory, the amount of adsorbed gas correlated to the total surface area of the particles. Since each N_2 molecule occupies 0.162 nm^2 at 77 K, the total surface area can be calculated. Figure 3.9 shows the BET surface area analyser used in this research.

Figure 3.9: Brunauer–Emmett–Teller (BET) Surface Area Analyser

3.5.7 Fourier Transform Infrared Spectroscopy (FTIR)

Fourier transform infrared spectroscopy (FTIR) was used to obtain an infrared spectrum emitted or absorbed by the sample. The FTIR test was undergone using Nicholet IS10 FT-IR to study the functional groups present on the magnetic catalyst. The effect of pyrolysis and sulphonation on the functional group during the preparation stages were compared. The samples were tested using 64 scans with a resolution of 4 cm^{-1} from 4000-650 cm^{-1}. Figure 3.10 shows the FTIR used in the study of functional group.

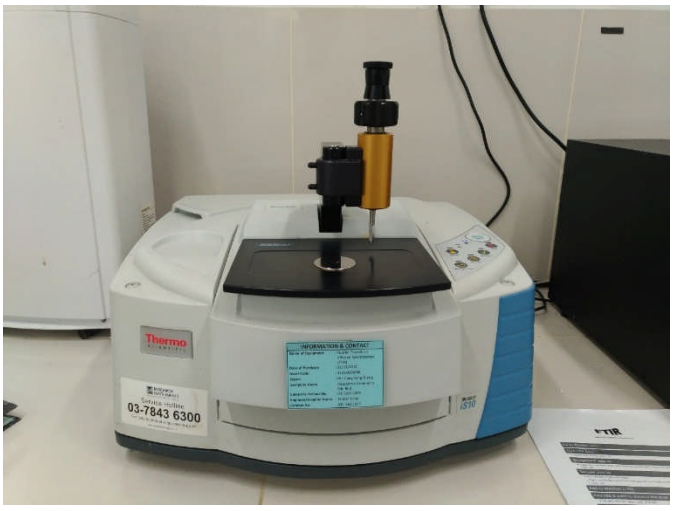

Figure 3.10: Fourier Transform Infrared Spectroscopy (FTIR) Used in the Study of Functional Group.

3.6 Characterization of Biodiesel

3.6.1 Acidic Value of Biodiesel

The methodology for acidic value testing for biodiesel was similar to the one in Section 3.4.1.

The conversion of PFAD was calculated using the Equation 3.3.

$$Conversion(\%) = \frac{Acidic\,Value\,of\ Feedstock - Acidic\,Value\,of\ Biodiesel}{Acidic\,Value\,of\ Feedstock} \quad (3.3)$$

3.6.2 Gas Chromatography (GC)

Gas Chromatography (GC) used a technique of separating and analysing the samples at vapour state by determining their retention time. Clarus 500 Gas Chromatography was used in the test to determine the conversion and composition of fatty acid methyl ester, FAME in biodiesel as shown in Figure 3.11. Before injection, preparation of sample injection was required.

Firstly, 1 g of biodiesel was transferred to the beaker. It was diluted with 10 ml of hexane for every gram of biodiesel. The beaker was then swirled to mix it well. The syringe was rinsed with hexane before extracting 1 µL of liquid from the mixture. It was ensured that there were no bubbles inside the syringe before injecting the sample into the GC for testing. The results were saved.

Figure 3.11: Gas Chromatography (GC) to Determine the Concentration of FAME in Biodiesel.

3.7 Catalyst Reusability

Catalyst obtained from the first experiment was washed with hexane to ensure there was neither biodiesel nor fatty acid stain on it before it was separated with a magnet. The catalyst was then dried in an oven at 80 °C. The catalyst was reused for another test under the same optimum condition. The reusability of a catalyst was based on the rate of change in conversion on the subsequence reaction.

3.8 Summary

The flow chart of the methodology is shown in Figure 3.12

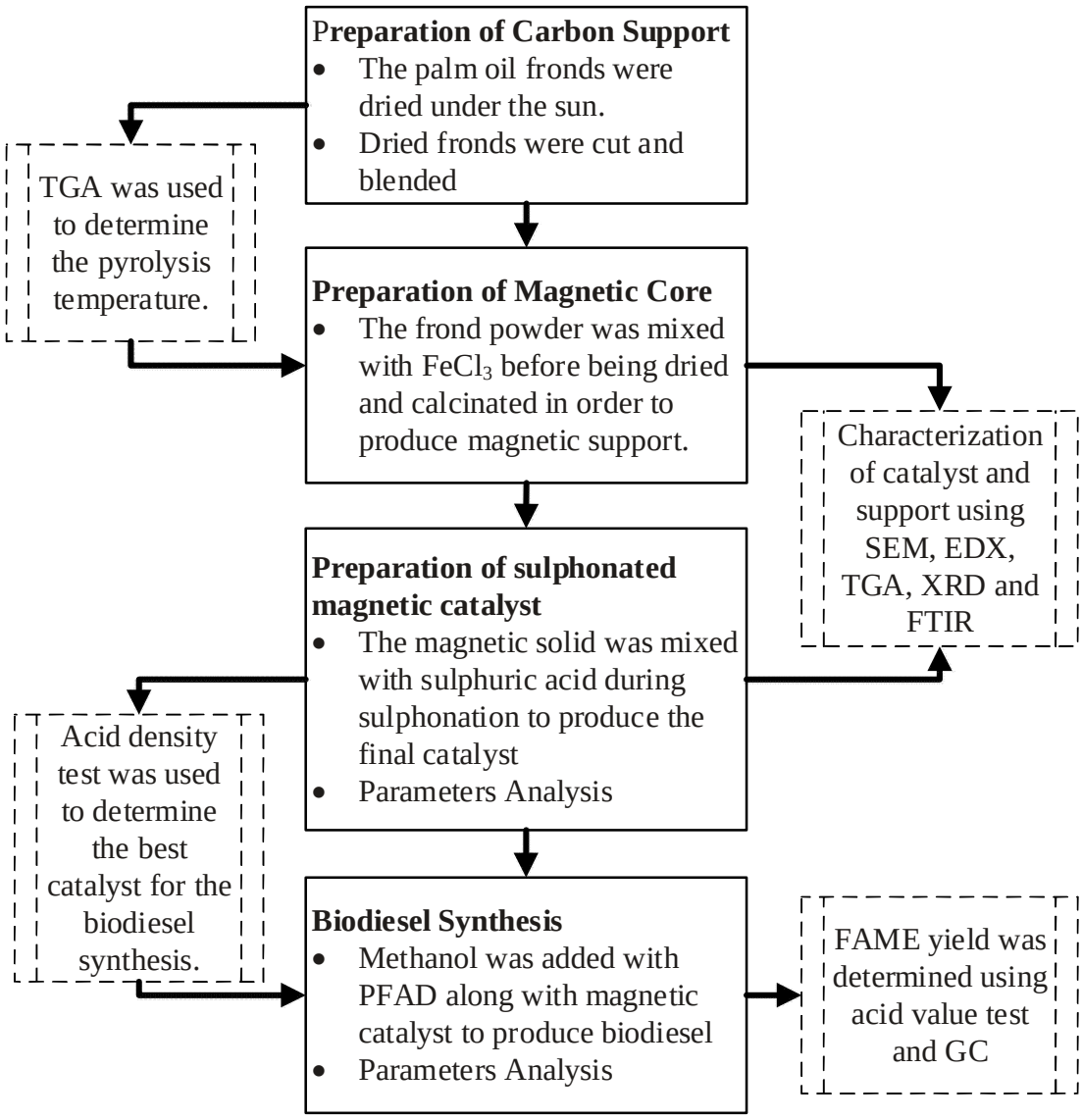

Figure 3.12: Summary of the Experiment

CHAPTER 4

RESULTS AND DISCUSSIONS

4.1 Preliminary Stage Observation

Magnetic catalysts were prepared according on the parameters as shown in Table 4.2. The best catalyst was determined using acid density test before chosen for esterification process. The biodiesel preparation parameters were varied to determine the optimum biodiesel condition. After production of biodiesel, the excess methanol was removed by simple distillation process.

Figure 4.1 shows the magnetic catalyst as attracted by the magnet where the strength of the magnet was able to support the weight of the paper. As seen in Figure 4.2(a), the lighter top layer was methanol due to lower density while the heavier lower part was the biodiesel with unreacted PFAD. Meanwhile in Figure 4.2(b), the black droplets are the glycerol. After removal of methanol, only one layer will remain as shown in Figure 4.3 and 4.4.

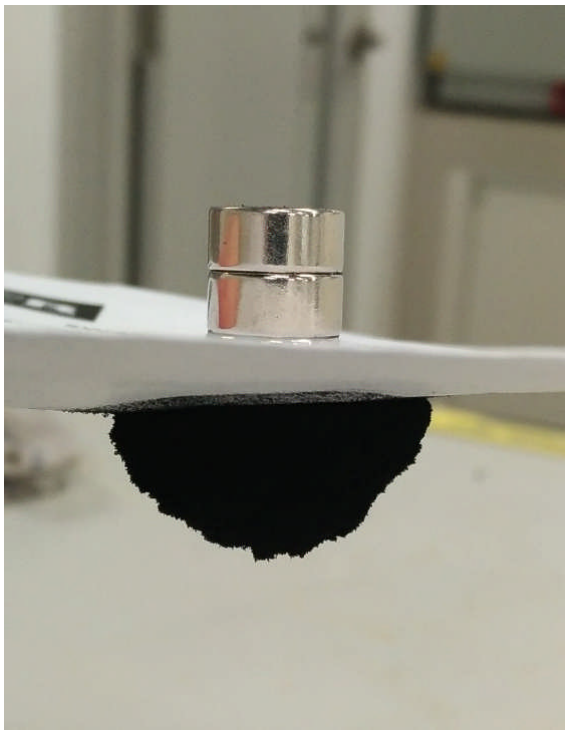

Figure 4.1: Magnetic Catalyst as Attracted by Magnet.

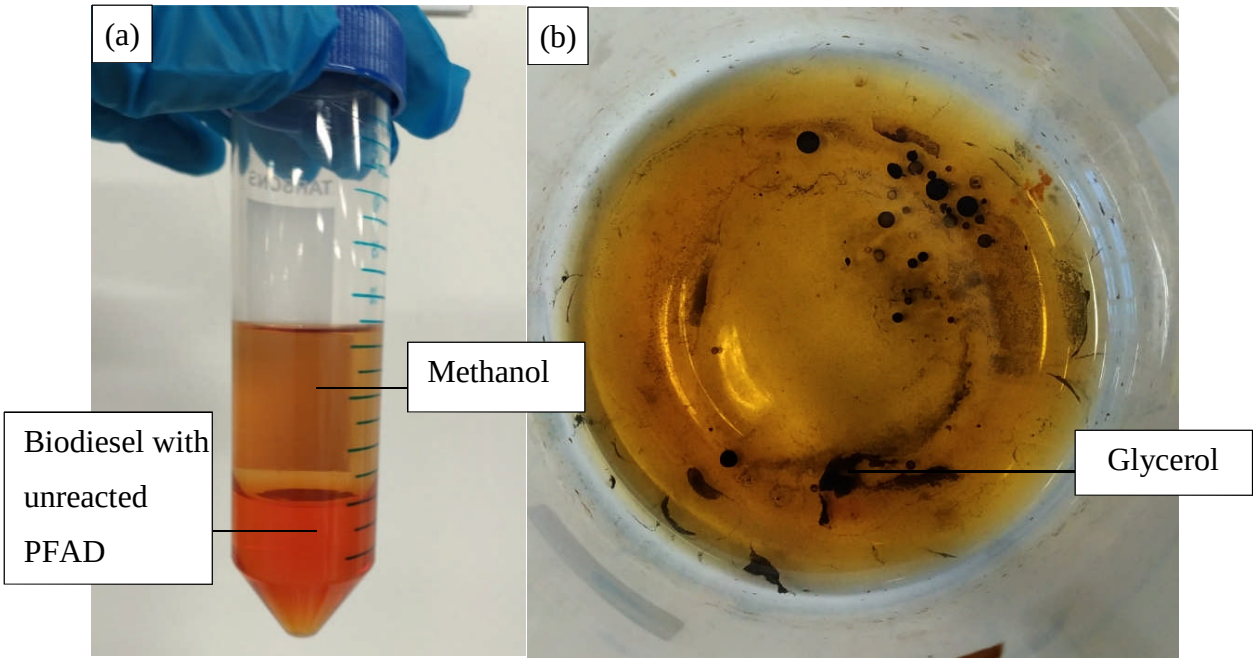

Figure 4.2: Biodiesel with By-product Before the Removal of Methanol: Side View (a), Top View (b).

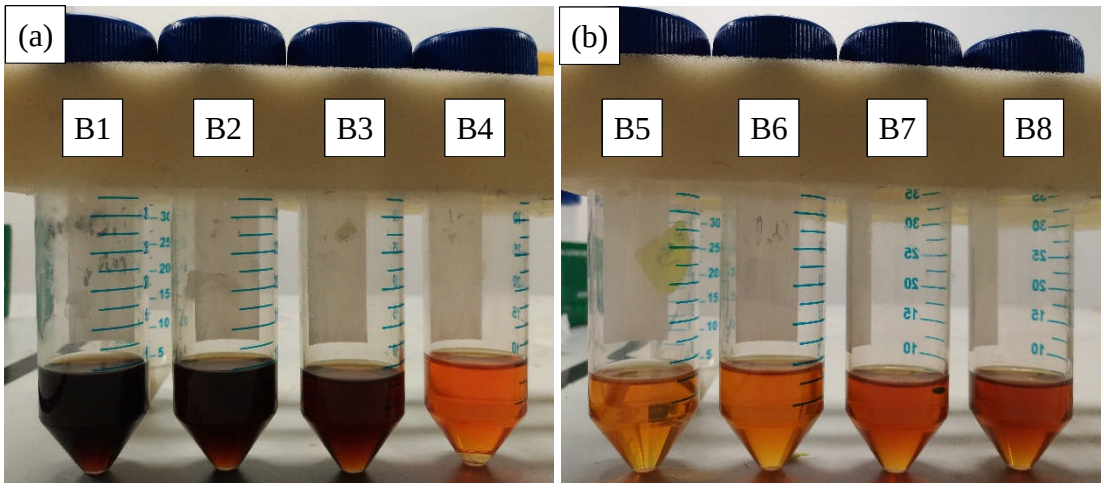

Figure 4.3: Production of Biodiesel with (a) Different Esterification Duration of 0.5, 1.0, 2.0, 3.0 h and (b) Catalyst Mass Loading of 0.5, 1.0 , 7.5, 10.0 wt %.

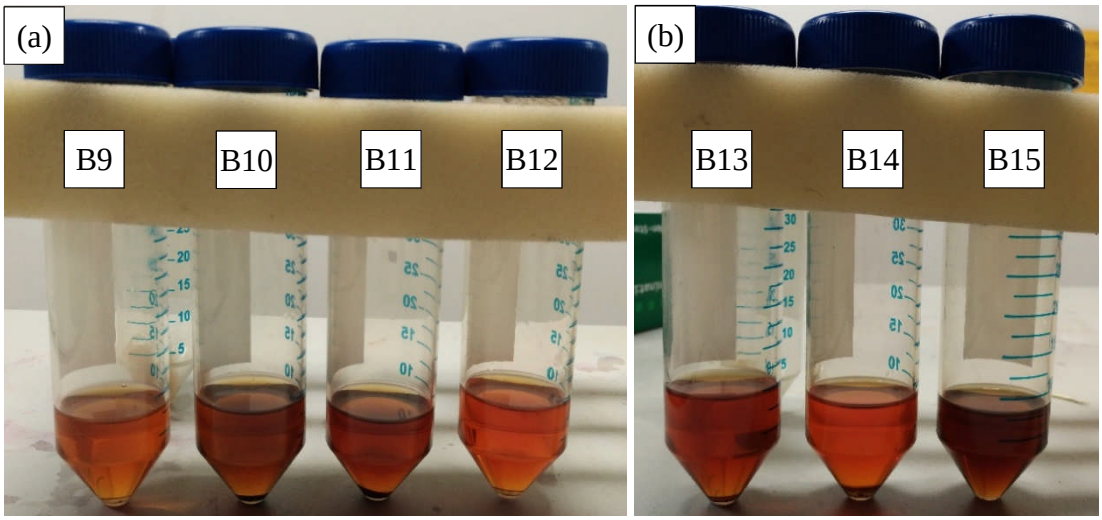

Figure 4.4: Production of Biodiesel with (a) Different Methanol to Oil Ratio of 15:1, 25:1, 30:1, 35:1 and (b) Esterification Temperature of 50, 75, 125 °C.

4.2 Preparation of Magnetic Support

4.2.1 Addition of $FeCl_3$

A fixed mass of $FeCl_3$ was mixed with 250 ml of distilled water before mixing with frond dust at 200 °C for 2 hours until all of the liquid is evaporated. The sample was dried and tested with EDX. It was detected that Fe (wt%) increases with mass of $FeCl_3$ used as shown in Figure 4.5 which confirmed the successful physisorption and chemisorption of $FeCl_3$ to the frond dust. The optimum mass of $FeCl_3$ was 20 g where the elemental Fe composition was at 13.22 wt %.

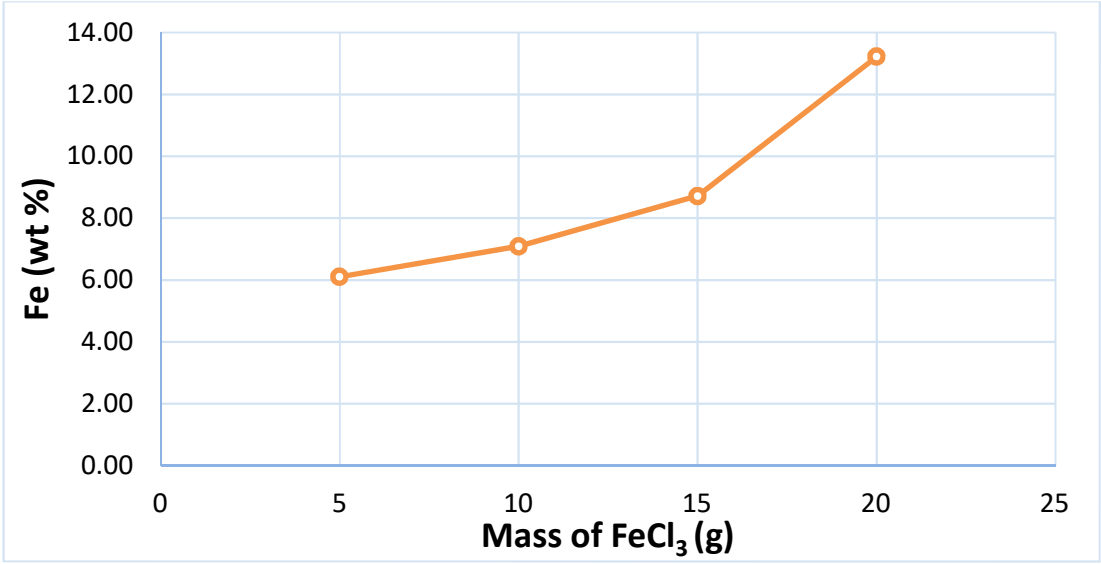

Figure 4.5: Elemental Composition of Fe (wt%) After Addition of $FeCl_3$ to the Frond Support.

4.2.2 Calcination Temperature

Calcination temperature parameter was determined by TGA where the range was within the mass loss range. There were two stages of mass loss. The first stage which was the gradual weight loss occurred at approximately 25 to 200 °C which was due to the dehydration of water content and released of volatile organic compound as shown in Figure 4.6. The second rapid mass loss stage was the decomposition of the samples into H_2O, CO and CO_2 (Liu et al., 2013). $FeCl_3$ added frond dust has higher weight percentage at higher temperature. This was due to the presence of Fe which cannot be easily decomposed as compared to the carbon based frond dust. The slight increase in mass for $FeCl_3$ added fronds sample was probably due to the formation of Fe_3O_4 where the oxygen was used to oxidise the Fe instead of carbon structure, reducing the formation and release of H_2O, CO and CO_2 as gaseous phase. Therefore, the temperature between 300 to 700 °C was selected as a range for the calcination temperature parameter.

There were two major effects of different calcination temperature on the magnetic catalyst support which were the magnetic strength and BET specific surface area. Both effects will be discussed in detail in the following subsection.

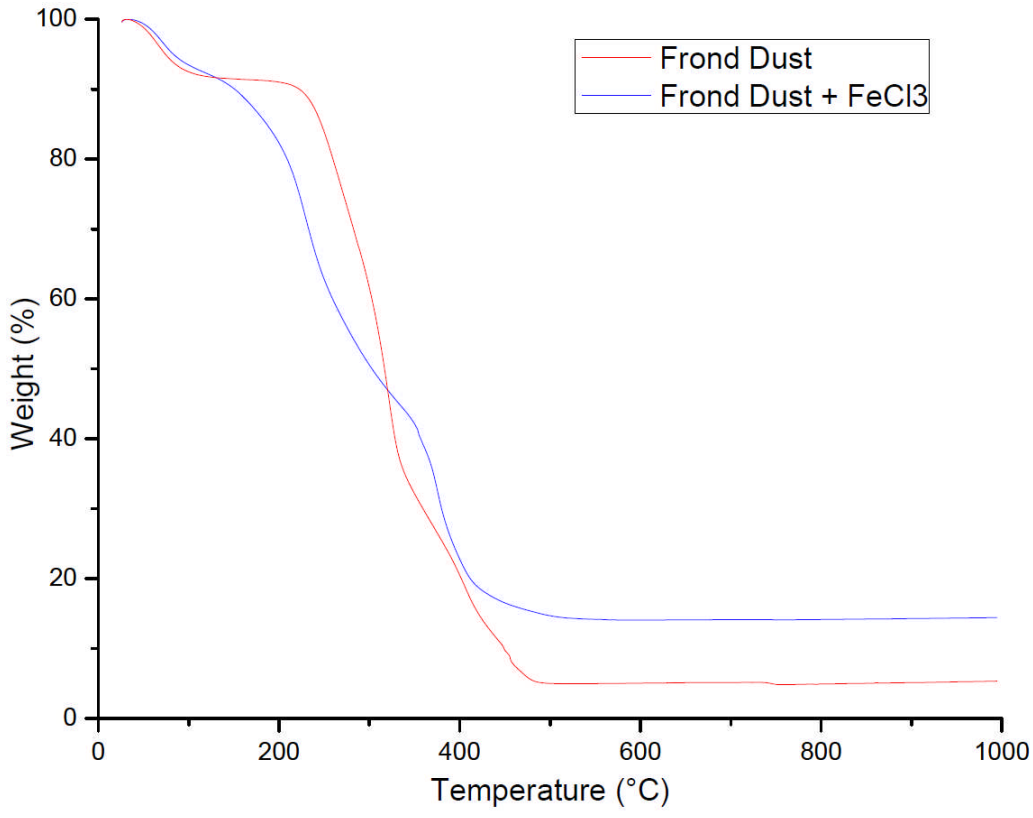

Figure 4.6: TGA of Frond Dust Before and After Addition of $FeCl_3$ in Air.

4.2.2.1 Magnetic Strength

The magnetic strength of magnetic support for different calcination temperatures were tested with a neodymium magnet with a magnetic strength of 2000 Gs as there was no other equipment available. It should be noted that before calcination, there was no magnetic properties detected on the sample.

$Fe(OH)_3$ was first bounded to the frond powder through physisorption and chemisorption in the precipitation of $FeCl_3$. The $Fe(OH)_3$ will then be oxidised to Fe_3O_4 which provided the magnetic properties. According to Liu et al. (2013), by-products such as CO, CO_2 and H_2O will be released as gases during the formation of Fe_3O_4 as shown in the chemical equation 4.1, 4.2, 4.3, 4.4 and 4.5 below.

$$FeCl_3 + 3\,H_2O \rightarrow Fe(OH)_3 + 3\,HCl \quad (4.1)$$

$$Fe\,(OH)_3 \rightarrow FeO(OH) + H_2O \quad (4.2)$$

$$6\,FeO(OH) + 4\,H_2 \rightarrow 2\,Fe_3O_4 + 4\,H_2O \quad (4.3)$$

$$6\,FeO(OH) + 4\,C \rightarrow 2\,Fe_3O_4 + 2\,CO \quad (4.4)$$

$$6\,FeO(OH) + 4\,CO \rightarrow 2\,Fe_3O_4 + 4\,CO_2 \quad (4.5)$$

Calcination of 300 to 400 °C produced no observable magnetic properties. This was probably due to the oxidation occurring at a very slow rate which was unobservable. According to Figure 4.7, the magnetic strength increased when the calcination temperature increased from 400 to 700 °C. At higher temperature, the oxidation of Fe was more prevalent as can be proven by the resulted higher magnetic strength. The higher magnetic strength was due to the higher rate of oxidation promoted by the higher calcination temperature.

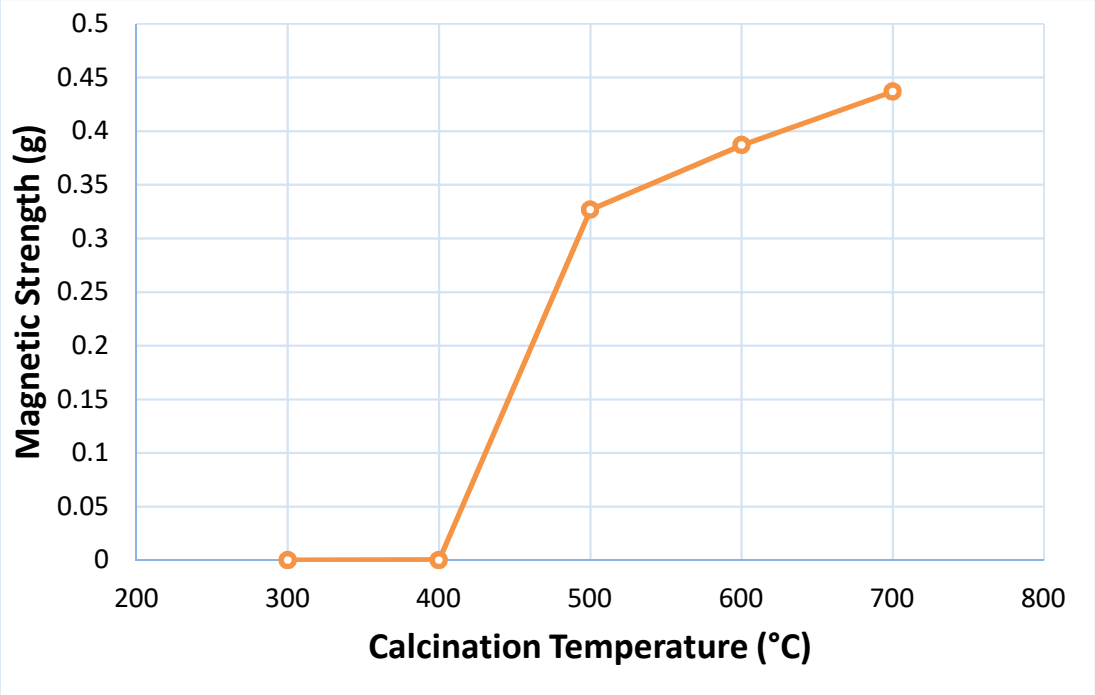

Figure 4.7: The Graph of Magnetic Strength vs the Calcination Temperature.

4.2.2.2 Specific Surface Area

According to Feyzi et al. (2013), calcination temperature will increase the surface area to a maximum point before decreasing due to sintering effect. BET analyser shows an increment in the specific surface area with calcination temperature as shown in Table 4.1. The sintering effect probably occurs at a higher temperature as compared to the one in Feyzi et al. (2013). At high calcination temperature, volatile component can be removed as gaseous phase. At the same time, pores will be formed. Catalyst consisted of larger pores will provide easier attachment of $–SO_3H$ functional groups to the support (Shu et al., 2010). This will increase the catalytic activity of catalyst as confirmed by the result in Hu et al. (2011).

Table 4.1: BET Specific Surface Area for Different Calcination Temperature

Calcination Temperature (°C)	Specific Surface Area (m^2/g)
400	182.69
500	251.94
600	321.47
700	339.94

4.3 Sulphonation Optimization

Magnetic catalyst was prepared following the sulphonation condition as shown in Table 4.2. The catalysts were then compared based on their acid density with different parameters of sulphonation temperature, duration and concentration.

Table 4.2: Catalyst Preparation Parameter and its Acid Density

Catalyst	Sulphonation Condition			Acid Density (mmol/g)
	Temperature (°C)	Duration (h)	Concentration (M)	
C1	50	2	5	2.89
C2	100	2	5	2.53
C3	150	2	5	2.24
C4	200	2	5	2.10
C5	50	0.5	5	2.62
C6	50	1	5	2.74
C7	50	3	5	2.89
C8	50	3	0.5	2.41
C9	50	3	1	2.74
C10	50	3	10	3.16

Note: Mass of $FeCl_3$ during addition of FeCl3 and Calcination Temperature was at 20 g and 700 °C respectively for all catalyst preparation.

4.3.1 Effect of Temperature

As the temperature increased from 50 to 200 °C, the acid density of the catalyst decreased from 2.89 to 2.10 mmol/g as shown in Figure 4.8. This was because fracture of the condensed structure may occur at high temperature which will damage the catalyst structure and reducing its effectiveness. At very high temperature around 200 °C, carbonisation of the catalyst may occur which counteracts the sulphonation reaction (Zhang et al., 2016). According to Wu et al. (2014), acidity of the catalyst was an important factor to increase the catalytic performance. In general, catalyst with higher acid density will produce higher yield of biodiesel.

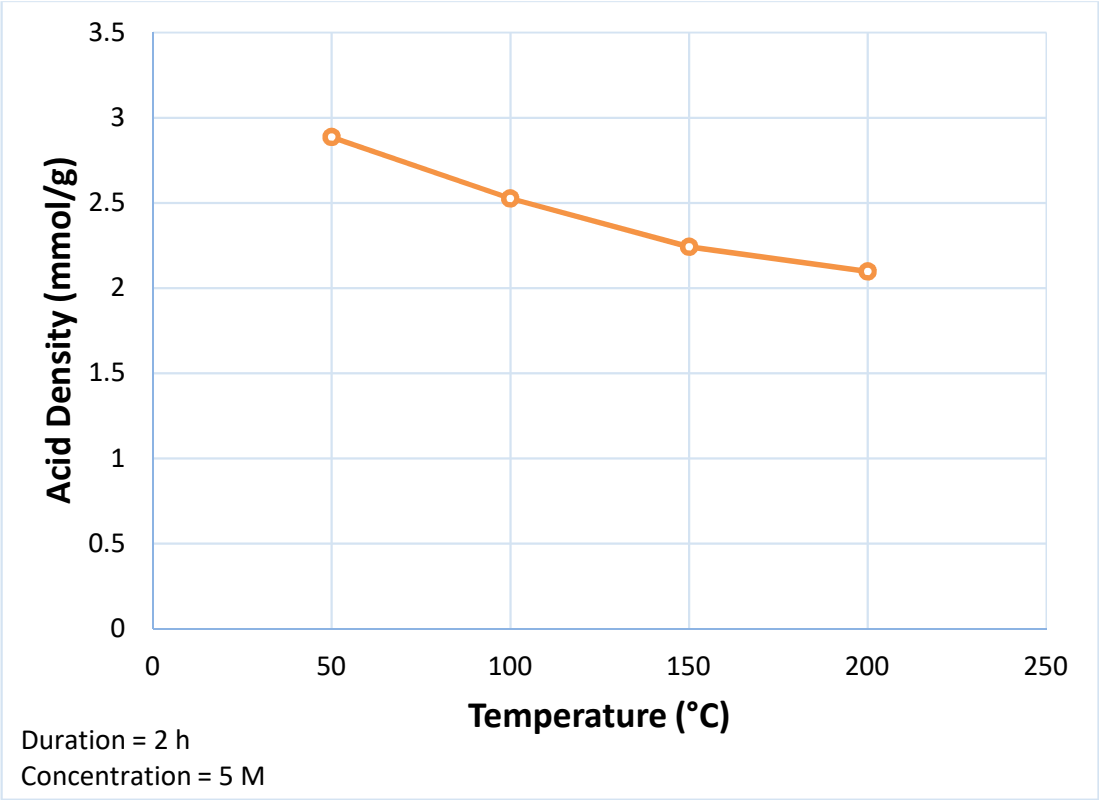

Figure 4.8: The Graph of Acid Density vs Temperature

4.3.2 Effect of Sulphonation Duration

Based on Figure 4.9, the acid density increased from 2.62 to 2.89 mmol/g when the sulphonation duration increased from 0.5 to 2 h. It should be noted that there was only a slight increase in acid density from the 2 to 3 h as the acid sites became saturated. The magnetic support cannot be further attached with more -SO_3H functional group. According to Zhang et al. (2016), the increase in sulphonation time will lead to completion of sulphonation, which in turn led to higher yield. This was due to the sulphuric acid being a strong oxidiser which oxidised the –OH group into –COOH increasing the acidity.

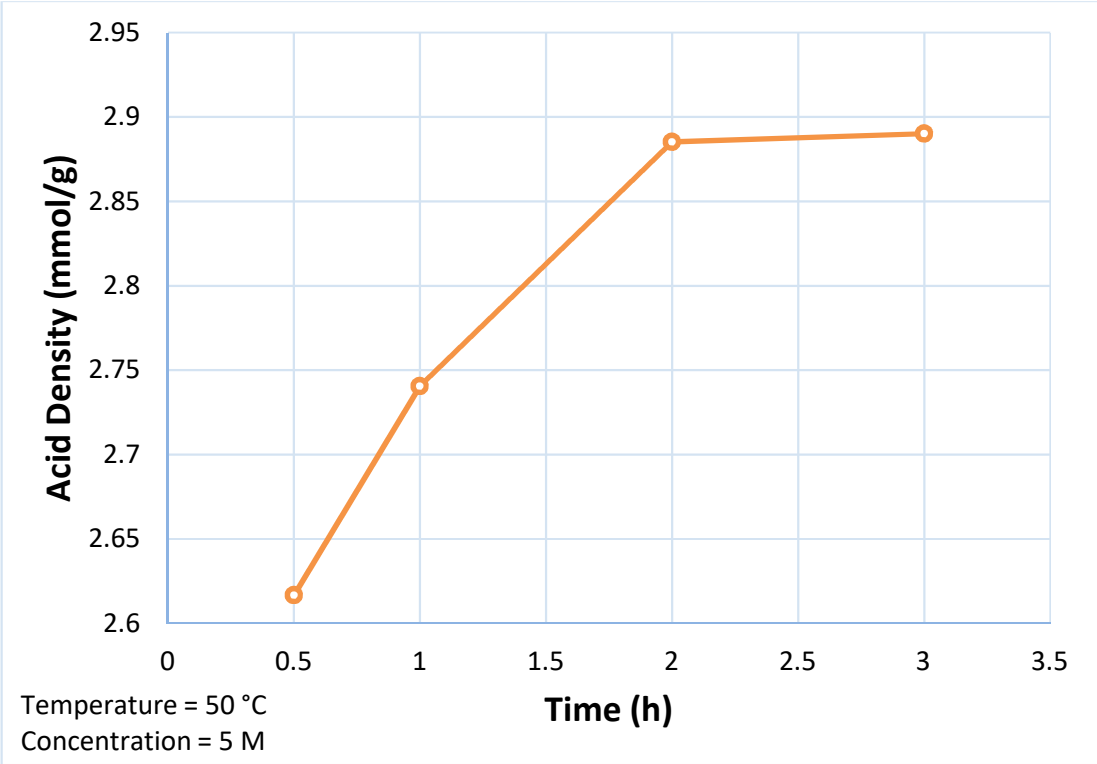

Figure 4.9: The Graph of Acid Density vs Time

4.3.3 Effect of Molarity

It can be seen from Figure 4.10 that the acid density increased with molarity due to the fact that more $–SO_3$ function group were available for the attachment to the amorphous carbon structure. The acid density increased drastically from 0.5 to 1 M before decreasing in rate from 1 M to 10 M. At 10 M, the acid density achieved the highest acid density of 3.16 mmol/g. The catalyst with the highest acid density, C10 was chosen as the best catalyst and will be tested for its optimum esterification condition. In general, higher concentration of sulphonation will increase the acid density of the catalyst. This was confirmed by the results in Zillillah et al. (2014) where the highest phosphonation concentration produced the highest acidity.

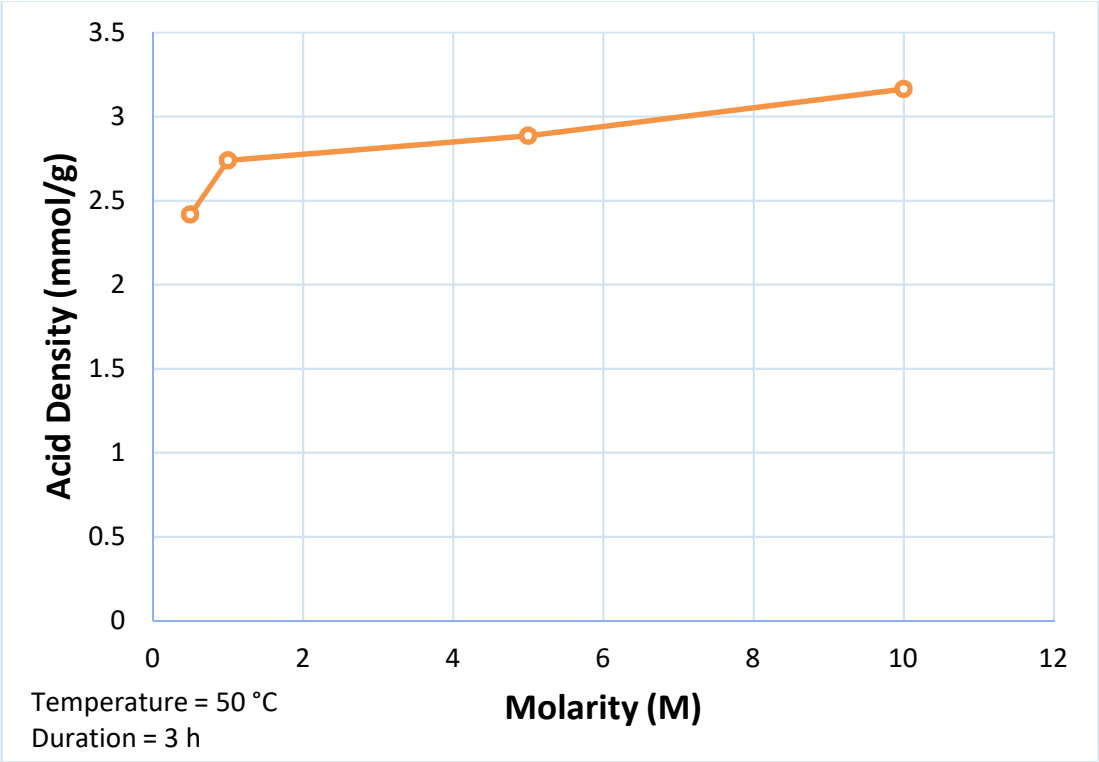

Figure 4.10: The Graph of Acid Density vs Molarity

4.4 Catalyst Characterisation

The final catalyst were being characterized by several equipment such as TGA, SEM, EDX, XRD and FTIR.

4.4.1 Thermogravimetric Analysis (TGA)

TGA was done under the atmosphere of air with a rate of 10 °C/min. Based on Figure 4.11, gradual weight loss was observed at 100 °C followed by a reduction of 80% in mass from 400 to 700 °C. After 700 °C, there was no observable weight loss, after 700 °C. The first stage was due to the evaporation of water content followed by the decomposition of catalyst at the second stage. It can be concluded that the catalyst was chemically and thermally stable up to 400 °C in air and will not oxidise or decompose easily during the biodiesel esterification process.

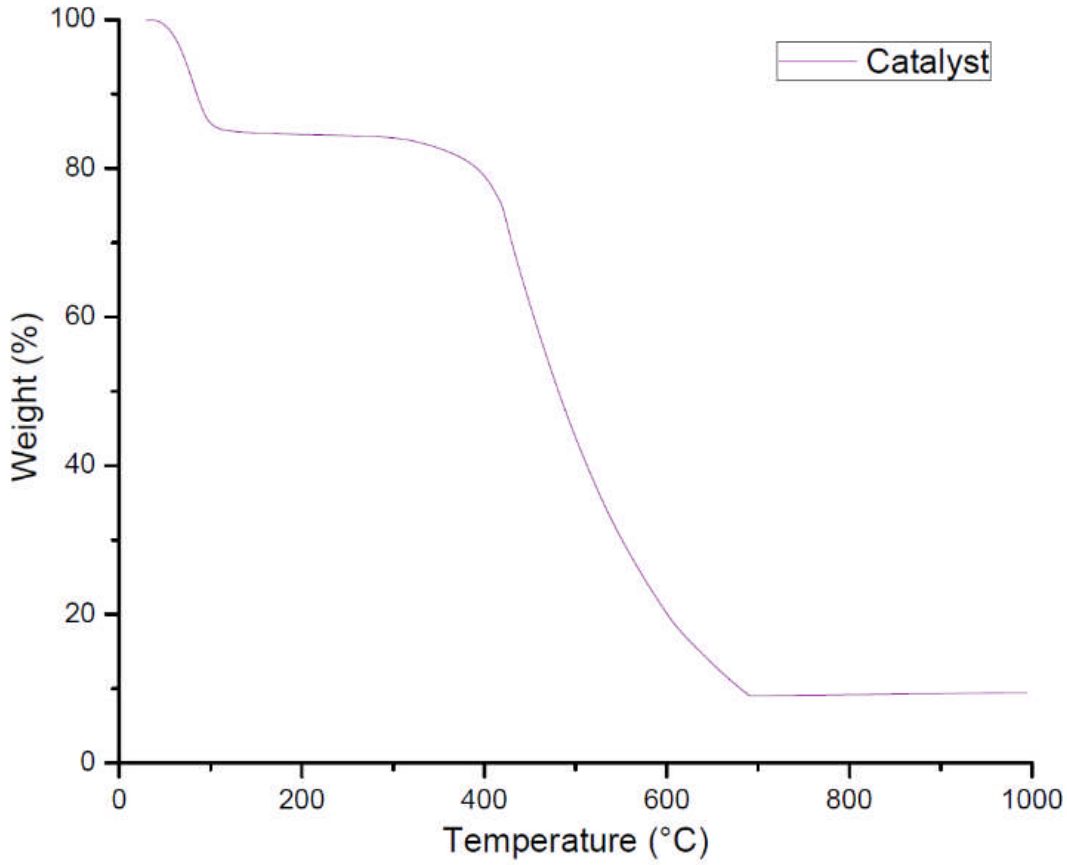

Figure 4.11: Mass Loss of Catalyst in Air.

4.4.2 Scanning Electron Microscope (SEM)

After addition of $FeCl_3$, the surface showed an increase in roughness as can be seen from the Figure 4.12 (b) and (d). This was due to the physisorption and chemisorption of $FeCl_3$. After calcination, the structure appeared to be smoother. At the same time, there are more cracks and pores as can be seen in Figure 4.12 (f) which was caused by the evaporation of volatile component such as oxygen, nitrogen and chlorine.

There was no clear change in structure after the sulphonation process. This was consistent with Zhang et al. (2013) where the magnetic core was stable and will not easily change its structure.

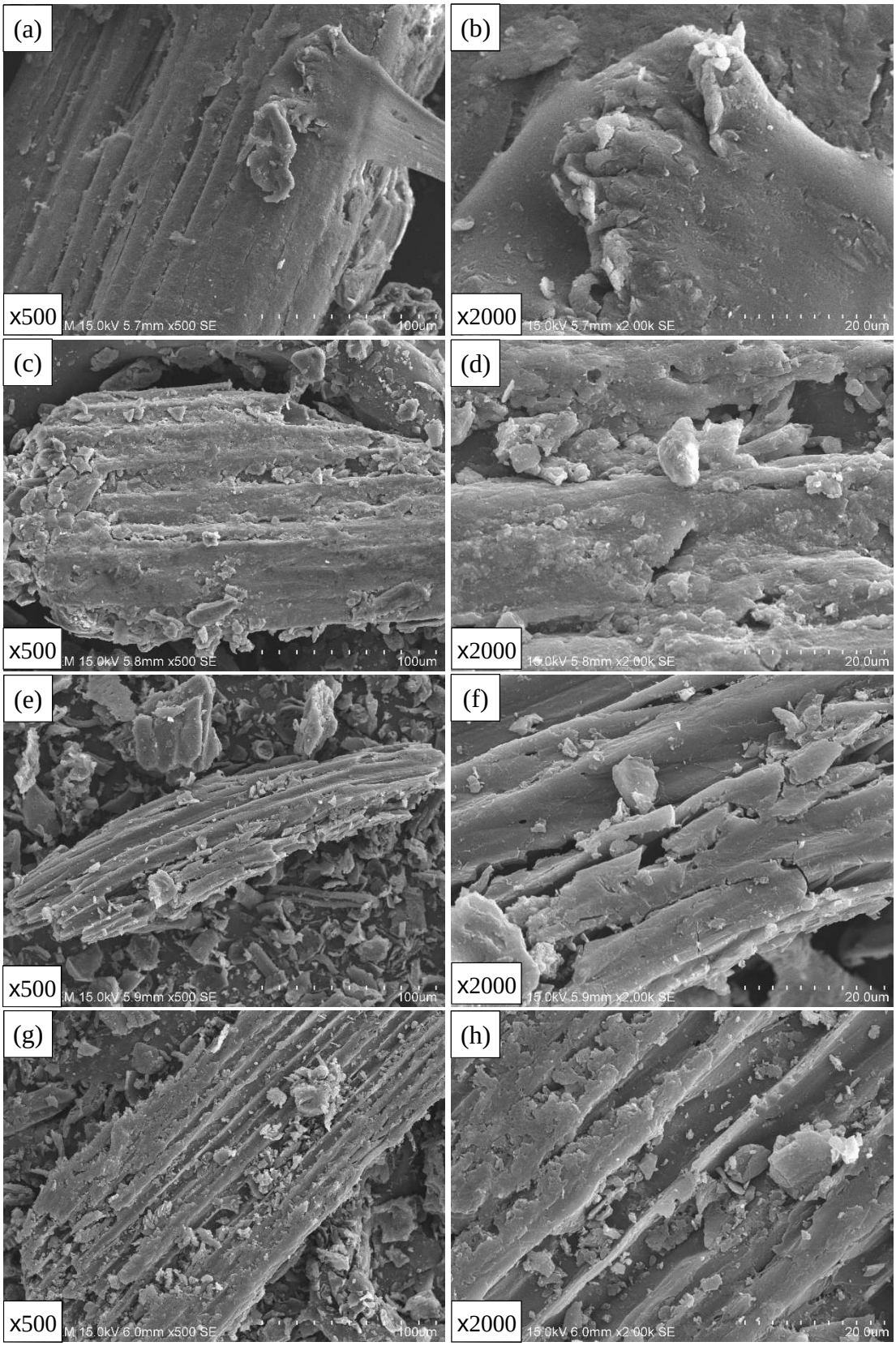

Figure 4.12: SEM Images of the Frond Dust (a), (b) Before and (c), (d) After the Addition of $FeCl_3$, (e), (f) Magnetic Support After Calcination and (g), (h) Catalyst After Sulphonation at a Magnification of 500x and 2000x.

4.4.3 Electron Dispersive X-ray (EDX)

The raw frond dust was started with only C and O element with minimal Cl, Fe and S. After addition of $FeCl_3$, the elemental composition of Fe rose drastically from 0.09 wt% to 10.38 wt% as shown in Table 4.3.

It was noticed that after calcination, the elemental composition of oxygen decreased from 38.26 wt % to 10.28 wt% as most of the O are released as CO_2 and H_2O as by-product during the formation of Fe_2O_3 and Fe_3O_4. At the same time, Cl was released as HCl gas which showed reduction in composition as well. Fe did not experience any mass loss due to decomposition. The increased composition of Fe from 10.8 wt% to 18.39 wt% was due to the mass loss of other element.

After sulphonation, the S concentration increased from 0.86 to 2.47 wt %. However, it was noted that at the same time, Fe will be leached out as $FeSO_4$ during the process which reduced the magnetic properties strength and Fe composition to 3.78 wt %. Similarly, the increase in carbon concentration was due to the leaching of Fe and O as $FeSO_4$.

Table 4.3: Elemental Composition of the Samples Throughout the Experiment

Element	**Frond Dust**		**Addition of $FeCl_3$**		**After Calcination**		**After Sulphonation**	
	Wt %	At %	Wt %	At %	Wt %	At %	Wt %	At %
C	46.72	54.74	21.33	32.16	49.29	71.91	71.28	84.01
O	49.87	43.88	38.26	45.62	10.28	11.32	10.25	9.07
Cl	2.76	1.10	29.28	17.66	21.18	10.50	12.21	4.88
Fe	0.09	0.02	10.38	4.08	18.39	5.80	3.78	0.96
S	0.56	0.25	0.75	0.47	0.86	0.47	2.47	1.09

4.4.4 X-Ray Diffraction (XRD) Analysis

The broad weak diffraction peak of 2θ at 10-30° for the catalyst confirmed the amorphous carbon in the magnetic catalyst (Liang, 2015; Hara et al., 2004). The board peak which described amorphous phase, remained even after calcination and sulphonation as shown in Figure 4.13. The amorphous structure allowed the attachment of $-SO_3H$ active site functional group.

For the magnetic support after calcination, XRD showed the peaks of 2θ at 32.8°, 35.1°, 38.1°, 44.4°, 53.7°, 64.8° and 77.9° which were corresponded to the planes (220), (311), (222), (400), (422), (440) and (622) of Fe_3O_4 respectively as shown in Figure 4.13 (b) (Liang, 2015; Liu et al., 2013). This showed the formation of Fe_3O_4 after calcination of the $FeCl_3$ added frond dust. After sulphonation, the presence of peaks proved that Fe_3O_4 were still tightly bonded to the carbon support. However, there was a slight reduction of peaks of Fe_3O_4 which showed the decreasing Fe_3O_4 content due to leaching during the sulphonation process when comparing Figure 4.13 (b) and (c).

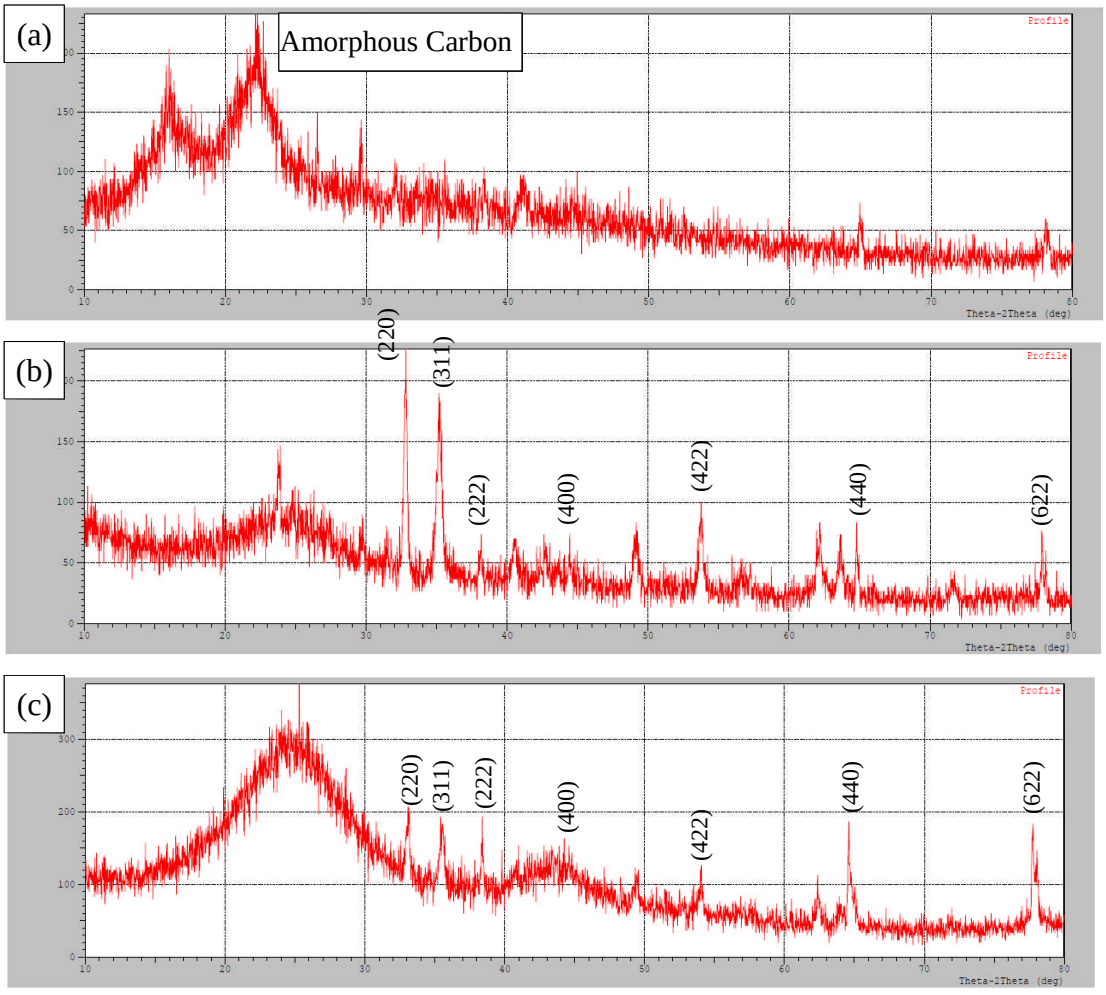

Figure 4.13: XRD for Frond Dust (a) After the Addition of $FeCl_3$, (b) Magnetic Support After Calcination and (c) Catalyst After Sulphonation.

4.4.5 Fourier Transform-Infrared Spectroscopy (FTIR)

All of the functional groups that were applicable in this research are shown in Table 4.4. The FTIR spectrum shown by the frond dust is consistent with the result of Liang (2015) where its mainly consisted of carbon materials. As can be seen from Figure 4.14, From 950 – 1250 cm^{-1}, the peak showed strong broad absorbability due to the C-O stretching vibration, which confirmed the high oxygen-containing groups in the frond dust before and after addition of $FeCl_3$. Other functional groups observed were C=O at 180 cm^{-1} and O-H group at 3331.02 cm^{-1}. Both O-H and C-O groups were important in providing active sites for the sulphonation process according to Liang (2015).

After calcination, the magnetic support showed a reduction in O-H groups due to the evaporation of water content at high temperature. There was also a cleaner FTIR spectrum from 1500 to 1250 cm^{-1} as most of the volatile impurities were evaporated during the calcination process. Formation of Fe-O group can be observed by the peak at 561.18 cm^{-1} which was similar to Feyzi et al. (2013) result. This showed the formation of iron oxide during the calcination process which further validated the presence of Fe_3O_4 as shown in the XRD analysis.

By comparing the spectra of before and after sulphonation, the peak at 1041.72 cm^{-1} showed the presence S-O group. This showed successful attachment of S-O group on the surface of the amorphous carbon. At the same time, the Fe-O still maintained after sulphonation at 561.18 cm^{-1} confirming the fact that the magnetic properties was not eliminate after sulphonation.

Table 4.4: Possible Functional Groups Detected from FTIR

Wavenumber (cm^{-1})	**Possible bond**
<400	*Fe- / Fe-S*
500-600	*Fe-O*
1000-1300	*S-O*
1400-1600	*C-O*
1500-1650	*C=O*
2800-3000	*C-H*
2800-3400	*O-H*

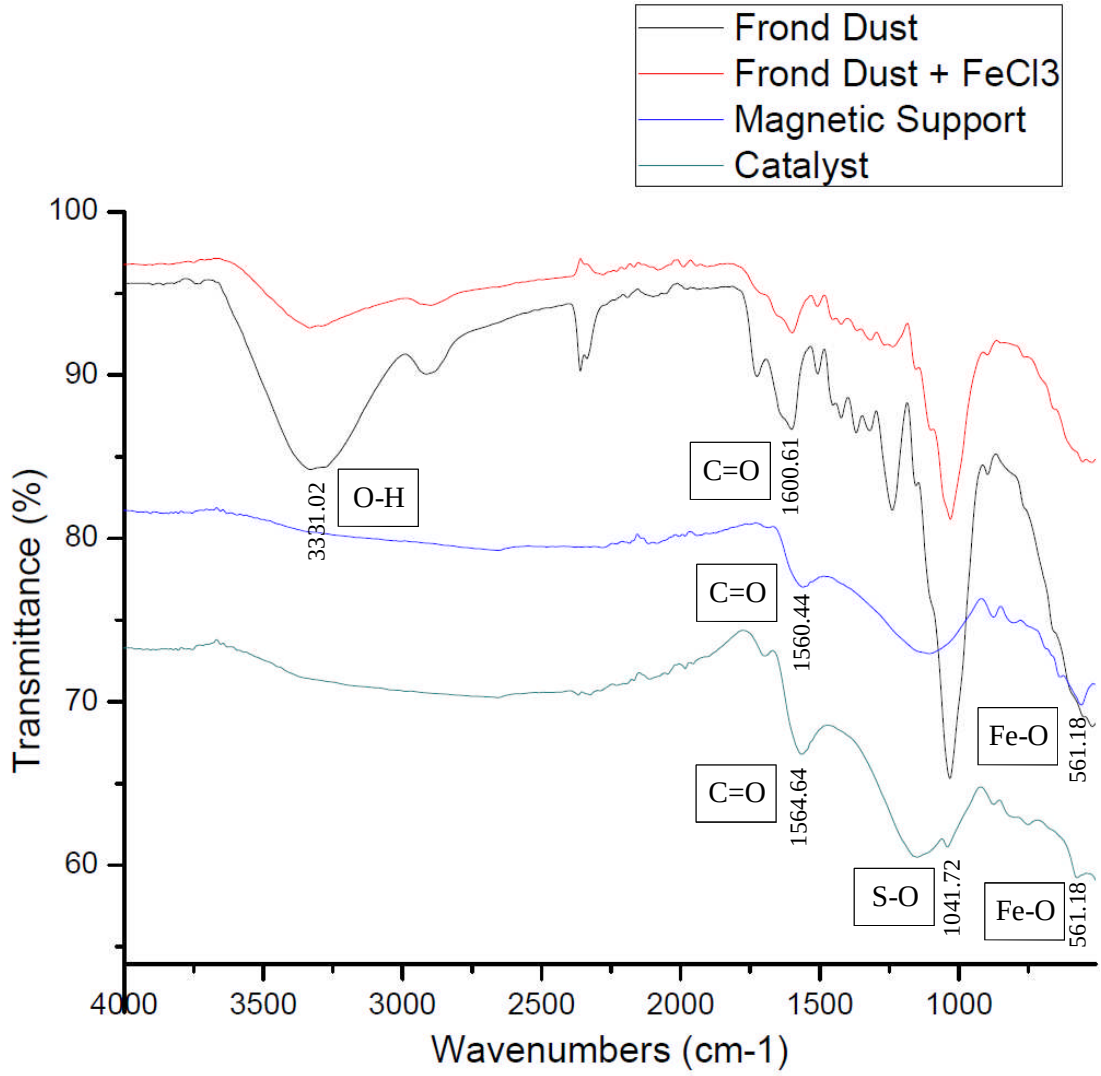

Figure 4.14: FTIR Spectra of Frond Dust Before and After Addition of $FeCl_3$, Magnetic Support and Catalyst.

4.5 Biodiesel Optimization

Table 4.5 showed the conversion of different esterification parameters such as esterification duration, catalyst mass loading, methanol to oil ratio, temperature and acid number during the production of biodiesel. As can be seen from Table 4.5, the highest conversion was at 87.56 % where the optimum esterification condition was 3 h, 10 wt % catalyst loading, 20:1 methanol to oil ratio, at 75 °C.

Table 4.5: Effect of Different Parameters on the Conversion of Biodiesel.

	Duration (h)	**Catalyst Loading (wt%)**	**Methanol to Oil Ratio**	**Temperature (°C)**	**Acid Number**	**Conversion (%)**
B1	0.5	5	20:1	100	293.95	33.11
B2	1	5	20:1	100	251.25	42.82
B3	2	5	20:1	100	183.12	58.33
B4	3	5	20:1	100	157.98	64.05
B5	3	0.5	20:1	100	412.24	6.19
B6	3	1	20:1	100	324.13	26.24
B7	3	7.5	20:1	100	128.69	70.71
B8	3	10	20:1	100	90.03	79.51
B9	3	10	15:1	100	147.47	66.44
B10	3	10	25:1	100	94.22	78.56
B11	3	10	30:1	100	104.92	76.12
B12	3	10	35:1	100	120.60	72.56
B13	3	10	20:1	50	142.69	67.53
B14	3	10	20:1	75	54.68	87.56
B15	3	10	20:1	125	88.61	79.83

Note: C10 with the sulphonation condition of 50 °C, 3h and 10 M was used in esterification process.

4.5.1 Duration

Based on Figure 4.15, the conversion increases with esterification duration. According to Lokman et al. (2016), other conditions such as catalyst mass loading, methanol to oil ratio and reaction temperature affected the rate of reaction. In other words, the time required for the reaction to reach equilibrium was affected. Similarly as proven by Fadhil et al. (2016), the conversion will always increase with time despite the catalyst loading, methanol to oil ratio and esterification temperature were different

It can be seen that the esterification and transesterification required approximate 3 hours to achieve 64.05 % conversion. The maximum conversion and yield occurred at equilibrium point when the forward and backward reaction was equal. Since the increase of conversion was almost constant from 2 h to 3 h, it can be said that equilibrium had been achieved.

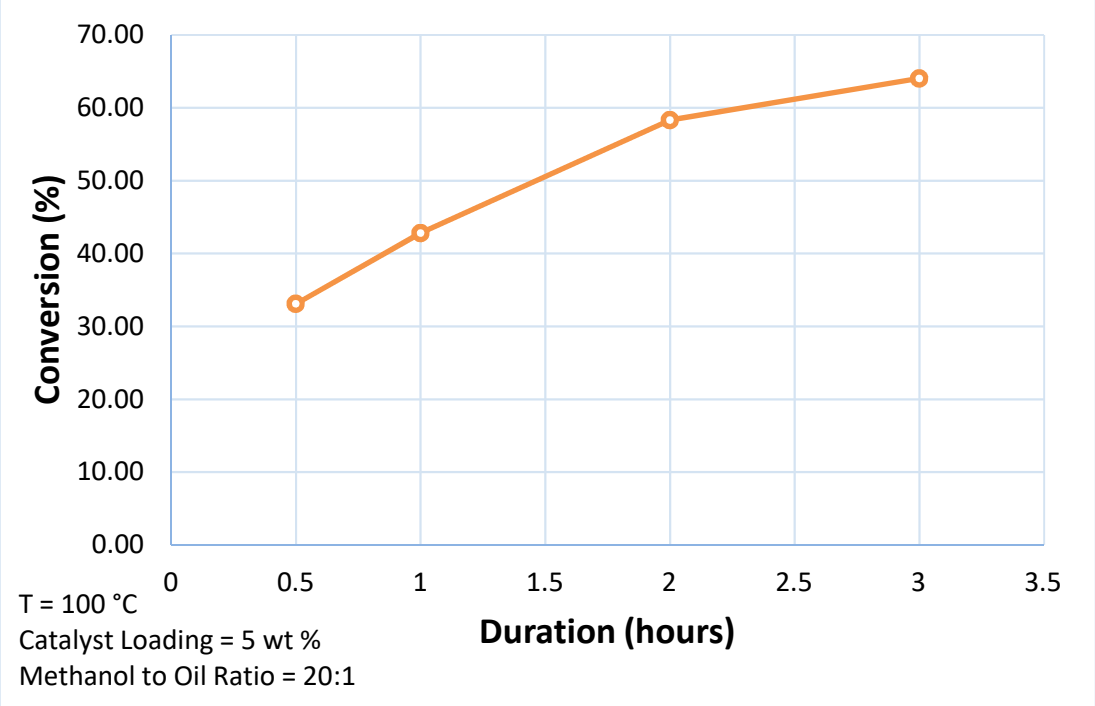

Figure 4.15: Conversion vs Esterification Duration

4.5.2 Catalyst Mass Loading

The effect of catalyst loading against the conversion are shown in Figure 4.16. The catalyst loading was varied from 0.5 to 10 wt %. It can be seen that the conversion increases drastically from 6.19 to 70.71 % when the catalyst loading increased from 0.5 wt% to 5 wt% before slowly stabilizing at approximately 7.5 wt%.

The increase in conversion can be explained by the increase in the total number of available active sites which in turn reduced the duration to achieve reaction equilibrium (Hidayat et al., 2016). Therefore, the rate of reaction will be higher resulting in the higher final conversion after 3 h. According to Fadhil et al. (2016), the presence of various hydrophilic surface functional groups such as –COOH, -OH and –SO_3H attributed to the high conversion. The functional groups acted as the anchoring sites for attachment of polar FFAs and methanol. Therefore, the higher catalyst loading will result in higher number of the active functional groups presence which increased the rate of reaction and subsequent final conversion.

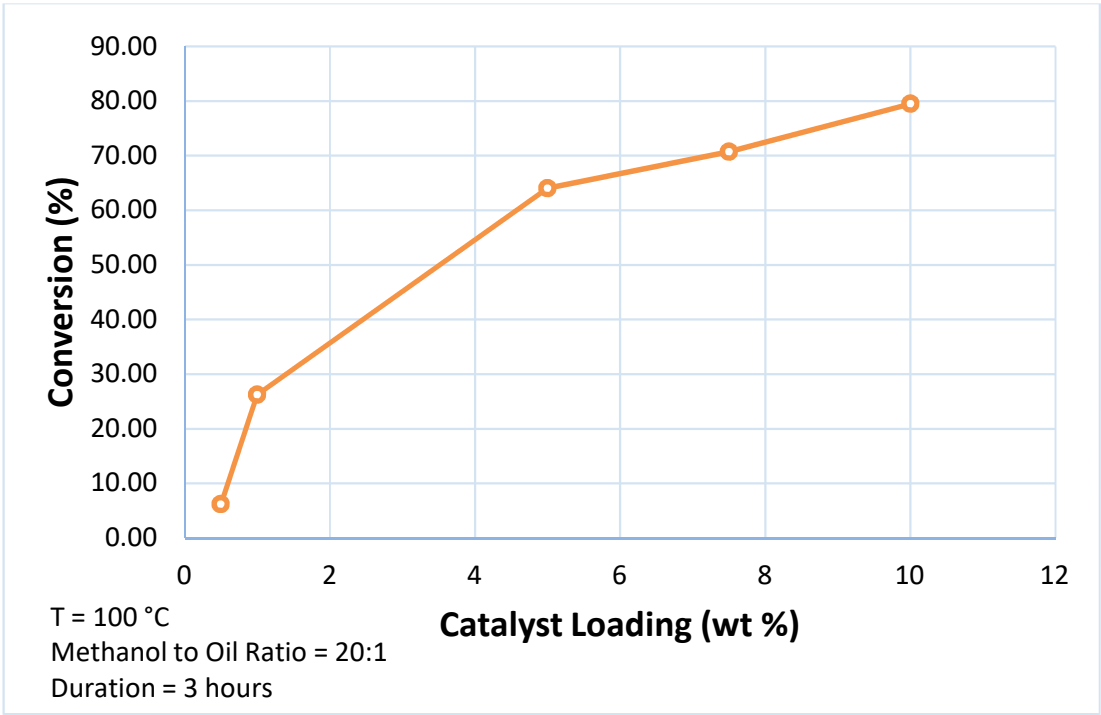

Figure 4.16: Conversion vs Catalyst Loading

4.5.3 Methanol to Oil ratio

Methanol to oil ratio is one of the factors which affects the conversion and yield of biodiesel. The stoichiometric methanol to oil ratio for transesterification and esterification is 3:1 and 1:1 respectively. Since the reaction is reversible for both transesterification and esterification process. Higher methanol to oil ratio which was usually used in practice will shift the equilibrium to the right as stated in Le Chatelier's principle, increasing the biodiesel formation. It should be noted that PFAD was solid at room temperature. As methanol was added to the PFAD, the nonpolar hydrocarbon

chain of the methanol was able to dissolve the oil. This will increase the miscibility of the mixture forming a homogeneous solution which in turn improved the mixing and reaction contact time (Musa, 2016).

The decrease in conversion due to methanol to oil ratio as shown in Figure 4.17 was due to the distillation method utilised during the removal of excess methanol. Both transesterification and esterification will undergo reverse reaction during the heating of crude biodiesel and methanol. Higher methanol to oil ratio required longer distillation duration which may promote reversible reaction.

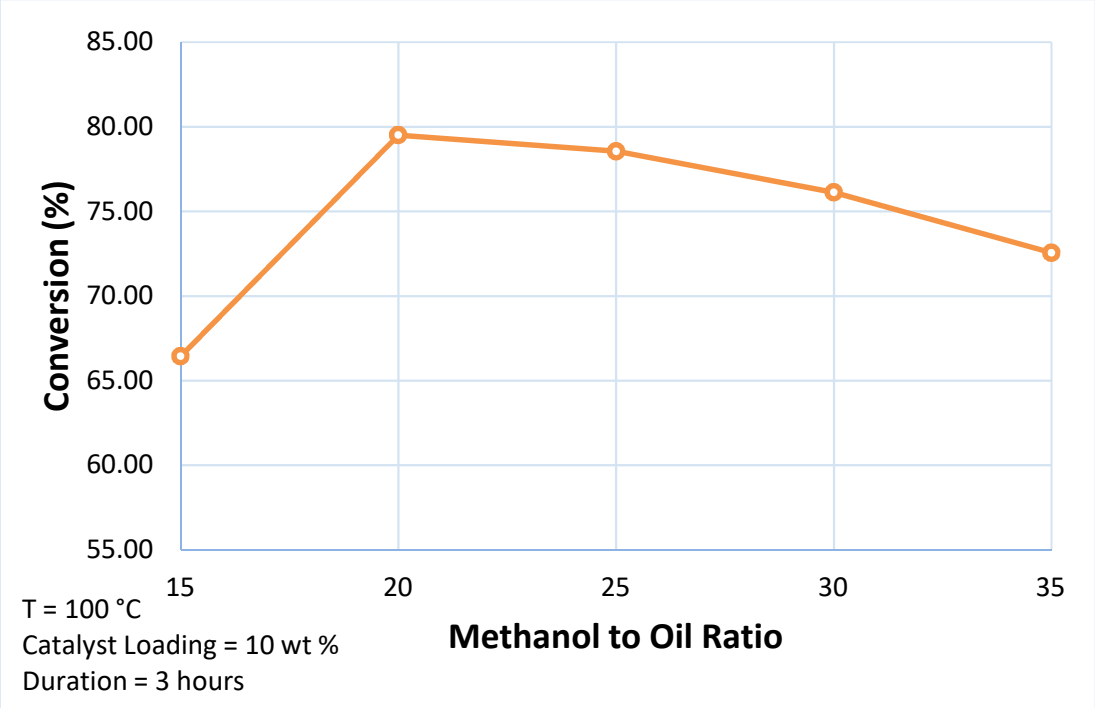

Figure 4.17: Conversion vs Methanol to Oil Ratio

4.5.4 Temperature

Based on Figure 4.18, as the temperature increases, the conversion increases, reaching the optimum point of 75 °C where 87.56 % of conversion was achieved. As mentioned by Mathiyazhagan and Ganapathi (2011) the higher temperature will reduce the viscosity of the oil. The reduce in viscosity will improve the mass transfer between reactant and catalyst as the reactant molecules gain kinetic energy. (Hidayat et al., 2016).

However, as the temperature further increases beyond the optimum point, the conversion decreases slightly. Methanol is a very volatile liquid with a boiling point

of 64.7 °C. As the temperature increases, more methanol was evaporated which could not be fully condensed by the liebig condenser. Some of the methanol will eventually slowly escaped, decreasing the methanol to oil ratio overtime (Zhang, Tian et al., 2017). As mentioned previously, low methanol to oil ratio will enable the reaction to shift to the left, reducing conversion. Therefore the optimum temperature is 75 °C where the both the rate of evaporation of methanol and viscosity of the oil is kept minimum.

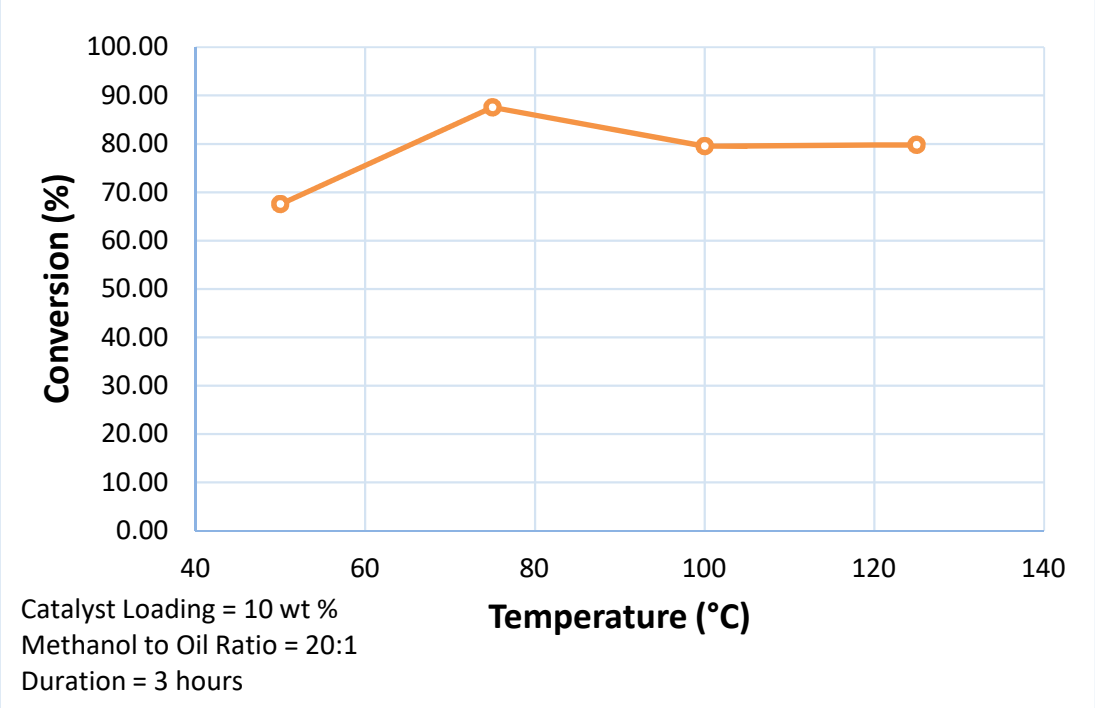

Figure 4.18: Graph of Conversion vs Temperature

4.6 Characterization of Biodiesel

The four main component of fatty acids in PFAD are palmitic, stearic, oleic and linoleic acid. All these four components will produce methyl palmitate, methyl stearate, metyl oleate, methyl linoleate respectively. The retention time based on the calibration curve for the following esters were shown in Table 4.6.

As can be seen from Figure 4.19, there was only three peaks at approximately 9.8, 13.7 and 14.7 min which showed the presence of methyl palmitate, methyl oleate and a small peak for methyl linoleate respectively. There was no observation of methyl stearate. This was due to the low concentration of Stearic Acid contained in PFAD.

The concentration of methyl palmitate and methyl oleate were calculated using the calibration curve as 0.943429 and 0.053706 g/L respectively whereas the methyl linoleate peak was too low to be detected by the gas chromatograph.

Table 4.6: PFAD Fatty Acid Composition and its Counterpart Biodiesel Retention Time

Fatty Acid	**Weight percentage in PFAD wt %**	**Biodiesel**	**Retention Time (min)**
Palmitic	46.9	Methyl Palmitate	9.4
Oleic	36.7	Methyl Oleate	13.5
Linoleic	9.34	Methyl Linolate	14.5
Stearic	4.3	Methyl Stearate	12.5
Others	2.76	-	-

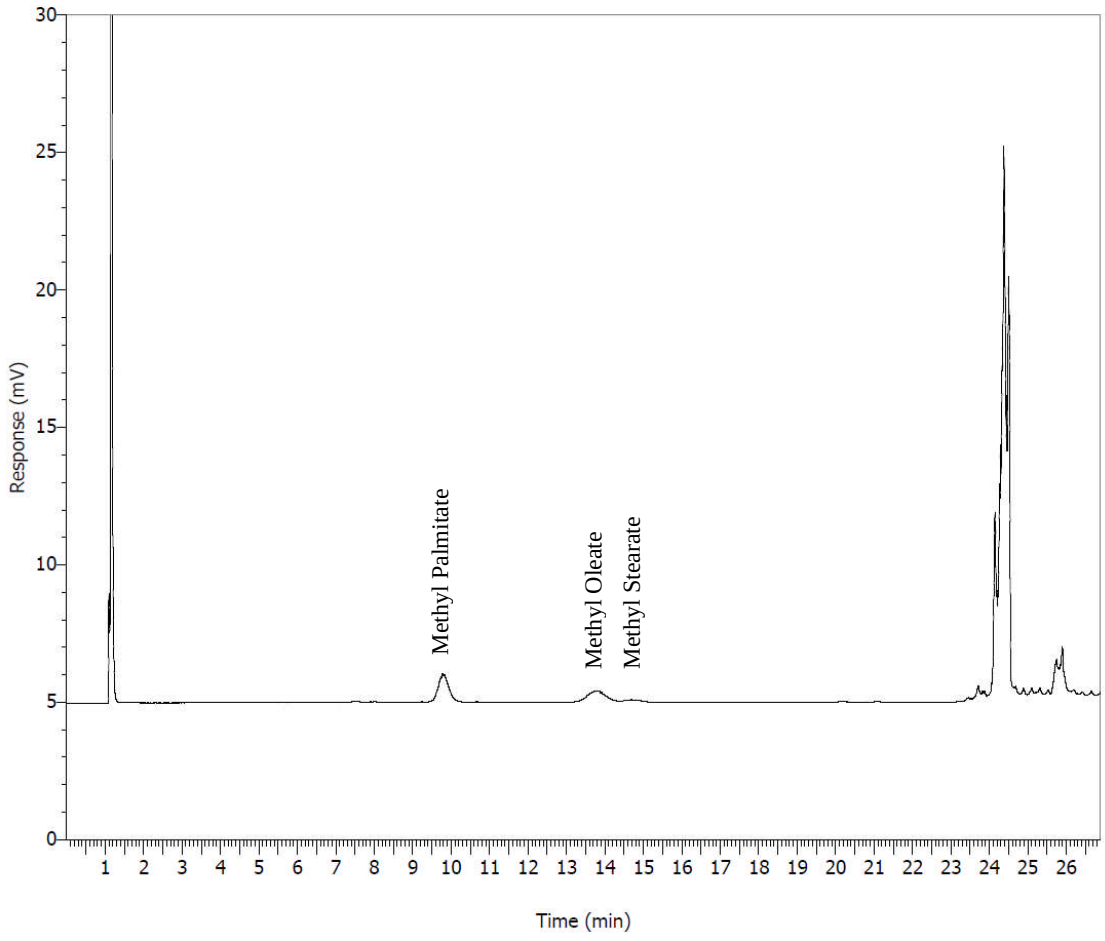

Figure 4.19: Gas Chromatography Spectrum

4.7 Reusability Test

The reusability test was carried out following the optimum esterification condition as investigated in Figure 4.20. The conversion decreased to 44.51 % in the 1st run. It was a reduction of approximately 50 % in conversion. On the 3rd and 4th run, the conversion decreased to 18.59 % and 5.32 % respectively. The loss of catalytic activities may be affected by the combination of two major factors, the leaching of the active functional group of the catalyst and the blockage of the pores of the catalyst by the oil (Lokman et al., 2016). Figure 4.21 shows the biodiesel from the first 4 runs.

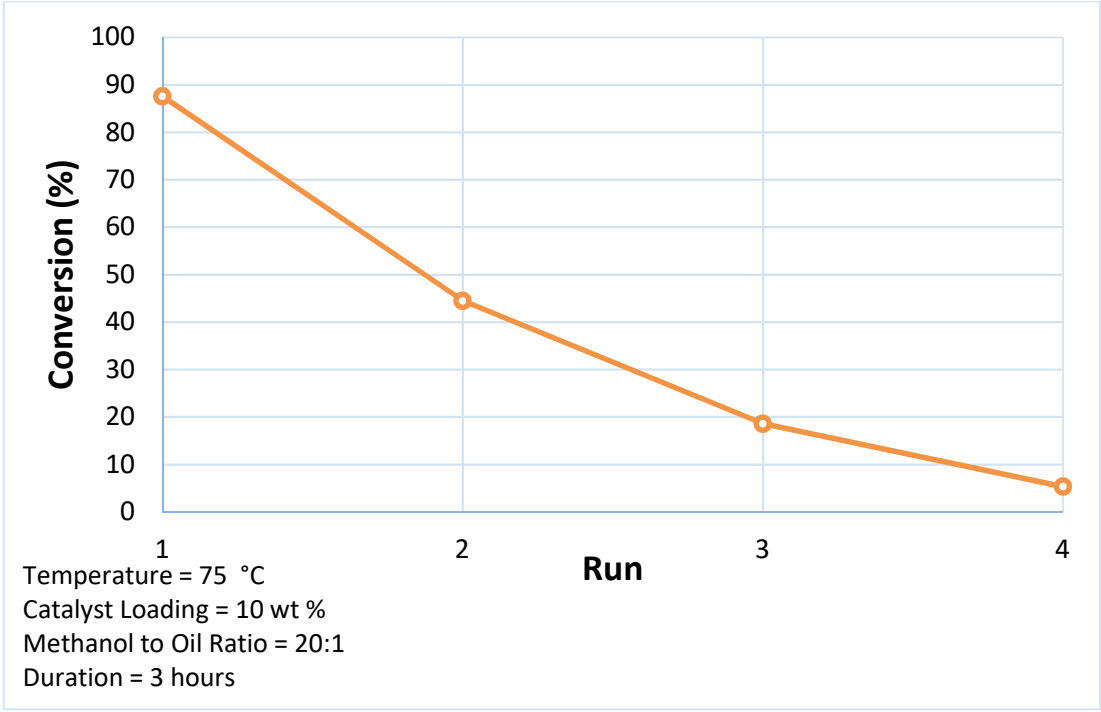

Figure 4.20: The Reusability of the Catalyst.

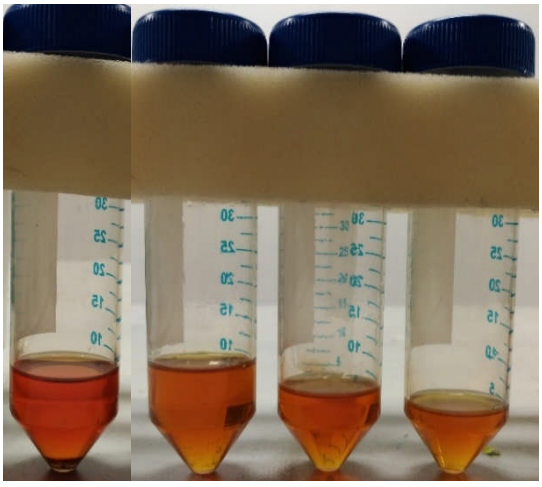

Figure 4.21: Biodiesel from First, Second, Third and Fourth run.

CHAPTER 5

CONCLUSION AND RECOMMENDATIONS

5.1 Conclusion

Frond dust, a waste product initially was used to produce carbon support before being magnetised and sulphonated to produce magnetic solid acid catalyst. The iron oxides which provide the magnetic catalyst was successfully bonded to the catalyst as shown by the EDX, FTIR and XRD analysis. For the sulphonation process, the functional group -SO_3H was also successfully bonded to the amorphous carbon support as proven by EDX and FTIR respectively. Despite SEM did not capture the difference of before and after sulphonation process, it should be noted that both the EDX and XRD still showed the presence Fe and Fe_3O_4 despite a slight decrease in concentration due to leaching effect by sulphuric acid. In other words, the carbon-based magnetic solid acid catalyst was successful synthesised. The optimum catalyst was C10 where the sulphonation condition was 50 °C, 3 h and 10 M.

For esterification process, the optimum condition was B14 with a condition of 10 wt% catalyst loading, 20:1 methanol to oil ratio, 75 °C and 3 h where the a maximum yield of 87.56 % was achieved. The concentration of methyl palmitate and methyl oleate produced was 0.943429 and 0.053706 g/L respectively. Meanwhile, the reusability decreased drastically with every run and decreased to 5.32 % at the fourth run.

5.2 Recommendation

No matter how good a research is, there is always a room for improvement. Firstly, the calcination temperature relation to the yield should be tested as there is no guarantee that higher specific surface area and magnetic properties will have higher yield. Next, the reusability of the catalyst can be further researched. The leaching effect was considerably high and could be further studied. Properties of the biodiesel such as the density, viscosity, stability, calorific value, flash point, octane number and so on must be tested as it is important that the biodiesel produce can be used in the market and do not cause fouling to the fuel filters and engine. Last but not least, the magnetic properties of the catalyst should be further tested with proper equipment such as the magnetometer in order to determine the magnetic strength of the catalyst accurately.

REFERENCES

Abdullah, N. and Sulaiman, F., 2013. The oil palm wastes in Malaysia. *Biomass Now – Sustainable Growth and Use*, (December), pp.75–100.

Alenezi, R., Santos, R.C.D., Raymahasay, S. and Leeke, G.A., 2013. Improved biodiesel manufacture at low temperature and short reaction time. *Renewable Energy*, 53, pp.242–248. Available at: http://dx.doi.org/10.1016/j.renene.2012.11.019.

Amaro, S., 2016. January is "the first big test" for OPEC production deal: Analysts. *CNBC*. Available at: http://www.cnbc.com/2016/12/30/january-is-the-first-big-test-for-opec-production-deal-analysts.html.

Borgelt, S.C., Kolb, T.S. and Schumacher, L.G., 1994. Biodiesel: World Status. *Proceedings of an Alternative Energy Conference*. 1994 ASAE, St. Joseph, pp. 67–76.

Dalai, A.K., Issariyakul, T. and Baroi, C., 2012. Biodiesel Production Using Homogeneous and Heterogeneous Catalysts: A Review. In: Guczi, L. and Erdóhelyi, A., (eds.) *Catalysis for Alternative Energy Generation*. Springer, New York, pp. 237–262.

Dean, D., 2015. *Thermal Gravimetric Analysis*, Birmingham.

Duncan, J., 2003. Costs of biodiesel production. *Environmental Protection*, (May), p.26. Available at: http://www.globalbioenergy.org/uploads/media/0305_Duncan_-_Cost-of-biodiesel-production.pdf.

Dunn, R.O., 2005. The Biodiesel Handbook. In: Gerhard Knothe, Jon Van Gerpen and Krahl, J., (eds.) *The Biodiesel Handbook*. AOCS Press, Champaign, pp. 232–254.

Fadhil, A.B., Aziz, A.M. and Al-Tamer, M.H., 2016. Biodiesel production from Silybum marianum L. seed oil with high FFA content using sulfonated carbon catalyst for esterification and base catalyst for transesterification. *Energy Conversion and Management*, 108, pp.255–265. Available at: http://dx.doi.org/10.1016/j.enconman.2015.11.013.

Feyzi, M., Hassankhani, A. and Rafiee, H.R., 2013. Preparation and characterization of Cs/Al/Fe3O4 nanocatalysts for biodiesel production. *Energy Conversion and Management*, 71, pp.62–68. Available at: http://dx.doi.org/10.1016/j.enconman.2013.03.022.

Gapor Md Top, A., 2010. Production and utilization of palm fatty acid distillate (PFAD). *Lipid Technology*, 22(1), pp.11–13.

Guo, F. and Fang, Z., 2011. Biodiesel Production with Solid Catalysts. *Biodiesel Feedstocks and Processing Technologies*, pp.1–21.

Guo, P., Huang, F., Zheng, M., et al., 2012. Magnetic solid base catalysts for the production of biodiesel. *JAOCS, Journal of the American Oil Chemists' Society*, 89(5), pp.925–933.

Guo, P., Huang, F. and Zheng, M., 2012. Magnetic Solid Base Catalysts for the Production of Biodiesel. , pp.925–933.

Hara, M. et al., 2004. A carbon material as a strong protonic acid. *Angewandte Chemie - International Edition*, 43(22), pp.2955–2958.

Hidayat, A., Rochmadi, Wijaya, K. and Budiman, A., 2016. Removal of free fatty acid in Palm Fatty Acid Distillate using sulfonated carbon catalyst derived from biomass wastefor biodiesel production. *IOP Conference Series: Materials Science and Engineering*, 105, p.12026. Available at: http://stacks.iop.org/1757-899X/105/i=1/a=012026?key=crossref.94cbcaef25c0f4d1a6914f9e4da551e4.

Hu, S., Guan, Y., Wang, Y. and Han, H., 2011. Nano-magnetic catalyst KF/CaO-Fe3O4 for biodiesel production. *Applied Energy*, 88(8), pp.2685–2690. Available at: http://dx.doi.org/10.1016/j.apenergy.2011.02.012.

Iea, I.E.A., 2004. E N E R Gy a G E N C Y for for. *Transport*, (December), p.216. Available at: http://www.iea.org/textbase/nppdf/free/2004/biofuels2004.pdf.

Jüntgen, H., 1986. Activated carbon as catalyst support. *Fuel*, 65(10), pp.1436–1446.

Kaushik, N., Kumar, K. and Kumar, S., 2007. Potential of Jatropha curcas for Biofuels. *Journal of Biobased Materials and Bioenergy*, 1(3), pp.301–314. Available at: http://openurl.ingenta.com/content/xref?genre=article&issn=1556-6560&volume=1&issue=3&spage=301.

Kawashima, A., Matsubara, K. and Honda, K., 2008. Development of heterogeneous base catalysts for biodiesel production. *Bioresource Technology*, 99(9), pp.3439–3443.

Khalil, H.P.S.A., Alwani, M.S. and Omar, A.K.M., 2006. Chemical composition, anatomy, lignin distribution, and cell wall structure of Malaysian plant waste fibers. *BioResources*, 1, pp.220–232.

Knothe, G., 2001. Historical perspectives on vegetable oil based diesel fuels. *Inform*, 12(November), pp.1103–1107.

Konwar, L.J., Boro, J. and Deka, D., 2014. Review on latest developments in biodiesel production using carbon-based catalysts. *Renewable and Sustainable Energy Reviews*, 29, pp.546–564. Available at: http://dx.doi.org/10.1016/j.rser.2013.09.003.

Lee, H.V., Juan, J.C., Yun Hin, T.Y. and Ong, H.C., 2016. Environment-friendly heterogeneous alkaline-Based mixed metal oxide catalysts for biodiesel production. *Energies*, 9(8).

Li, J. and Liang, X., 2016. Magnetic solid acid catalyst for biodiesel synthesis from waste oil. *Energy Conversion and Management*. Available at:

http://dx.doi.org/10.1016/j.enconman.2016.06.072.

Liang, X., 2015. Novel magnetic carbon based solid acid for alkylation of benzene and dodecene. *Chemical Engineering Journal*, 264, pp.251–257. Available at: http://dx.doi.org/10.1016/j.cej.2014.11.105.

Lim, K.O., Zainal, Z.A., Quadir, G.A. and Abdullah, M.Z., 2000. Plant based energy potential and biomass utilisation in malaysia LIM.pdf. *international Energy Journal*, 1(September 2016), pp.77–88.

Lin, L. et al., 2013. Synthesis of magnetic calcium oxide hollow fiber catalyst for the production of biodiesel. *Environmental Progress & Sustainable Energy*, 32(4), pp.1255–1261. Available at: http://dx.doi.org/10.1002/ep.11721.

Liu, C. et al., 2010. The nanometer magnetic solid base catalyst for production of biodiesel. *Renewable Energy*, 35(7), pp.1531–1536. Available at: http://dx.doi.org/10.1016/j.renene.2009.10.009.

Liu, W.-J., Tian, K., Jiang, H. and Yu, H.-Q., 2013. Facile synthesis of highly efficient and recyclable magnetic solid acid from biomass waste. *Scientific reports*, 3, p.2419. Available at: http://www.pubmedcentral.nih.gov/articlerender.fcgi?artid=3741625&tool=pmcentrez&rendertype=abstract.

Liu, X. et al., 2008. Transesterification of soybean oil to biodiesel using CaO as a solid base catalyst. *Fuel*, 87(2), pp.216–221.

Lokman, I.M., Rashid, U. and Taufiq-Yap, Y.H., 2016. Meso- and macroporous sulfonated starch solid acid catalyst for esterification of palm fatty acid distillate. *Arabian Journal of Chemistry*, 9(2), pp.179–189. Available at: http://dx.doi.org/10.1016/j.arabjc.2015.06.034.

Lou, W.Y., Zong, M.H. and Duan, Z.Q., 2008. Efficient production of biodiesel from high free fatty acid-containing waste oils using various carbohydrate-derived solid acid catalysts. *Bioresource Technology*, 99(18), pp.8752–8758.

Ma, F. and Hanna, M.A., 1999. Biodiesel production: A review. *Bioresource Technology*, 70(1), pp.1–15.

Mathiyazhagan, M. and Ganapathi, A., 2011. Factors Affecting Biodiesel Production. *Research in Plant Biology*, 1(2), pp.1–5.

Mo, X. et al., 2008. A novel sulfonated carbon composite solid acid catalyst for biodiesel synthesis. *Catalysis Letters*, 123(1–2), pp.1–6.

Musa, I.A., 2016. The effects of alcohol to oil molar ratios and the type of alcohol on biodiesel production using transesterification process. *Egyptian Journal of Petroleum*, 25(1), pp.21–31. Available at: http://www.sciencedirect.com/science/article/pii/S1110062115000914.

Okamura, M. et al., 2006. Acid-catalyzed reactions on flexible polycyclic aromatic carbon in amorphous carbon. *Chemistry of Materials*, 18(13), pp.3039–3045.

PerkinElmer, 2010. *Thermogravimetric Analysis (TGA) A Beginner â€™ s Guide*, Waltham.

Shu, Q. et al., 2010. Synthesis of biodiesel from waste vegetable oil with large amounts of free fatty acids using a carbon-based solid acid catalyst. *Applied Energy*, 87(8), pp.2589–2596. Available at: http://dx.doi.org/10.1016/j.apenergy.2010.03.024.

Sivasamy, A. et al., 2009. Catalytic applications in the production of biodiesel from vegetable oils. *ChemSusChem*, 2(4), pp.278–300.

Strobel, R. and Pratsinis, S.E., 2009. Direct synthesis of maghemite, magnetite and wustite nanoparticles by flame spray pyrolysis. *Advanced Powder Technology*, 20(2), pp.190–194. Available at: http://dx.doi.org/10.1016/j.apt.2008.08.002.

Talha, N.S. and Sulaiman, S., 2016. Overview of catalysts in biodiesel production. *ARPN Journal of Engineering and Applied Sciences*, 11(1), pp.439–442.

Tang, S. et al., 2012. Study on preparation of Ca/Al/Fe 3O 4 magnetic composite solid catalyst and its application in biodiesel transesterification. *Fuel Processing Technology*, 95, pp.84–89. Available at: http://dx.doi.org/10.1016/j.fuproc.2011.11.022.

Toda, M. et al., 2005. Green chemistry: Biodiesel made with sugar catalyst. *Nature (London, U. K.)*, 438(Copyright (C) 2010 American Chemical Society (ACS). All Rights Reserved.), p.178.

Vaccaro, L., 2017. Use of Solids Suspension catalysts in Flow. In: *Sustainable Flow Chemistry: Methods and Applications*. Wiley, p. 293.

Vidal-Vidal, J., Rivas, J. and López-Quintela, M.A., 2006. Synthesis of monodisperse maghemite nanoparticles by the microemulsion method. *Colloids and Surfaces A: Physicochemical and Engineering Aspects*, 288(1–3), pp.44–51.

Wang, H. et al., 2015. Acid-Functionalized Magnetic Nanoparticle as Heterogeneous Catalysts for Biodiesel Synthesis. *Journal of Physical Chemistry C*, 119(46), pp.26020–26028.

Wu, H., Liu, Y., Zhang, J. and Li, G., 2014. In situ reactive extraction of cottonseeds with methyl acetate for biodiesel production using magnetic solid acid catalysts. *Bioresource Technology*, 174, pp.182–189. Available at: http://dx.doi.org/10.1016/j.biortech.2014.10.026.

Wu, W. et al., 2015a. Recent progress on magnetic iron oxide nanoparticles: synthesis, surface functional strategies and biomedical applications. *Science and Technology of Advanced Materials*, 16(2), p.23501. Available at: http://stacks.iop.org/1468-6996/16/i=2/a=023501?key=crossref.ce9f924b99d57e3eefcec91a1deff8b7.

Wu, W. et al., 2015b. Recent progress on magnetic iron oxide nanoparticles: synthesis, surface functional strategies and biomedical applications. *Science and Technology of Advanced Materials*, 16(2), p.23501.

Wu, W., He, Q. and Jiang, C., 2008. Magnetic iron oxide nanoparticles: Synthesis and surface functionalization strategies. *Nanoscale Research Letters*, 3(11), pp.397–415.

Xie, W. and Li, H., 2006. Alumina-supported potassium iodide as a heterogeneous catalyst for biodiesel production from soybean oil. *Journal of Molecular Catalysis A: Chemical*, 255(1–2), pp.1–9.

Yuan, C., Chen, W. and Yan, L., 2012. Amino-grafted graphene as a stable and metal-free solid basic catalyst. *Journal of Materials Chemistry*, 22(15), p.7456. Available at: http://xlink.rsc.org/?DOI=c2jm30442b.

Zhang, C. et al., 2013. Magnetic core-shell Fe3O4@C-SO3H nanoparticle catalyst for hydrolysis of cellulose. *Cellulose*, 20(1), pp.127–134.

Zhang, F., Tian, X.-F., et al., 2017. Catalytic production of Jatropha biodiesel and hydrogen with magnetic carbonaceous acid and base synthesized from Jatropha hulls. *Energy Conversion and Management*, 142, pp.107–116. Available at: http://linkinghub.elsevier.com/retrieve/pii/S0196890417302364.

Zhang, F., Fang, Z. and Wang, Y.T., 2015. Biodiesel production direct from high acid value oil with a novel magnetic carbonaceous acid. *Applied Energy*, 155, pp.637–647. Available at: http://dx.doi.org/10.1016/j.apenergy.2015.06.044.

Zhang, F., Tian, X., Shah, M. and Yang, W., 2017. Synthesis of magnetic carbonaceous acids derived from hydrolysates of Jatropha hulls for catalytic biodiesel production. *RSC Adv.*, 7(19), pp.11403–11413. Available at: http://xlink.rsc.org/?DOI=C6RA28796D.

Zhang, P. et al., 2016. Sr doping magnetic CaO parcel ferrite improving catalytic activity on the synthesis of biodiesel by transesterification. *Fuel*, 186, pp.787–791. Available at: http://dx.doi.org/10.1016/j.fuel.2016.09.024.

Zhang, X. et al., 2016. Preparation of Core-Shell Structure Magnetic Carbon- Based Solid Acid and its Catalytic Performance on Hemicellulose in Corncobs. *Core-shell catalyst*, 11(4), pp.10014–10029.

Zillillah, Ngu, T.A. and Li, Z., 2014. Phosphotungstic acid-functionalized magnetic nanoparticles as an efficient and recyclable catalyst for the one-pot production of biodiesel from grease via esterification and transesterification. *Green Chemistry*, 16(3), p.1202. Available at: http://pubs.rsc.org/en/content/articlehtml/2014/gc/c3gc41379a.

APPENDICES

APPENDIX A: Gantt Chart

ACTIVITY	STARTING WEEK	DURATION (WEEK)	WEEK
			1 2 3 4 5 6 7 8 9 10 11 12 13 14
Preparation of Catalyst (Parameter analysis)	1	7	
Acid Value of Feedstock	1	2	
TGA	2	1	
Characteristic Test for Catalyst	3	3	
Synthesis of Biodiesel	3	7	
Characteristic test for Biodiesel	8	3	
Catalyst Reusability	10	2	
Completion of Final Report	11	4	

APPENDIX B: Brunauer Emmett and Teller (BET) Analysis Report

Thermo ELECTRON CORPORATION

Date : 8/25/2017
Sample name : 400
Instrument type : Sorptomatic 1990
Filename : C:\Documents and Settings\Sorptomatic\My Documents\Data SO1990\Steven Lim\Leong Weng Fai\400_Analysis.199
Software version : 1.03

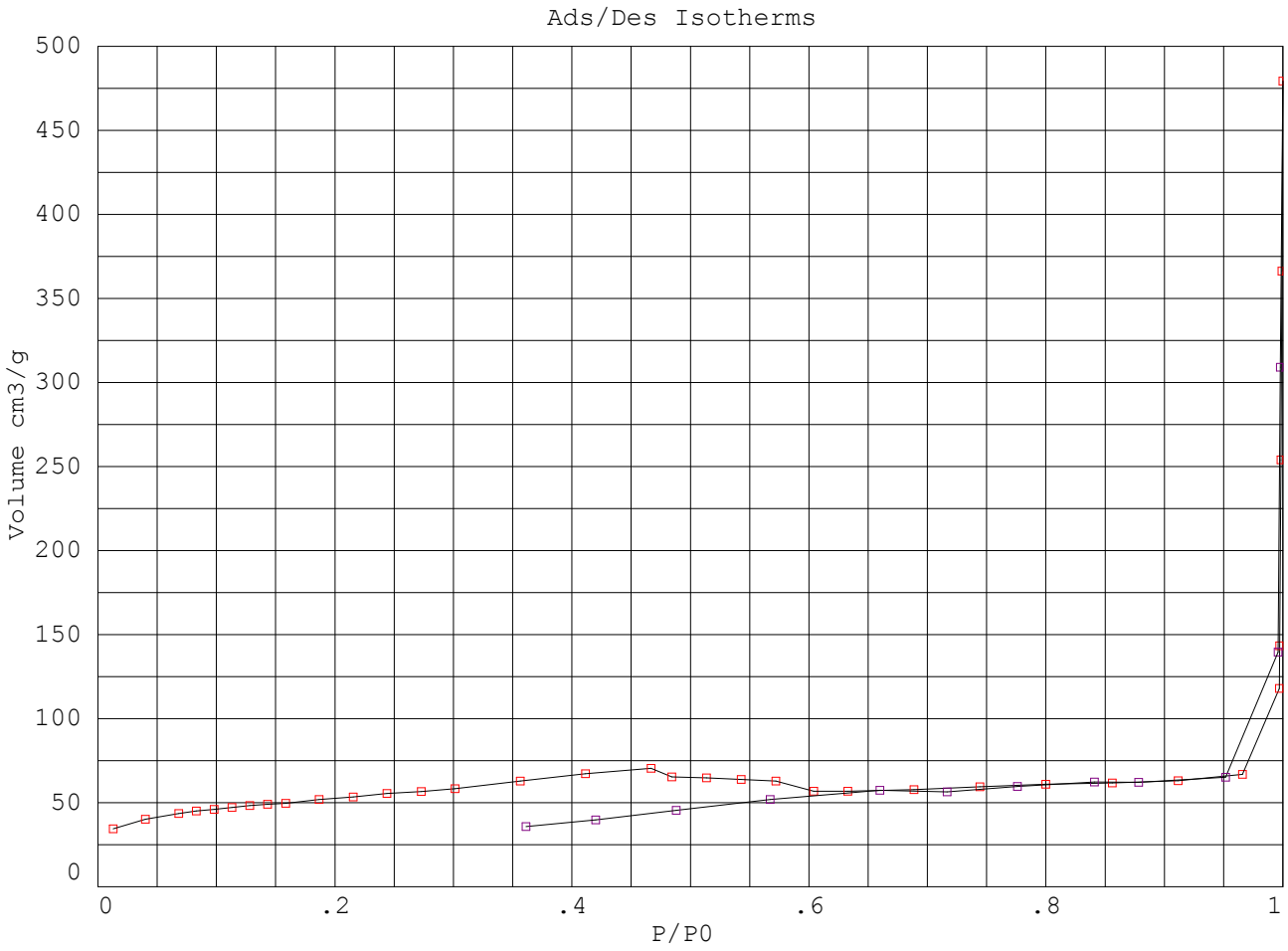

R E S U L T S

Calculation Method < B.E.T. >	
<B.E.T.> Initial-final P/P0 :	.04 - .3
Specific surface calculations	
Monolayer volume (cm3/g) :	41.9659882
Specific surface area (m²/g) :	182.686295
C value of BET equation :	772.1188
Correlation factor :	.9997224
Pore specific volume (cm3/g) :	.0975377
Pore specific volume at P/P0 :	.95
Total Adsorbed volume (cm3/g) :	479.36111
(Dol./Heal)	
Cumulative area max. (m²/g) :	63.677448
Pore volume max. (cm3/g) :	.079999216

P O R E S D I S T R I B U T I O N

Pore ranges (Å)	-[Radius] (Å)	Relative Vol.% (%)	Cumulative Vol.% (%)	Relative Vol. (cm3/g)	Cumulative Vol. (cm3/g)
150	134	0.05	0.05	0.000039	0.00004
134	119	0.05	0.09	0.000037	0.00008
119	106	0.04	0.13	0.000032	0.00011
106	95	0.03	0.17	0.000027	0.00013
95	84	0.67	0.84	0.000538	0.00067
84	75	3.44	4.28	0.002744	0.00342
75	67	3.05	7.33	0.002439	0.00586
67	60	3.44	10.77	0.002748	0.00860
60	53	3.56	14.34	0.002845	0.01145
53	47	2.97	17.31	0.002373	0.01382
47	42	1.10	18.40	0.000875	0.01470
42	38	0.88	19.28	0.000700	0.01540
38	34	10.13	29.40	0.008085	0.02348

PORES DISTRIBUTION

Pore ranges (Å)	-[Radius] (Å)	Relative Vol.% (%)	Cumulative Vol.% (%)	Relative Vol. (cm3/g)	Cumulative Vol. (cm3/g)
34	30	12.25	41.66	0.009784	0.03326
30	27	10.25	51.91	0.008186	0.04145
27	24	10.63	62.53	0.008486	0.04994
24	21	16.67	79.21	0.013314	0.06325
21	19	11.37	90.57	0.009076	0.07233
19	17	9.43	100.00	0.007528	0.07986
17	15	0.00	100.00	0.000000	0.07986

ADSORPTION DATA REPORT

Point N.	Press. Ads (Torr)	Rel. Press. (P/P0)	Vol. Introd. (cm3)	Vol. Adsorb. (cm3/g)	Thickness (Å)	B.E.T. (P/(P0-P)V/g)
1	10.00	0.0128	2.82	34.45	3.7	0.000377513
2	31.20	0.0400	5.66	40.05	4.1	0.001041407
3	53.10	0.0682	8.49	43.60	4.4	0.001677280
4	64.70	0.0831	9.97	45.02	4.5	0.002011861
5	76.40	0.0981	11.44	46.09	4.6	0.002360636
6	88.10	0.1132	12.91	47.08	4.7	0.002712032
7	99.70	0.1281	14.38	48.26	4.8	0.003045320
8	111.4	0.1432	15.85	49.11	4.9	0.003402301
9	123.2	0.1584	17.31	49.61	4.9	0.003792518
10	145.3	0.1868	20.11	51.88	5.1	0.004427338
11	167.6	0.2155	22.90	53.46	5.2	0.005138748
12	189.7	0.2440	25.68	55.41	5.4	0.005826581
13	212.0	0.2729	28.46	56.73	5.5	0.006617473
14	234.1	0.3014	31.24	58.40	5.7	
15	276.8	0.3565	36.66	62.89	6.0	
16	319.4	0.4115	42.06	67.19	6.3	
17	362.3	0.4669	47.45	70.48	6.6	
18	375.7	0.4842	48.85	65.34	6.7	
19	398.3	0.5136	51.58	64.80	6.9	
20	421.0	0.5429	54.31	63.82	7.1	
21	443.6	0.5722	57.03	62.92	7.4	
22	468.1	0.6041	59.75	56.88	7.6	
23	490.3	0.6327	62.46	56.81	7.9	
24	533.6	0.6888	67.80	57.67	8.4	
25	576.6	0.7442	73.14	59.48	9.1	
26	619.5	0.7999	78.47	60.98	10.0	
27	662.6	0.8561	83.78	61.67	11.3	
28	705.4	0.9117	89.09	63.11	13.4	
29	747.2	0.9659	94.39	66.89	18.6	
30	771.1	0.9970	99.69	117.86	41.9	
31	772.1	0.9972	100.99	143.37	43.2	
32	773.4	0.9984	106.29	254.02	51.9	
33	774.1	0.9993	111.58	366.21	68.7	
34	774.5	1.0000	116.88	479.36	280.8	

Thermo ELECTRON CORPORATION

Date : 8/25/2017
Sample name : 500
Instrument type : Sorptomatic 1990
Filename : C:\Documents and Settings\Sorptomatic\My Documents\Data SO1990\Steven Lim\Leong Weng Fai\500_Analysis.199
Software version : 1.03

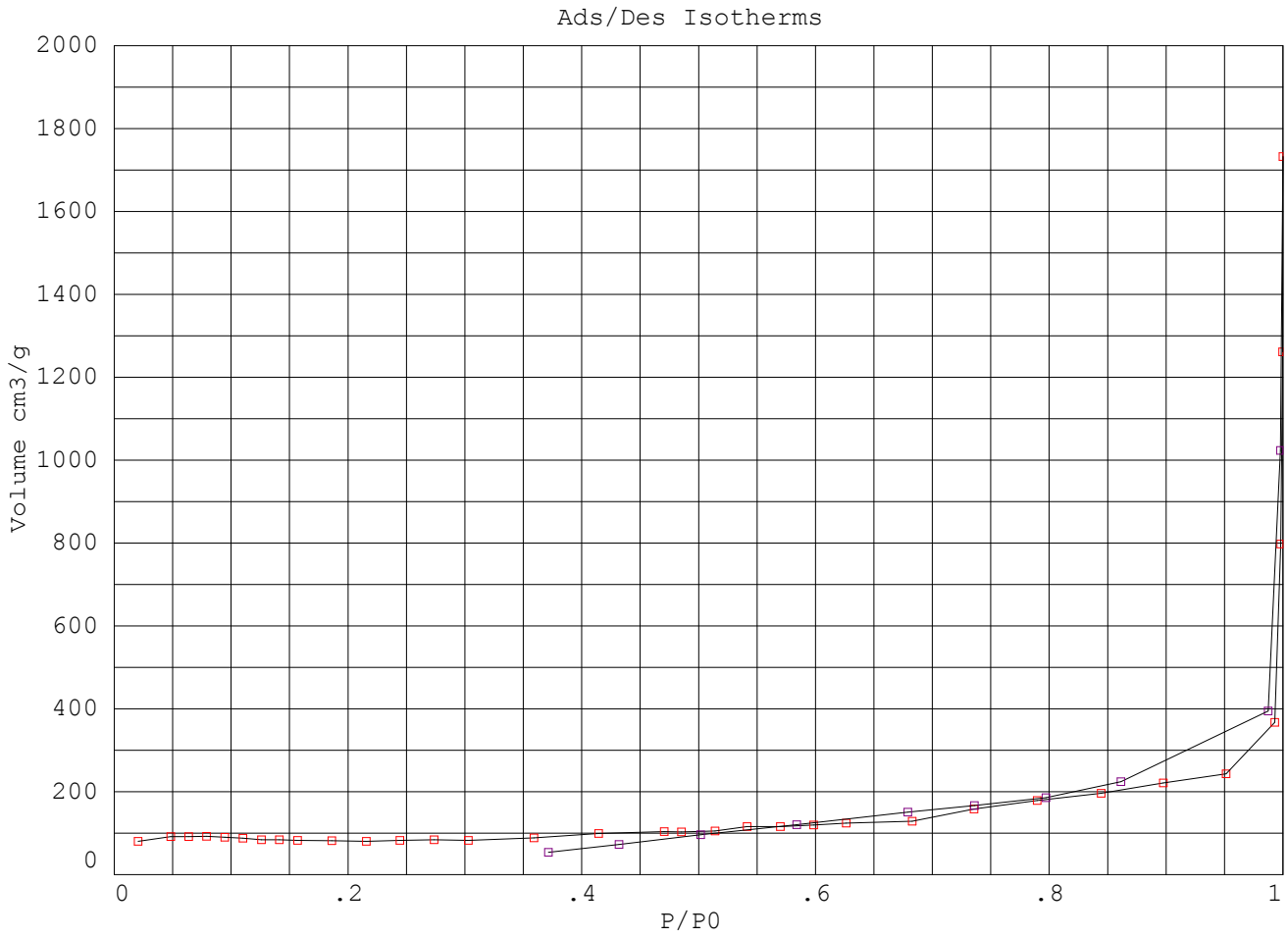

R E S U L T S

Calculation Method < B.E.T. >	
<B.E.T.> Initial-final P/P0 :	.04 - .3
Specific surface calculations	
Monolayer volume (cm3/g) :	57.6588745
Specific surface area (m²/g) :	251.000565
C value of BET equation :	-36.8286
Correlation factor :	.9980387
Pore specific volume (cm3/g) :	.3417916
Pore specific volume at P/P0 :	.95
Total Adsorbed volume (cm3/g) :	1732.73021
(Dol./Heal)	
Cumulative area max. (m²/g) :	276.908264
Pore volume max. (cm3/g) :	.415072471

P O R E S D I S T R I B U T I O N

Pore ranges (Å)	-[Radius] (Å)	Relative Vol.% (%)	Cumulative Vol.% (%)	Relative Vol. (cm3/g)	Cumulative Vol. (cm3/g)
150	134	0.54	0.54	0.001848	0.00185
134	119	0.50	1.04	0.001732	0.00358
119	106	0.44	1.48	0.001501	0.00508
106	95	0.37	1.85	0.001270	0.00635
95	84	0.37	2.22	0.001270	0.00762
84	75	0.50	2.72	0.001731	0.00935
75	67	3.94	6.66	0.013515	0.02287
67	60	3.44	10.11	0.011826	0.03469
60	53	3.44	13.55	0.011826	0.04652
53	47	4.64	18.19	0.015914	0.06243
47	42	4.11	22.30	0.014110	0.07654
42	38	8.11	30.40	0.027836	0.10438
38	34	12.19	42.59	0.041835	0.14622

PORES DISTRIBUTION

Pore ranges (Å)	-[Radius] (Å)	Relative Vol.% (%)	Cumulative Vol.% (%)	Relative Vol. (cm3/g)	Cumulative Vol. (cm3/g)
34	30	10.15	52.73	0.034832	0.18105
30	27	7.11	59.84	0.024399	0.20545
27	24	9.47	69.31	0.032515	0.23796
24	21	12.95	82.26	0.044451	0.28241
21	19	10.94	93.20	0.037554	0.31997
19	17	6.80	100.00	0.023350	0.34332
17	15	0.00	100.00	0.000000	0.34332

ADSORPTION DATA REPORT

Point N.	Press. Ads (Torr)	Rel. Press. (P/P0)	Vol. Introd. (cm3)	Vol. Adsorb. (cm3/g)	Thickness (Å)	B.E.T. (P/(P0-P)V/g)
1	16.00	0.0203	2.85	80.54	3.8	0.000257410
2	38.00	0.0483	5.67	91.48	4.2	0.000554892
3	50.00	0.0636	7.14	92.00	4.3	0.000738652
4	62.00	0.0790	8.61	92.15	4.4	0.000930626
5	74.10	0.0945	10.07	90.44	4.5	0.001154028
6	86.30	0.1102	11.53	87.51	4.7	0.001415287
7	98.50	0.1259	12.98	84.35	4.7	0.001707404
8	110.4	0.1413	14.43	84.12	4.8	0.001956194
9	122.4	0.1568	15.88	82.82	4.9	0.002244841
10	145.2	0.1861	18.65	81.52	5.1	0.002805139
11	168.1	0.2156	21.43	80.14	5.2	0.003429747
12	190.6	0.2445	24.20	82.35	5.4	0.003930894
13	213.1	0.2736	26.96	84.30	5.6	0.004469126
14	235.8	0.3029	29.71	82.86	5.7	
15	279.3	0.3590	35.07	88.66	6.0	
16	322.4	0.4144	40.42	98.95	6.3	
17	366.2	0.4707	45.79	103.50	6.7	
18	377.7	0.4854	47.18	103.05	6.7	
19	399.9	0.5140	49.89	105.08	6.9	
20	421.3	0.5415	52.61	115.69	7.1	
21	443.6	0.5701	55.31	116.22	7.3	
22	465.6	0.5985	58.02	119.58	7.6	
23	487.4	0.6265	60.71	124.22	7.8	
24	531.0	0.6828	66.03	129.12	8.3	
25	572.1	0.7358	71.33	158.64	9.0	
26	614.1	0.7897	76.62	178.47	9.8	
27	656.3	0.8444	81.90	196.05	10.9	
28	697.8	0.8976	87.18	221.16	12.7	
29	739.7	0.9515	92.46	242.94	16.5	
30	771.9	0.9931	97.72	367.67	31.7	
31	775.9	0.9982	102.97	797.56	50.1	
32	776.8	0.9997	108.22	1261.18	95.2	
33	777.0	1.0000	113.48	1732.73	280.8	

Thermo ELECTRON CORPORATION

Date : 8/25/2017
Sample name : 600
Instrument type : Sorptomatic 1990
Filename : C:\Documents and Settings\Sorptomatic\My Documents\Data SO1990\Steven Lim\Leong Weng Fai\600_Analysis.199
Software version : 1.03

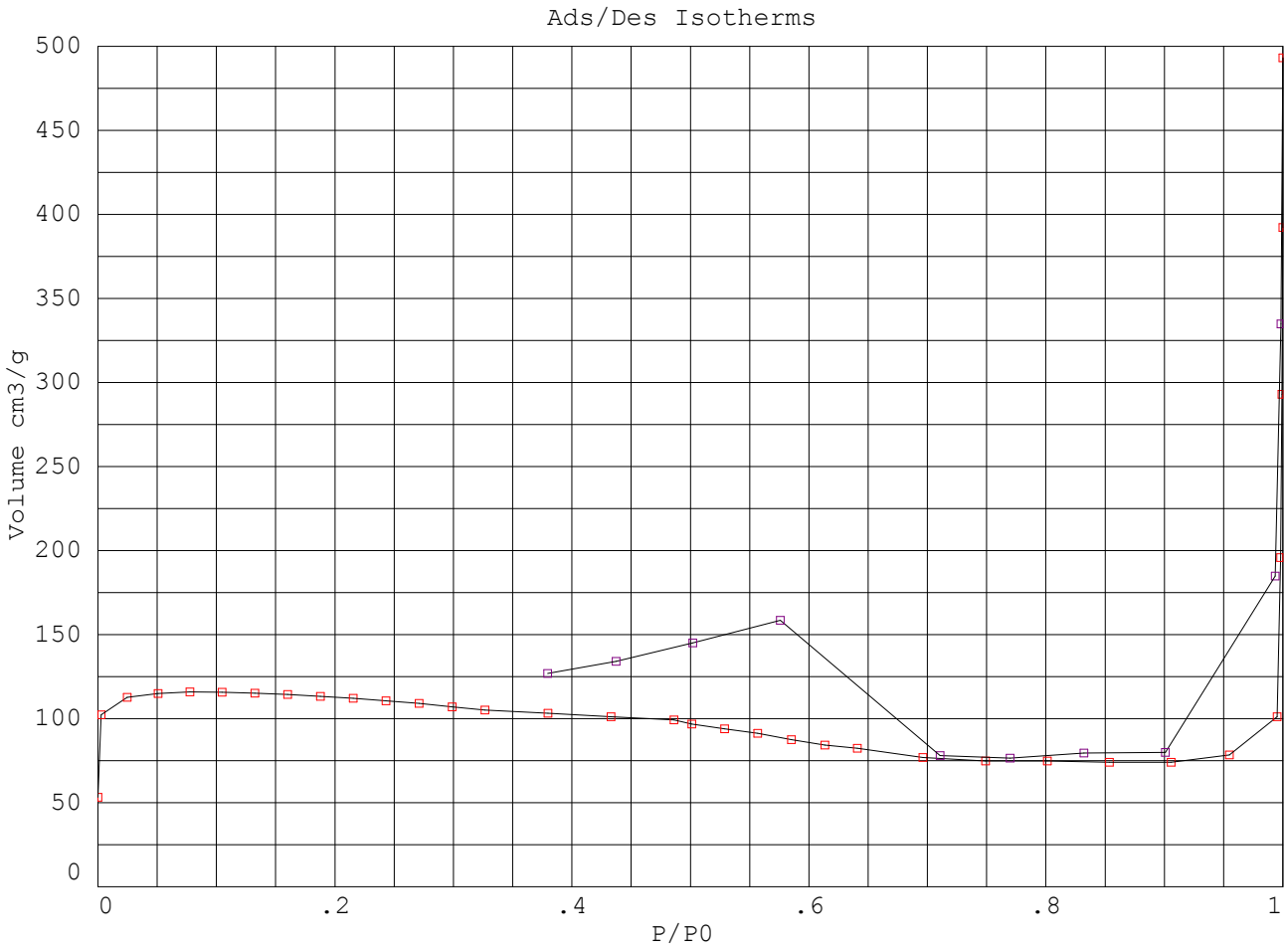

R E S U L T S

Calculation Method < B.E.T. >

<B.E.T.> Initial-final P/P0 : .04 - .3

Specific surface calculations

Monolayer volume (cm3/g) :	73.8477631
Specific surface area (m²/g) :	321.47403
C value of BET equation :	-30.9868
Correlation factor :	.9931195
Pore specific volume (cm3/g) :	.11439223
Pore specific volume at P/P0 :	.95
Total Adsorbed volume (cm3/g) :	493.18517

(Dol./Heal)

Cumulative area max. (m²/g) :	192.420288
Pore volume max. (cm3/g) :	.30273369

P O R E S D I S T R I B U T I O N

Pore ranges (Å)	-[Radius] (Å)	Relative Vol.% (%)	Cumulative Vol.% (%)	Relative Vol. (cm3/g)	Cumulative Vol. (cm3/g)
150	134	0.00	0.00	0.000012	0.00001
134	119	0.00	0.01	0.000011	0.00002
119	106	0.00	0.01	0.000010	0.00003
106	95	0.50	0.51	0.001509	0.00154
95	84	0.58	1.09	0.001743	0.00328
84	75	0.47	1.56	0.001426	0.00471
75	67	0.42	1.98	0.001267	0.00598
67	60	0.40	2.38	0.001212	0.00719
60	53	0.46	2.84	0.001381	0.00857
53	47	0.39	3.23	0.001184	0.00976
47	42	30.73	33.96	0.092711	0.10247
42	38	30.44	64.40	0.091839	0.19431
38	34	12.59	76.99	0.037990	0.23229

PORES DISTRIBUTION

Pore ranges (Å)	-[Radius] (Å)	Relative Vol.% (%)	Cumulative Vol.% (%)	Relative Vol. (cm3/g)	Cumulative Vol. (cm3/g)
34	30	3.62	80.61	0.010917	0.24321
30	27	2.71	83.32	0.008188	0.25140
27	24	3.69	87.01	0.011143	0.26254
24	21	6.88	93.90	0.020766	0.28331
21	19	4.10	98.00	0.012370	0.29568
19	17	2.00	100.00	0.006045	0.30172
17	15	0.00	100.00	0.000000	0.30172

ADSORPTION DATA REPORT

Point N.	Press. Ads (Torr)	Rel. Press. (P/P0)	Vol. Introd. (cm3)	Vol. Adsorb. (cm3/g)	Thickness (Å)	B.E.T. (P/(P0-P)V/g)
1	0.000	0.0000	2.67	53.32	3.5	0.000000000
2	1.976	0.0026	5.38	102.33	3.5	0.000025013
3	19.10	0.0247	8.08	112.61	3.9	0.000224544
4	39.30	0.0508	10.78	114.94	4.2	0.000465437
5	60.00	0.0776	13.47	115.92	4.4	0.000725405
6	81.10	0.1048	16.16	115.84	4.6	0.001010961
7	102.4	0.1324	18.84	115.15	4.8	0.001325658
8	123.7	0.1601	21.52	114.39	4.9	0.001665945
9	145.1	0.1878	24.19	113.30	5.1	0.002041035
10	166.5	0.2155	26.85	112.10	5.2	0.002450134
11	188.0	0.2432	29.51	110.58	5.4	0.002905831
12	209.5	0.2709	32.17	109.02	5.5	0.003408096
13	231.1	0.2989	34.82	107.10	5.7	0.003981351
14	252.7	0.3266	37.46	105.16	5.8	
15	294.2	0.3797	42.64	103.26	6.1	
16	335.7	0.4331	47.79	101.19	6.4	
17	377.1	0.4861	52.94	99.30	6.7	
18	388.6	0.5012	54.27	96.80	6.8	
19	410.3	0.5290	56.88	94.02	7.0	
20	432.0	0.5569	59.48	91.16	7.2	
21	454.0	0.5853	62.07	87.46	7.5	
22	475.8	0.6134	64.66	84.18	7.7	
23	497.0	0.6408	67.24	82.29	7.9	
24	539.6	0.6962	72.34	76.85	8.5	
25	580.7	0.7491	77.42	74.89	9.2	
26	621.0	0.8012	82.48	74.79	10.0	
27	661.6	0.8537	87.55	74.13	11.2	
28	701.9	0.9056	92.60	74.02	13.1	
29	740.3	0.9548	97.64	78.38	16.9	
30	771.4	0.9951	102.67	101.15	35.5	
31	773.8	0.9982	107.72	195.79	49.3	
32	775.1	0.9993	112.74	292.86	68.7	
33	775.5	1.0000	117.77	392.21	280.8	
34	775.3	0.9999	122.80	493.19	142.1	

Thermo ELECTRON CORPORATION

Date : 8/25/2017
Sample name : 700
Instrument type : Sorptomatic 1990
Filename : C:\Documents and Settings\Sorptomatic\My Documents\Data SO1990\Steven Lim\Leong Weng Fai\700_Analysis.199
Software version : 1.03

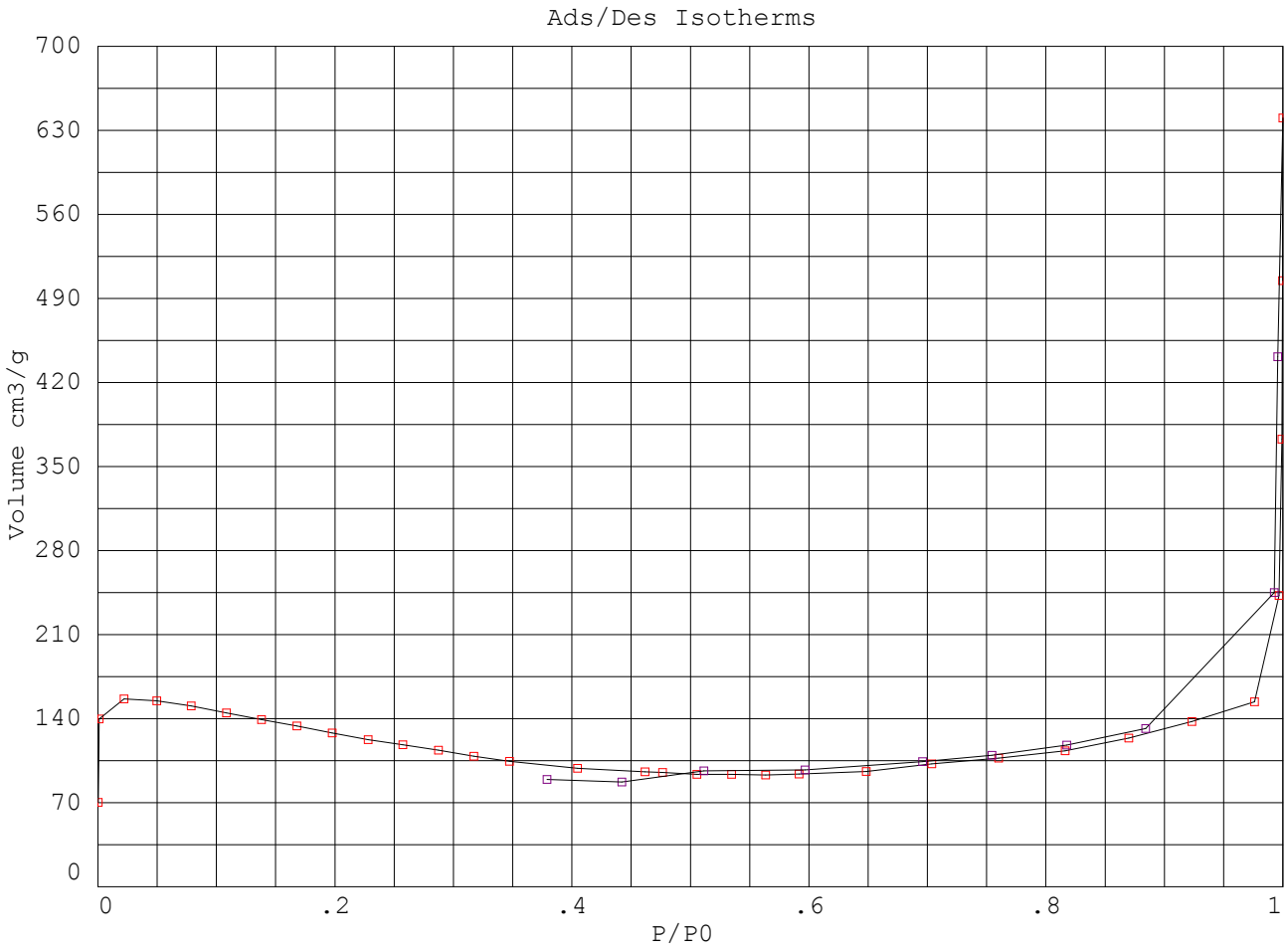

R E S U L T S

Calculation Method < B.E.T. >	
<B.E.T.> Initial-final P/P0 :	.04 - .3
Specific surface calculations	
Monolayer volume (cm3/g) :	78.0900879
Specific surface area (m²/g) :	339.941711
C value of BET equation :	-23.0356
Correlation factor :	.9888612
Pore specific volume (cm3/g) :	.21269788
Pore specific volume at P/P0 :	.95
Total Adsorbed volume (cm3/g) :	640.40329
(Dol./Heal)	
Cumulative area max. (m²/g) :	58.157513
Pore volume max. (cm3/g) :	.104818799

P O R E S D I S T R I B U T I O N

Pore ranges (Å)	-[Radius] (Å)	Relative Vol.% (%)	Cumulative Vol.% (%)	Relative Vol. (cm3/g)	Cumulative Vol. (cm3/g)
150	134	0.44	0.44	0.000346	0.00035
134	119	0.41	0.85	0.000324	0.00067
119	106	0.36	1.21	0.000281	0.00095
106	95	0.30	1.51	0.000238	0.00119
95	84	4.24	5.75	0.003343	0.00453
84	75	6.34	12.09	0.005000	0.00953
75	67	5.64	17.73	0.004444	0.01397
67	60	4.93	22.66	0.003889	0.01786
60	53	6.33	28.99	0.004991	0.02286
53	47	5.98	34.98	0.004716	0.02757
47	42	6.49	41.47	0.005119	0.03269
42	38	9.20	50.67	0.007250	0.03994
38	34	7.20	57.86	0.005673	0.04561

PORES DISTRIBUTION

Pore ranges (Å)	-[Radius] (Å)	Relative Vol.% (%)	Cumulative Vol.% (%)	Relative Vol. (cm3/g)	Cumulative Vol. (cm3/g)
34	30	0.00	57.86	0.000000	0.04561
30	27	0.00	57.86	0.000000	0.04561
27	24	15.73	73.60	0.012404	0.05802
24	21	21.84	95.44	0.017217	0.07523
21	19	3.24	98.68	0.002555	0.07779
19	17	1.32	100.00	0.001040	0.07883
17	15	0.00	100.00	0.000000	0.07883

ADSORPTION DATA REPORT

Point N.	Press. Ads (Torr)	Rel. Press. (P/P0)	Vol. Introd. (cm3)	Vol. Adsorb. (cm3/g)	Thickness (Å)	B.E.T. (P/(P0-P)V/g)
1	0.151	0.0002	2.77	70.15	3.5	0.000002751
2	0.847	0.0011	5.59	139.70	3.5	0.000007784
3	17.10	0.0219	8.41	156.45	3.9	0.000143405
4	38.80	0.0498	11.22	154.90	4.2	0.000338465
5	61.40	0.0788	14.03	150.50	4.4	0.000568510
6	84.50	0.1085	16.83	144.67	4.6	0.000841173
7	107.5	0.1380	19.63	139.34	4.8	0.001149387
8	130.6	0.1679	22.41	133.84	5.0	0.001507411
9	153.9	0.1978	25.20	128.01	5.2	0.001926637
10	177.2	0.2280	27.98	122.37	5.3	0.002413105
11	200.1	0.2574	30.76	118.27	5.5	0.002931316
12	223.2	0.2873	33.52	113.71	5.6	0.003544432
13	246.5	0.3172	36.28	108.61	5.8	
14	269.6	0.3472	39.04	104.63	5.9	
15	314.4	0.4048	44.43	98.71	6.3	
16	358.7	0.4616	49.81	95.62	6.6	
17	370.2	0.4765	51.21	95.07	6.7	
18	392.8	0.5055	53.94	93.70	6.9	
19	415.1	0.5347	56.67	93.58	7.1	
20	437.5	0.5634	59.38	93.24	7.3	
21	459.7	0.5917	62.10	93.86	7.5	
22	503.5	0.6483	67.45	95.87	8.0	
23	546.4	0.7037	72.82	102.43	8.6	
24	590.0	0.7601	78.15	107.09	9.3	
25	633.5	0.8162	83.48	113.22	10.3	
26	675.8	0.8701	88.80	123.86	11.7	
27	717.3	0.9232	94.10	137.63	14.1	
28	758.2	0.9761	99.38	153.99	20.9	
29	774.3	0.9969	104.68	242.74	41.4	
30	776.0	0.9992	109.97	372.72	66.0	
31	776.9	0.9997	115.25	504.90	90.8	
32	777.0	1.0000	120.57	640.40	280.8	

APPENDIX C: Fourier Transform Infrared Spectroscopy (FTIR) Report

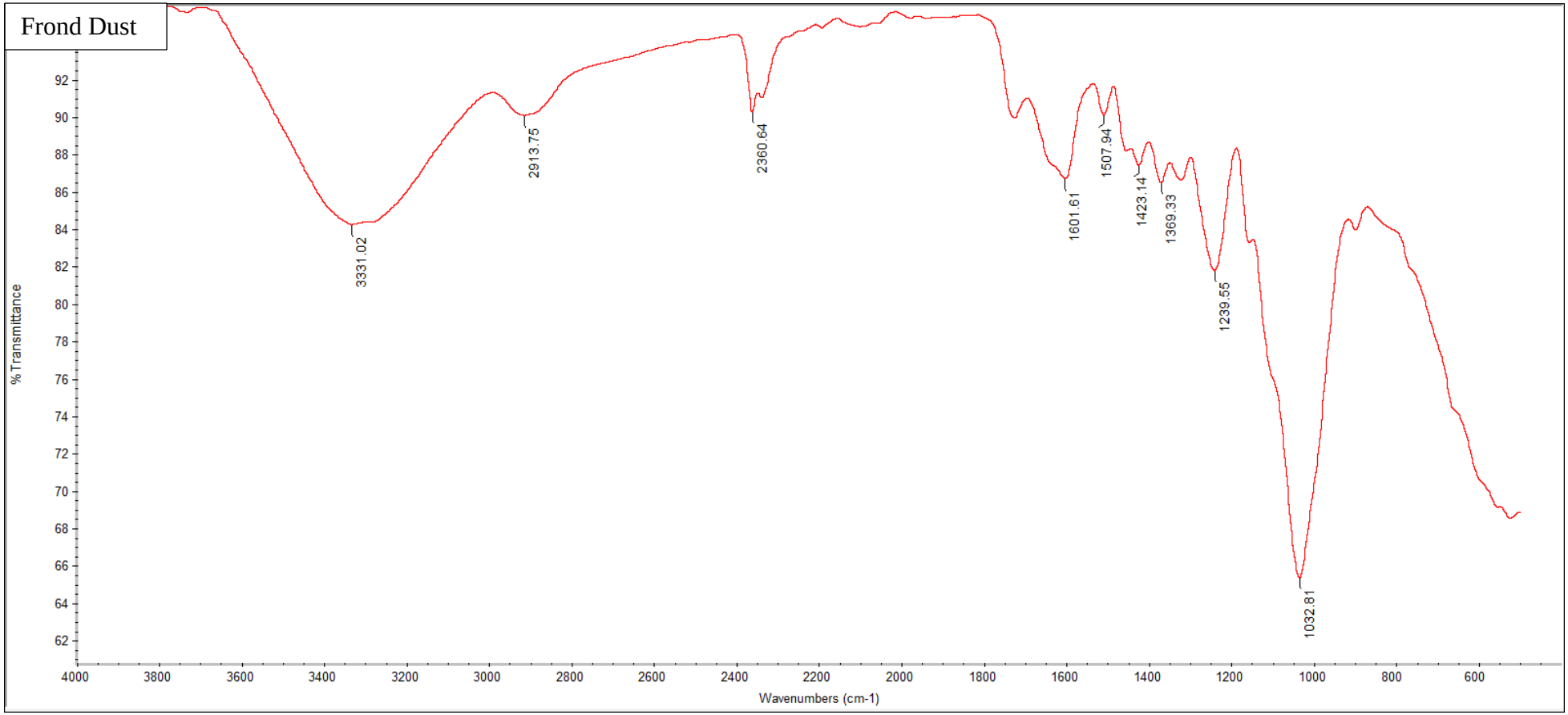
Frond Dust
% Transmittance
92
90
88
86
84
82
80
78
76
74
72
70
68
66
64
62
3331.02
2913.75
2360.64
1601.61
1507.94
1423.14
1369.33
1239.55
1032.81
4000
3800
3600
3400
3200
3000
2800
2600
2400
2200
2000
1800
1600
1400
1200
1000
800
600
Wavenumbers (cm-1)

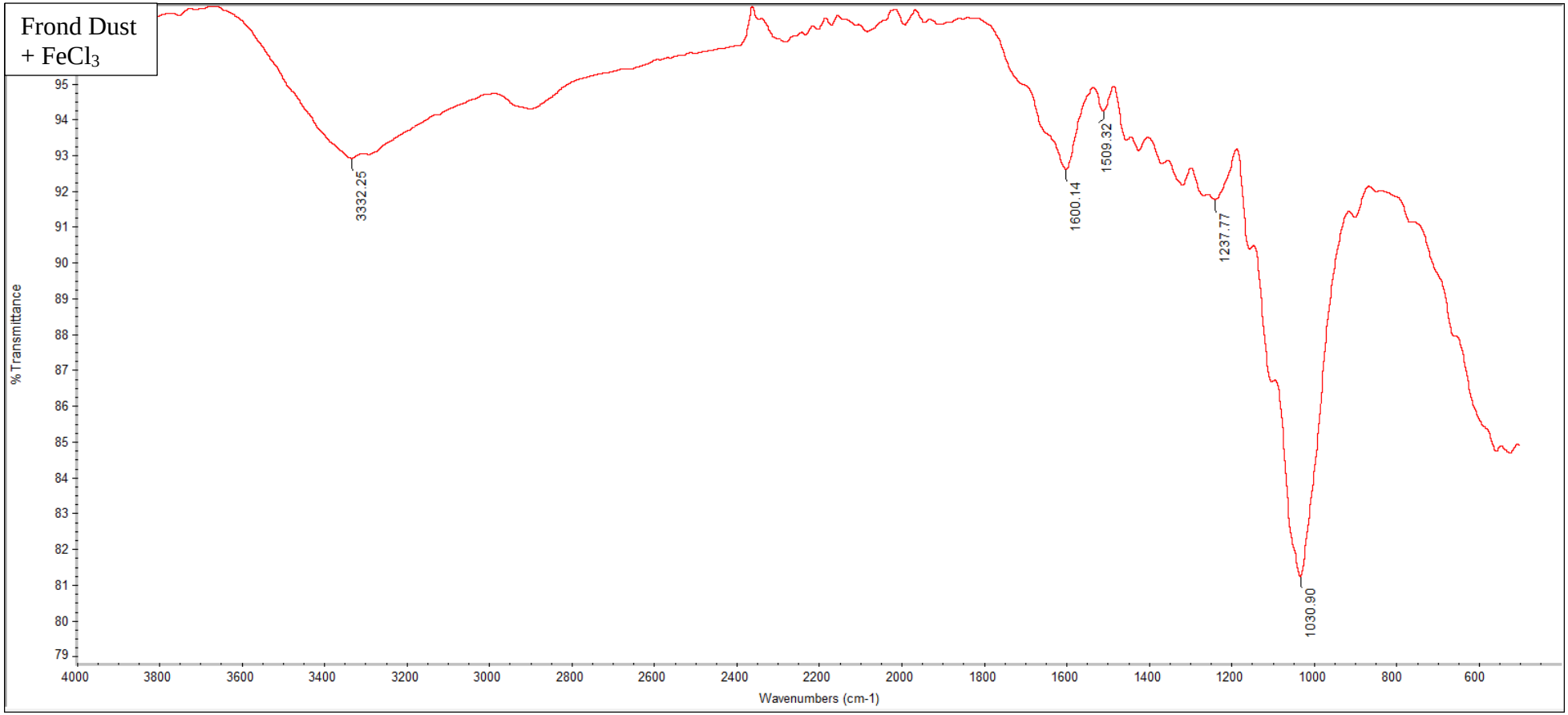
Frond Dust
+ FeCl3
% Transmittance
Wavenumbers (cm-1)
3332.25
1600.14
1509.32
1237.77
1030.90
95
94
93
92
91
90
89
88
87
86
85
84
83
82
81
80
79
4000
3800
3600
3400
3200
3000
2800
2600
2400
2200
2000
1800
1600
1400
1200
1000
800
600

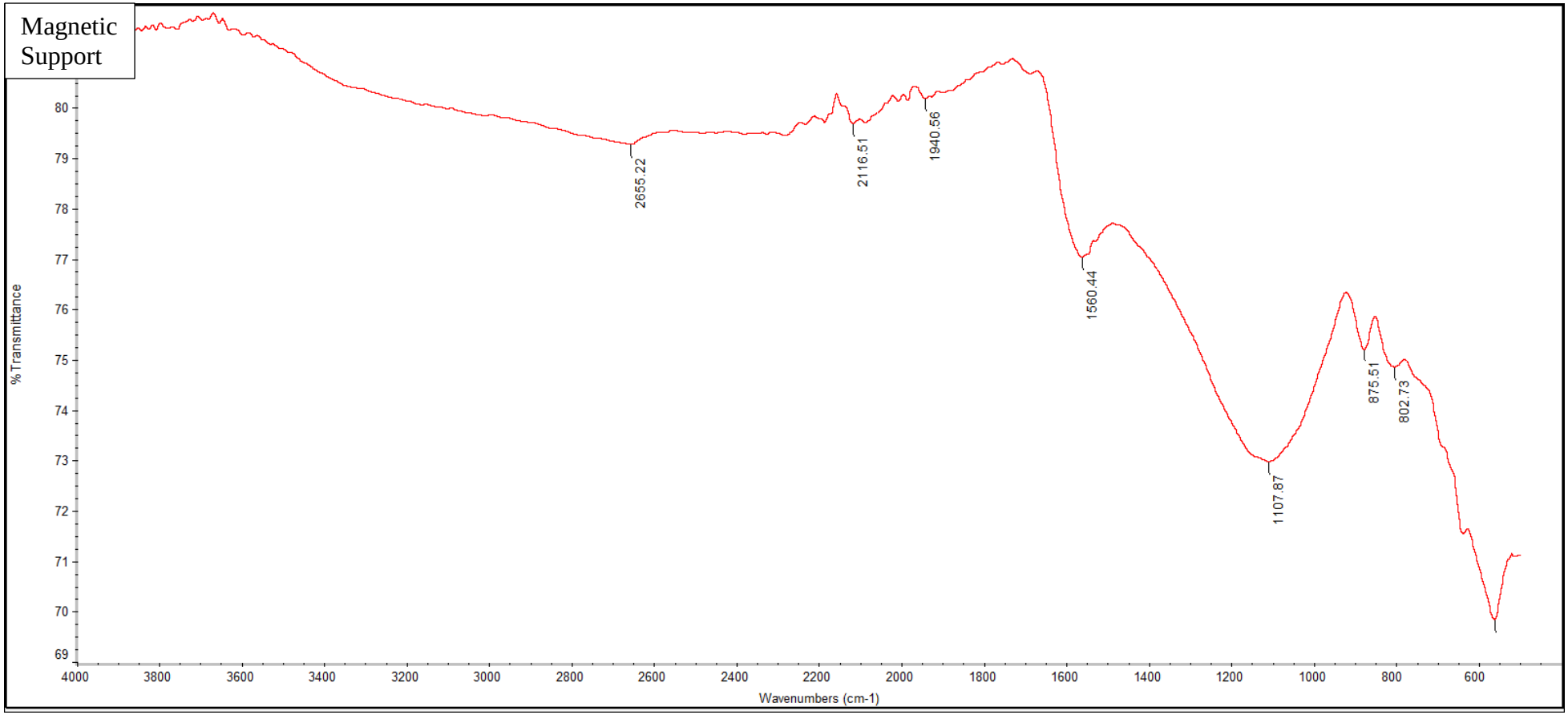
Magnetic
Support
% Transmittance
80
79
78
77
76
75
74
73
72
71
70
69
2655.22
2116.51
1940.56
1560.44
1107.87
875.51
802.73
4000
3800
3600
3400
3200
3000
2800
2600
2400
2200
2000
1800
1600
1400
1200
1000
800
600
Wavenumbers (cm-1)

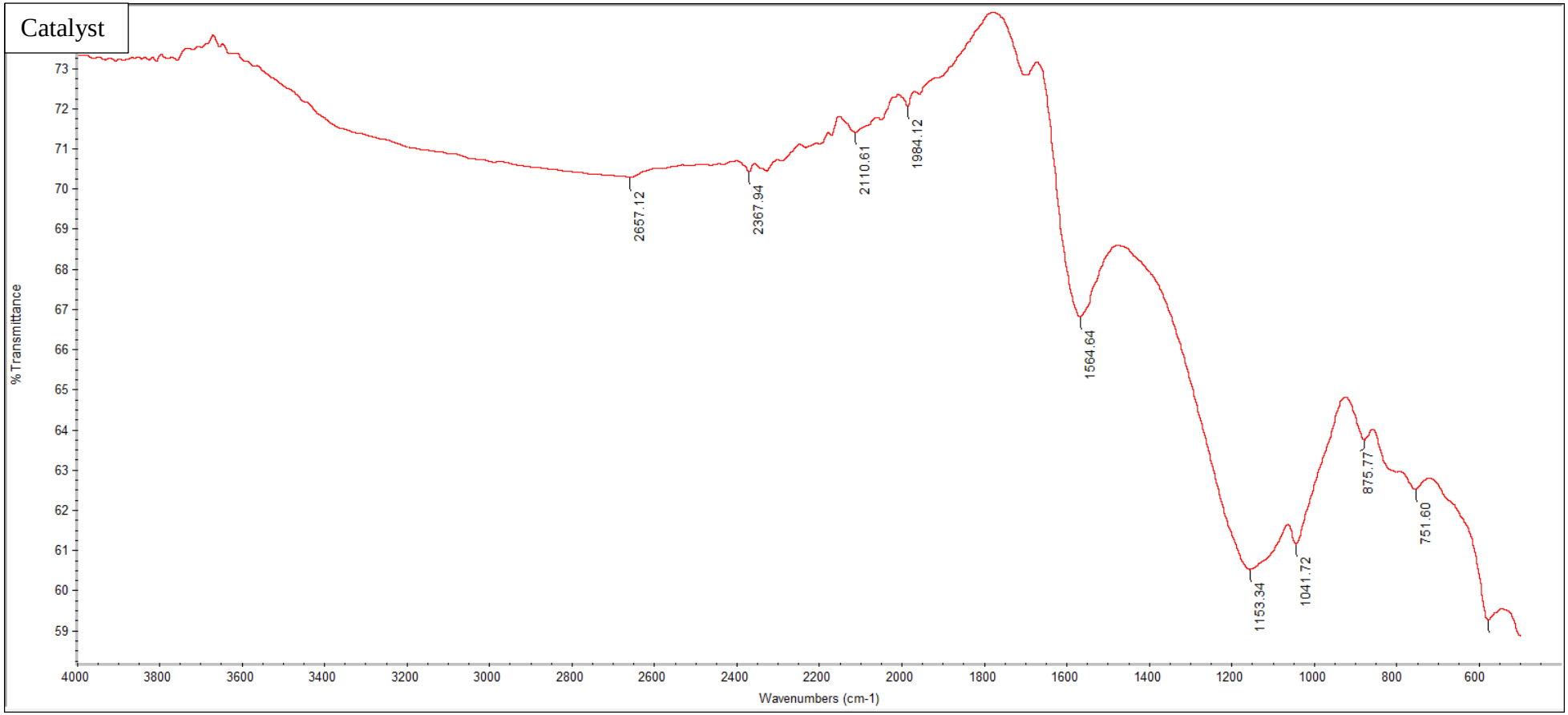
Catalyst
% Transmittance
Wavenumbers (cm-1)
2657.12
2367.94
2110.61
1984.12
1564.64
1153.34
1041.72
875.77
751.60

APPENDIX D: X-Ray Diffraction (XRD) Analysis Report

*** Basic Data Process ***

Group : StevenLim
Data : LeongWF_2

Strongest 3 peaks

no.	peak no.	2Theta (deg)	d (A)	I/I1	FWHM (deg)	Intensity (Counts)	Integrated Int (Counts)
1	12	22.0800	4.02258	100	2.00000	32	2172
2	6	15.9100	5.56594	69	1.10000	22	1172
3	13	23.0200	3.86040	59	0.00000	19	0

Peak Data List

peak no.	2Theta (deg)	d (A)	I/I1	FWHM (deg)	Intensity (Counts)	Integrated Int (Counts)
1	10.4700	8.44248	13	0.26000	4	89
2	11.1600	7.92200	9	0.04000	3	19
3	12.1500	7.27864	6	0.14000	2	21
4	13.7800	6.42112	19	0.44000	6	236
5	14.6400	6.04580	28	0.28000	9	178
6	15.9100	5.56594	69	1.10000	22	1172
7	16.9600	5.22364	31	0.68000	10	278
8	17.4200	5.08673	19	0.48000	6	152
9	17.9200	4.94591	6	0.00000	2	0
10	19.6700	4.50965	19	0.34000	6	130
11	20.8600	4.25500	53	1.12000	17	866
12	22.0800	4.02258	100	2.00000	32	2172
13	23.0200	3.86040	59	0.00000	19	0
14	23.7000	3.75115	31	0.48000	10	623
15	25.3200	3.51470	6	0.04000	2	10
16	26.5000	3.36081	9	0.04000	3	22
17	27.6900	3.21902	9	0.10000	3	40
18	28.6400	3.11437	3	0.00000	1	0
19	29.5600	3.01950	31	0.52000	10	311
20	31.9800	2.79632	19	0.48000	6	163
21	33.6300	2.66280	9	0.06000	3	31
22	34.5750	2.59215	9	0.05000	3	33
23	35.5600	2.52257	9	0.04000	3	22
24	36.5200	2.45843	3	0.00000	1	0
25	38.2500	2.35113	22	0.42000	7	203
26	39.0800	2.30308	9	0.12000	3	36
27	39.7600	2.26525	3	0.00000	1	0
28	41.0600	2.19648	28	0.48000	9	258
29	42.1700	2.14119	6	0.06000	2	16
30	44.7400	2.02398	16	0.12000	5	79
31	45.7000	1.98367	3	0.00000	1	0
32	48.9400	1.85965	6	0.04000	2	12
33	50.8000	1.79584	3	0.00000	1	0
34	54.5200	1.68177	9	0.04000	3	22
35	55.6000	1.65163	6	0.04000	2	13
36	56.3800	1.63062	3	0.00000	1	0
37	59.3700	1.55543	6	0.10000	2	32
38	60.6400	1.52586	6	0.20000	2	55
39	62.1400	1.49258	6	0.08000	2	20
40	62.8400	1.47763	9	0.12000	3	58
41	63.7400	1.45892	3	0.00000	1	0
42	64.9100	1.43542	22	0.46000	7	218
43	67.3400	1.38941	3	0.00000	1	0
44	69.3300	1.35431	6	0.06000	2	22
45	70.4200	1.33599	3	0.00000	1	0
46	73.0200	1.29470	9	0.08000	3	44
47	74.3800	1.27436	3	0.00000	1	0
48	78.1050	1.22264	28	0.45000	9	247

```
         ***  Basic Data Process  ***

# Data Infomation
          Group               : StevenLim
          Data                : LeongWF_2
          Sample Nmae         : LeongWF_2
          Comment             :
          Date & Time         : 08-10-17 09:26:40

# Measurement Condition
    X-ray tube
          target              : Cu
          voltage             : 40.0 (kV)
          current             : 30.0 (mA)
    Slits
          Auto Slit           : not Used
          divergence slit     :   1.00000 (deg)
          scatter slit        :   1.00000 (deg)
          receiving slit      :   0.30000(mm)
    Scanning
          drive axis          : Theta-2Theta
          scan range          :   10.0000 - 80.0000 (deg)
          scan mode           : Continuous Scan
          scan speed          :    2.0000 (deg/min)
          sampling pitch      :    0.0200 (deg)
          preset time         :    0.60 (sec)

# Data Process Condition
    Smoothing                 [ AUTO ]
          smoothing points    : 51
    B.G.Subtruction           [ AUTO ]
          sampling points     : 51
          repeat times        : 30
    Ka1-a2 Separate           [ MANUAL ]
          Ka1 a2 ratio        : 50 (%)
    Peak Search               [ AUTO ]
          differential points : 51
          FWHM threhold       : 0.050 (deg)
          intensity threhold  : 30 (par mil)
          FWHM ratio  (n-1)/n : 2
    System error Correction   [ NO ]
    Precise peak Correction   [ NO ]
```

< Group: StevenLim Data: LeongWF_2 >

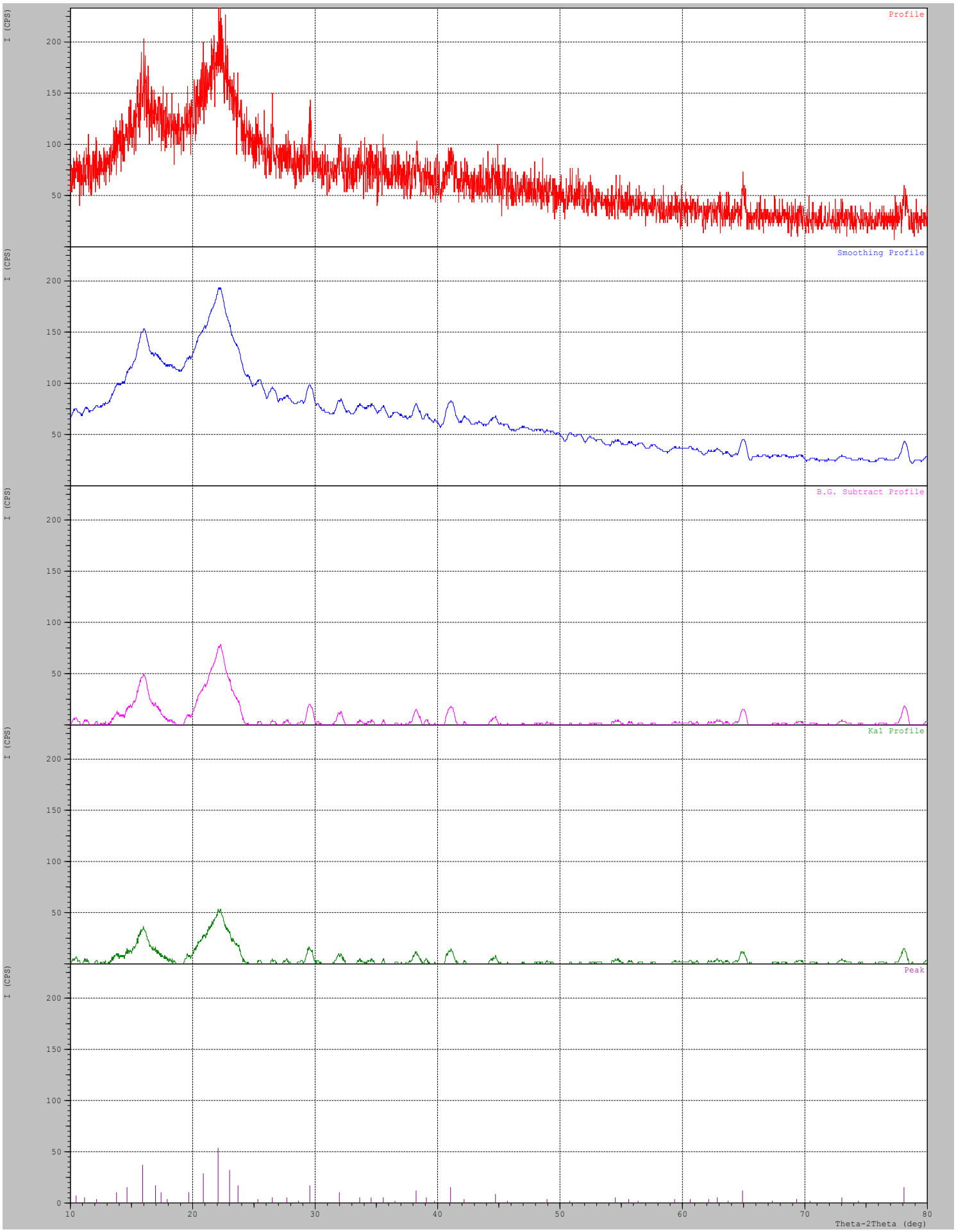

*** Basic Data Process ***

Group : StevenLim
Data : LeongWF_3

Strongest 3 peaks

no.	peak no.	2Theta (deg)	d (A)	I/I1	FWHM (deg)	Intensity (Counts)	Integrated Int (Counts)
1	58	32.7646	2.73112	100	0.25930	70	1004
2	63	35.1426	2.55157	79	0.41870	55	1039
3	108	53.7025	1.70543	40	0.32500	28	446

Peak Data List

peak no.	2Theta (deg)	d (A)	I/I1	FWHM (deg)	Intensity (Counts)	Integrated Int (Counts)
1	10.4466	8.46134	9	0.10670	6	40
2	10.8060	8.18072	9	0.26800	6	93
3	11.3333	7.80125	9	0.09330	6	36
4	11.5100	7.68188	10	0.18000	7	94
5	11.7800	7.50641	4	0.00000	3	0
6	12.1650	7.26970	4	0.05000	3	15
7	12.6200	7.00860	4	0.16000	3	52
8	12.8800	6.86770	3	0.00000	2	0
9	13.1800	6.71205	4	0.04000	3	26
10	13.5500	6.52959	7	0.06000	5	34
11	13.7666	6.42734	7	0.14670	5	59
12	14.2100	6.22776	6	0.06000	4	30
13	14.5700	6.07469	6	0.06000	4	43
14	15.1650	5.83766	3	0.05000	2	6
15	15.4600	5.72692	3	0.04000	2	5
16	15.7266	5.63043	6	0.05330	4	14
17	16.6400	5.32337	3	0.12000	2	24
18	17.2233	5.14437	4	0.04670	3	12
19	17.8350	4.96929	9	0.15000	6	46
20	18.2800	4.84931	7	0.04000	5	17
21	18.4800	4.79728	3	0.04000	2	16
22	18.9400	4.68179	4	0.08000	3	18
23	19.4500	4.56016	6	0.12000	4	32
24	19.8633	4.46620	7	0.07330	5	24
25	20.1750	4.39790	6	0.05000	4	24
26	20.4500	4.33937	6	0.06000	4	19
27	20.6600	4.29574	4	0.04000	3	11
28	21.1600	4.19535	4	0.02000	3	14
29	21.5400	4.12218	3	0.02000	2	4
30	21.9200	4.05157	6	0.12000	4	47
31	22.1550	4.00913	6	0.05000	4	14
32	22.4800	3.95190	7	0.08000	5	54
33	22.8200	3.89378	3	0.04000	2	19
34	23.0700	3.85215	11	0.10000	8	51
35	23.3650	3.80417	6	0.07000	4	21
36	23.7650	3.74104	29	0.25000	20	270
37	24.7400	3.59577	10	0.16000	7	89
38	25.2550	3.52360	7	0.11000	5	33
39	25.4550	3.49637	6	0.07000	4	17
40	25.7450	3.45764	7	0.07000	5	33
41	26.0725	3.41494	13	0.08500	9	44
42	26.2600	3.39098	6	0.02660	4	15
43	26.8300	3.32022	4	0.06000	3	17
44	27.3800	3.25476	10	0.12000	7	74
45	27.7450	3.21277	3	0.05000	2	6
46	28.2050	3.16141	4	0.03000	3	16
47	28.5100	3.12828	7	0.10000	5	52
48	29.0750	3.06876	7	0.05000	5	29
49	29.5400	3.02150	13	0.12000	9	82

peak no.	2Theta (deg)	d (A)	I/I1	FWHM (deg)	Intensity (Counts)	Integrated Int (Counts)
50	29.7600	2.99966	16	0.12000	11	104
51	30.2200	2.95504	4	0.04000	3	14
52	30.4600	2.93230	3	0.08000	2	16
53	31.0100	2.88154	4	0.04000	3	13
54	31.4750	2.84002	13	0.15000	9	83
55	31.7700	2.81432	11	0.12000	8	48
56	31.9900	2.79546	6	0.10000	4	20
57	32.3000	2.76934	9	0.14000	6	68
58	32.7646	2.73112	100	0.25930	70	1004
59	33.5400	2.66974	3	0.12000	2	19
60	33.8200	2.64827	7	0.08000	5	27
61	34.3333	2.60984	6	0.18670	4	38
62	34.7600	2.57878	14	0.20000	10	108
63	35.1426	2.55157	79	0.41870	55	1039
64	35.6900	2.51368	6	0.10000	4	32
65	35.8583	2.50227	4	0.05670	3	11
66	36.2100	2.47877	6	0.10000	4	23
67	36.7300	2.44486	3	0.06000	2	18
68	37.3100	2.40817	4	0.10000	3	17
69	38.0750	2.36153	14	0.27000	10	143
70	39.4600	2.28177	4	0.04000	3	11
71	40.1800	2.24253	4	0.12000	3	26
72	40.4950	2.22581	19	0.29000	13	207
73	40.9250	2.20341	4	0.03000	3	11
74	41.1866	2.19002	7	0.05330	5	29
75	41.3400	2.18225	6	0.00000	4	0
76	41.8300	2.15781	4	0.06000	3	19
77	42.0300	2.14800	6	0.06000	4	24
78	42.3633	2.13187	7	0.16670	5	49
79	42.6833	2.11663	19	0.15330	13	108
80	42.9400	2.10456	7	0.04000	5	28
81	43.4500	2.08104	6	0.14000	4	33
82	43.6166	2.07347	6	0.19330	4	44
83	44.4200	2.03782	13	0.16000	9	78
84	44.7350	2.02420	4	0.05000	3	16
85	44.9766	2.01388	7	0.11330	5	34
86	45.4750	1.99296	7	0.11000	5	33
87	45.7150	1.98306	6	0.11000	4	22
88	45.8950	1.97570	6	0.11000	4	23
89	46.1450	1.96557	6	0.13000	4	25
90	46.5100	1.95100	4	0.06000	3	18
91	46.8400	1.93802	9	0.12000	6	33
92	47.0800	1.92870	4	0.04000	3	10
93	47.3500	1.91833	6	0.10000	4	27
94	48.4300	1.87804	4	0.06000	3	12
95	49.0800	1.85468	24	0.40000	17	372
96	49.6000	1.83644	7	0.04000	5	21
97	49.9400	1.82473	4	0.04000	3	13
98	50.0900	1.81962	6	0.14000	4	38
99	50.5000	1.80581	3	0.04000	2	8
100	51.1000	1.78600	6	0.12000	4	27
101	51.3400	1.77821	4	0.04000	3	16
102	51.6850	1.76715	3	0.03000	2	5
103	51.9300	1.75939	3	0.10000	2	12
104	52.1800	1.75155	3	0.08000	2	9
105	52.7400	1.73426	6	0.12000	4	26
106	53.0250	1.72561	4	0.13000	3	23
107	53.3200	1.71676	9	0.12000	6	48
108	53.7025	1.70543	40	0.32500	28	446
109	54.1400	1.69267	7	0.08000	5	39
110	55.1400	1.66432	3	0.12000	2	16
111	55.5050	1.65424	3	0.03000	2	4

peak no.	2Theta (deg)	d (A)	I/I1	FWHM (deg)	Intensity (Counts)	Integrated Int (Counts)
112	56.1250	1.63742	4	0.07000	3	22
113	56.5700	1.62559	11	0.18000	8	86
114	56.9400	1.61591	7	0.16000	5	43
115	57.2400	1.60815	13	0.12000	9	58
116	57.5800	1.59946	4	0.08000	3	16
117	58.1650	1.58476	3	0.03000	2	8
118	58.7300	1.57085	6	0.18000	4	38
119	59.4000	1.55472	3	0.04000	2	6
120	59.7100	1.54739	6	0.10000	4	23
121	60.1350	1.53746	4	0.03000	3	7
122	61.1850	1.51357	3	0.05000	2	9
123	62.0000	1.49562	23	0.22000	16	172
124	62.2200	1.49086	26	0.13600	18	134
125	62.5900	1.48293	6	0.10000	4	33
126	63.5933	1.46193	24	0.26670	17	246
127	64.0950	1.45169	7	0.05000	5	29
128	64.7950	1.43769	33	0.18000	23	215
129	65.2300	1.42915	7	0.10000	5	30
130	65.6300	1.42141	6	0.10000	4	25
131	66.0600	1.41319	6	0.16000	4	39
132	66.4650	1.40556	3	0.05000	2	7
133	67.0400	1.39489	3	0.08000	2	16
134	67.4700	1.38705	4	0.06000	3	15
135	68.3350	1.37158	3	0.07000	2	10
136	68.5700	1.36745	3	0.06000	2	15
137	69.1200	1.35791	3	0.04000	2	10
138	69.8600	1.34533	6	0.12000	4	22
139	70.3400	1.33732	4	0.04000	3	12
140	70.6000	1.33303	3	0.04000	2	7
141	71.1700	1.32374	4	0.18000	3	44
142	71.6250	1.31645	11	0.35000	8	149
143	72.1150	1.30871	4	0.03000	3	9
144	72.3850	1.30449	4	0.03000	3	13
145	73.5000	1.28743	4	0.04000	3	11
146	73.8800	1.28174	6	0.08000	4	25
147	74.1500	1.27774	3	0.06000	2	14
148	74.4800	1.27290	4	0.04000	3	16
149	74.8450	1.26759	3	0.03000	2	7
150	75.1300	1.26349	4	0.10000	3	36
151	75.4050	1.25956	4	0.05000	3	16
152	75.7350	1.25489	7	0.07000	5	27
153	76.1466	1.24913	6	0.13330	4	41
154	76.3900	1.24576	6	0.06000	4	32
155	76.7800	1.24040	4	0.02000	3	13
156	77.0500	1.23672	6	0.19340	4	57
157	77.4700	1.23106	13	0.18000	9	86
158	77.9371	1.22485	34	0.19430	24	247
159	78.2933	1.22017	6	0.05330	4	20
160	78.9500	1.21166	3	0.06000	2	12
161	79.4800	1.20490	3	0.04000	2	5

```
         ***  Basic Data Process  ***

# Data Infomation
          Group               : StevenLim
          Data                : LeongWF_3
          Sample Nmae         : LeongWF_3
          Comment             :
          Date & Time         : 08-10-17 10:07:50

# Measurement Condition
    X-ray tube
          target              : Cu
          voltage             : 40.0 (kV)
          current             : 30.0 (mA)
    Slits
          Auto Slit           : not Used
          divergence slit     :   1.00000 (deg)
          scatter slit        :   1.00000 (deg)
          receiving slit      :   0.30000(mm)
    Scanning
          drive axis          : Theta-2Theta
          scan range          :   10.0000 - 80.0000 (deg)
          scan mode           : Continuous Scan
          scan speed          :    2.0000 (deg/min)
          sampling pitch      :    0.0200 (deg)
          preset time         :    0.60 (sec)

# Data Process Condition
    Smoothing                 [ AUTO ]
          smoothing points    : 15
    B.G.Subtruction           [ AUTO ]
          sampling points     : 17
          repeat times        : 30
    Ka1-a2 Separate           [ MANUAL ]
          Ka1 a2 ratio        : 50 (%)
    Peak Search               [ AUTO ]
          differential points : 15
          FWHM threhold       : 0.050 (deg)
          intensity threhold  : 30 (par mil)
          FWHM ratio  (n-1)/n : 2
    System error Correction   [ NO ]
    Precise peak Correction   [ NO ]
```

< Group: StevenLim Data: LeongWF_3 >

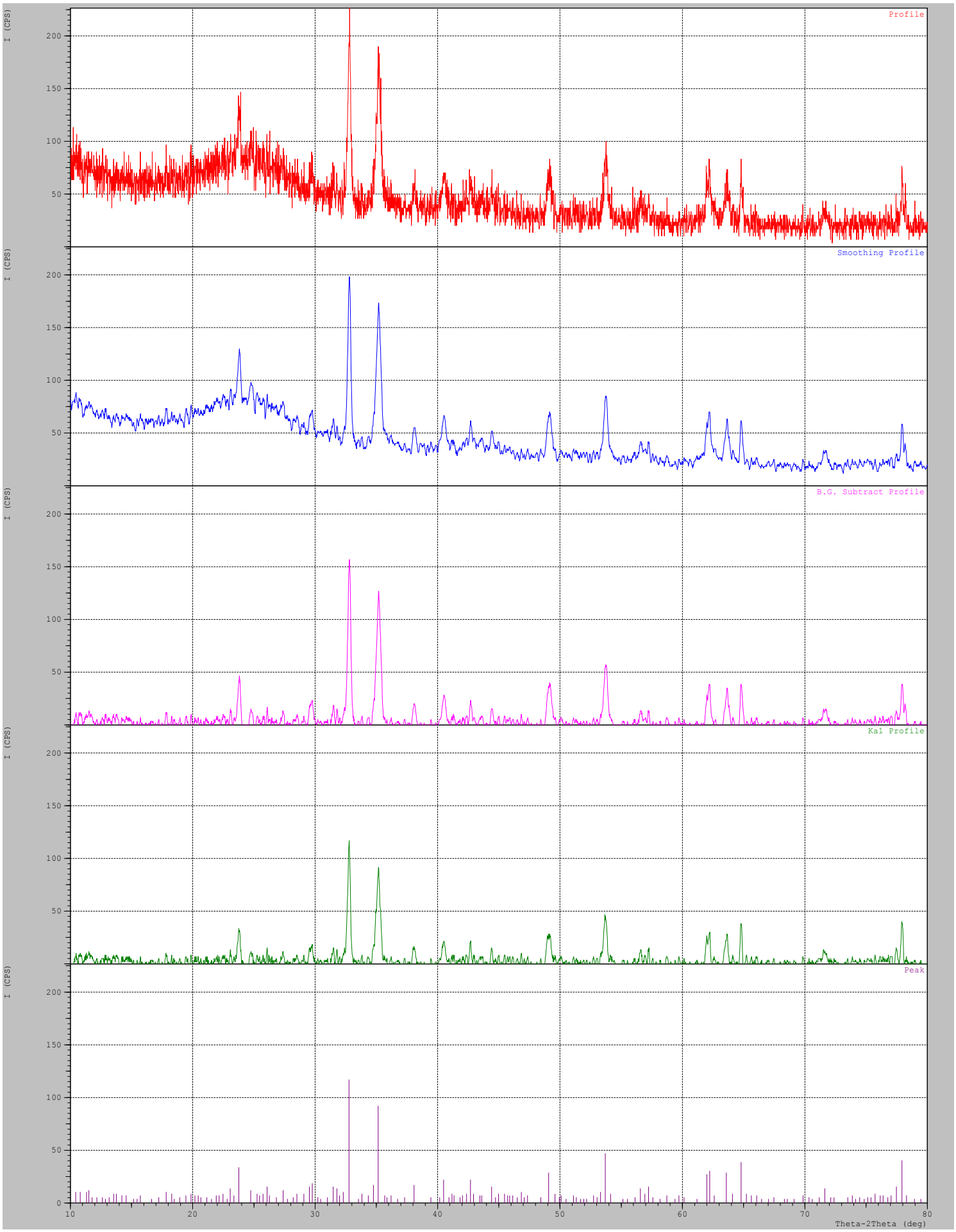

*** Basic Data Process ***

Group : StevenLim
Data : LeongWF_4

Strongest 3 peaks

no.	peak no.	2Theta (deg)	d (A)	I/I1	FWHM (deg)	Intensity (Counts)	Integrated Int (Counts)
1	10	24.1600	3.68076	100	0.00000	51	0
2	11	25.3000	3.51744	96	0.00000	49	0
3	45	77.7950	1.22673	73	0.59000	37	1137

Peak Data List

peak no.	2Theta (deg)	d (A)	I/I1	FWHM (deg)	Intensity (Counts)	Integrated Int (Counts)
1	11.4300	7.73547	4	0.22000	2	31
2	13.1200	6.74261	4	0.12000	2	27
3	14.3900	6.15026	6	0.06000	3	30
4	15.4550	5.72876	10	0.31000	5	142
5	17.3200	5.11587	4	0.08000	2	14
6	18.8600	4.70147	14	0.16000	7	191
7	19.7800	4.48482	18	0.08000	9	94
8	21.2000	4.18752	43	1.56000	22	2875
9	22.7200	3.91069	71	0.00000	36	0
10	24.1600	3.68076	100	0.00000	51	0
11	25.3000	3.51744	96	0.00000	49	0
12	26.9200	3.30933	69	0.00000	35	0
13	27.7600	3.21107	49	0.00000	25	0
14	28.3600	3.14448	45	0.00000	23	0
15	28.9000	3.08694	35	1.10000	18	947
16	29.8800	2.98789	18	0.44000	9	260
17	30.9700	2.88517	12	0.42000	6	275
18	33.0200	2.71058	39	0.54000	20	545
19	35.4700	2.52877	43	0.54000	22	589
20	38.2850	2.34906	27	0.51000	14	393
21	40.1400	2.24467	10	0.12000	5	74
22	40.6600	2.21716	24	0.48000	12	339
23	41.5600	2.17120	20	0.36000	10	477
24	42.7800	2.11206	20	0.00000	10	0
25	43.3200	2.08698	27	0.00000	14	0
26	44.3000	2.04306	24	1.52000	12	1022
27	45.7200	1.98285	10	0.24000	5	114
28	46.7600	1.94115	4	0.12000	2	38
29	47.3650	1.91775	4	0.03000	2	11
30	49.3300	1.84586	22	0.50000	11	330
31	52.6000	1.73855	4	0.20000	2	26
32	53.9500	1.69819	25	0.54000	13	387
33	55.1300	1.66460	6	0.06000	3	27
34	56.8850	1.61734	8	0.29000	4	128
35	57.7100	1.59616	6	0.18000	3	49
36	59.0600	1.56286	6	0.04000	3	18
37	60.2900	1.53388	6	0.14000	3	55
38	62.3500	1.48806	27	0.58000	14	435
39	63.8400	1.45687	16	0.44000	8	166
40	64.6333	1.44090	57	0.62670	29	948
41	69.6300	1.34921	6	0.10000	3	52
42	71.8800	1.31240	8	0.16000	4	70
43	74.7100	1.26955	8	0.18000	4	65
44	76.7700	1.24053	4	0.10000	2	25
45	77.7950	1.22673	73	0.59000	37	1137
46	78.7900	1.21371	10	0.18000	5	47
47	78.9400	1.21178	4	0.04000	2	5

```
         ***  Basic Data Process  ***

# Data Infomation
          Group               : StevenLim
          Data                : LeongWF_4
          Sample Nmae         : LeongWF_4
          Comment             :
          Date & Time         : 08-10-17 10:58:02

# Measurement Condition
    X-ray tube
          target              : Cu
          voltage             : 40.0 (kV)
          current             : 30.0 (mA)
    Slits
          Auto Slit           : not Used
          divergence slit     :   1.00000 (deg)
          scatter slit        :   1.00000 (deg)
          receiving slit      :   0.30000(mm)
    Scanning
          drive axis          : Theta-2Theta
          scan range          :   10.0000 - 80.0000 (deg)
          scan mode           : Continuous Scan
          scan speed          :    2.0000 (deg/min)
          sampling pitch      :    0.0200 (deg)
          preset time         :    0.60 (sec)

# Data Process Condition
    Smoothing                 [ AUTO ]
          smoothing points    : 51
    B.G.Subtruction           [ AUTO ]
          sampling points     : 51
          repeat times        : 30
    Ka1-a2 Separate           [ MANUAL ]
          Ka1 a2 ratio        : 50 (%)
    Peak Search               [ AUTO ]
          differential points : 51
          FWHM threhold       : 0.050 (deg)
          intensity threhold  : 30 (par mil)
          FWHM ratio  (n-1)/n : 2
    System error Correction   [ NO ]
    Precise peak Correction   [ NO ]
```

< Group: StevenLim Data: LeongWF_4 >

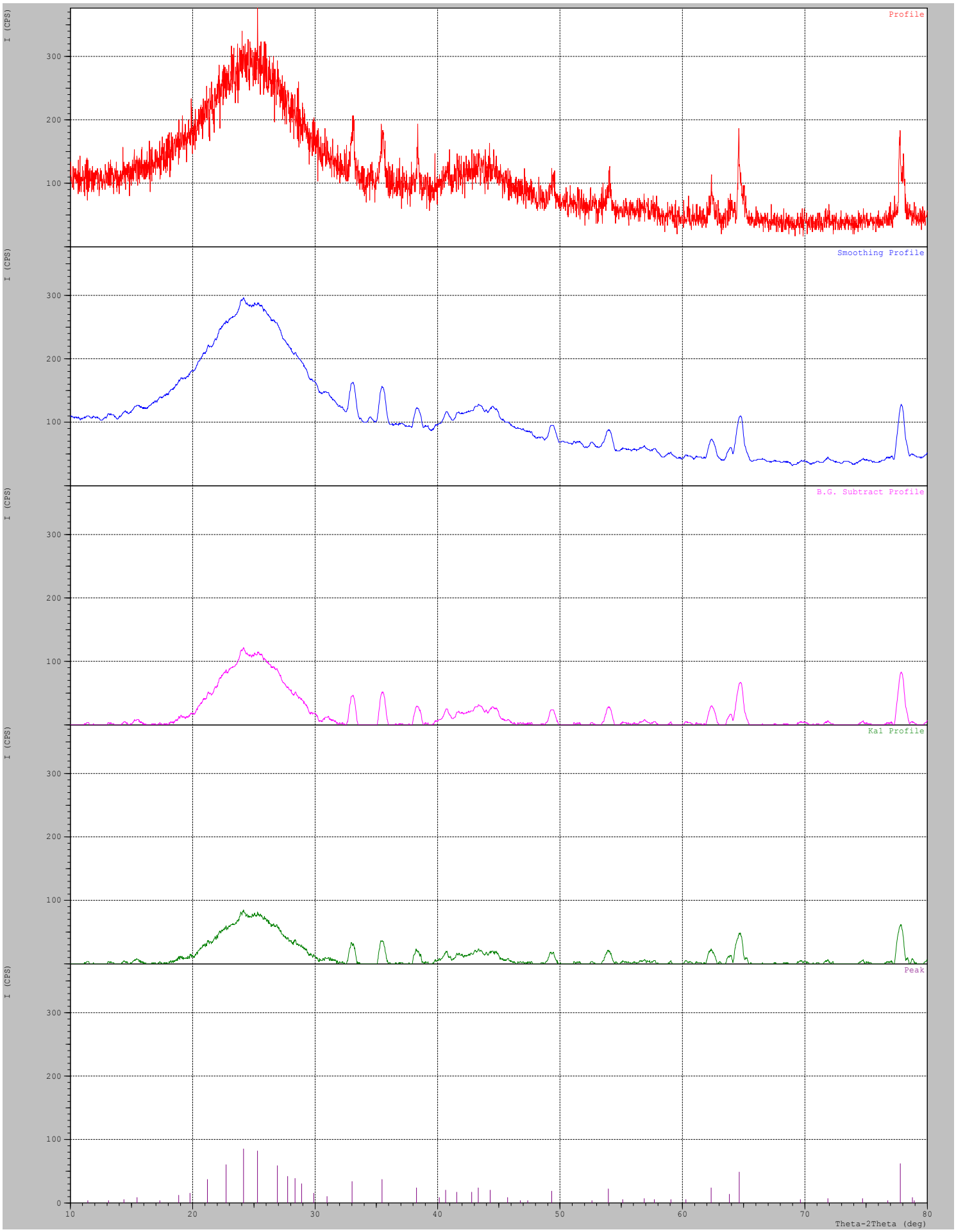

APPENDIX E: Gas Chromatography Report

Software Version	: 6.3.1.0504	Date	: 8/11/2017 10:32:52 AM
Operator	: FES	Sample Name	:
Sample Number	:	Study	:
AutoSampler	: NONE	Rack/Vial	: 0/0
Instrument Name	: Clarus500	Channel	: A
Instrument Serial #	: None	A/D mV Range	: 1000
Delay Time	: 0.00 min	End Time	: 26.89 min
Sampling Rate	: 12.5000 pts/s		
Sample Volume	: 1.000000 ul		
Sample Amount	: 1.0000	Area Reject	: 0.000000
Data Acquisition Time	: 8/11/2017 9:35:37 AM	Dilution Factor	: 1.00
		Cycle	: 1

Raw Data File : C:\GC\Data\1-20170811-093544.raw
Result File : C:\Documents and Settings\FES\Desktop\Result\2017\Leong Weng Fai\75 C.rst
Inst Method : C:\GC\Method\0_Biodiesel (20130308) from C:\GC\Data\1-20170811-093544.raw
Proc Method : C:\GC\Method\0_Biodiesel (20130308) from C:\Documents and Settings\FES\Desktop\Result\2017\Leong Weng Fai\75 C.rst
Calib Method : C:\GC\Method\0_Biodiesel (20130308) from C:\Documents and Settings\FES\Desktop\Result\2017\Leong Weng Fai\75 C.rst
Report Format File: C:\GC\Method\0_Biodiesel (20130308).rpt
Sequence File : C:\GC\Method\1-20170811-085914.seq

DEFAULT REPORT

Peak #	Time [min]	Area [µV·s]	Height [µV]	Area [%]	Norm. Area [%]	BL	Area/Height [s]
1	1.101	5500.03	3966.26	0.34	0.34	BV	1.3867
2	1.144	1334915.84	988900.27	83.42	83.42	VB	1.3499
3	9.745	1808.91	318.66	0.11	0.11	BV	5.6766
4	9.782	825.83	362.70	0.05	0.05	VV	2.2769
5	9.821	528.39	233.67	0.03	0.03	VB	2.2613
6	13.574	95.16	22.02	0.01	0.01	BB	4.3221
7	13.614	46.75	38.47	0.00	0.00	BV	1.2153
8	13.678	36.95	22.65	0.00	0.00	VB	1.6317
9	13.740	64.48	39.28	0.00	0.00	BB	1.6414
10	13.790	16.61	21.79	0.00	0.00	BB	0.7623
11	13.886	35.29	24.40	0.00	0.00	BB	1.4461
12	23.458	195.11	49.62	0.01	0.01	BB	3.9319
13	23.703	795.99	315.45	0.05	0.05	BV	2.5233
14	23.720	481.33	304.55	0.03	0.03	VB	1.5805
15	23.820	29.99	41.92	0.00	0.00	BB	0.7156
16	23.881	245.00	143.57	0.02	0.02	BB	1.7065
17	23.974	44.46	22.61	0.00	0.00	BB	1.9667
18	24.144	16911.52	6572.71	1.06	1.06	BV	2.5730
19	24.163	8043.96	5984.47	0.50	0.50	VV	1.3441
20	24.199	5692.09	3679.93	0.36	0.36	VV	1.5468
21	24.268	19683.84	7503.36	1.23	1.23	VV	2.6233
22	24.292	12087.37	8908.87	0.76	0.76	VV	1.3568
23	24.337	27093.65	12417.36	1.69	1.69	VV	2.1819
24	24.367	24320.10	17510.30	1.52	1.52	VV	1.3889
25	24.383	58847.35	19735.69	3.68	3.68	VV	2.9818
26	24.452	15477.36	10588.15	0.97	0.97	VV	1.4618
27	24.480	12635.05	12716.67	0.79	0.79	VV	0.9936
28	24.500	44377.91	14918.19	2.77	2.77	VB	2.9748
29	24.663	54.02	71.83	0.00	0.00	BV	0.7521
30	24.689	317.93	152.05	0.02	0.02	VB	2.0909
31	24.811	25.60	26.57	0.00	0.00	BV	0.9636
32	24.889	781.43	226.48	0.05	0.05	VB	3.4503

8/11/2017 10:32:52 AM Result: C:\Documents and Settings\FES\Desktop\Result\2017\Leong Weng Fai\75 C.rst

Peak #	Time [min]	Area [µV·s]	Height [µV]	Area [%]	Norm. Area [%]	BL	Area/Height [s]
33	25.103	1071.80	240.04	0.07	0.07	BV	4.4650
34	25.318	1173.36	238.17	0.07	0.07	VB	4.9265
35	25.532	443.92	137.66	0.03	0.03	BB	3.2247
36	25.746	3703.09	688.10	0.23	0.23	BV	5.3816
37	25.797	348.96	205.26	0.02	0.02	VV	1.7001
38	25.857	123.49	58.61	0.01	0.01	VB	2.1071
39	25.892	302.39	254.09	0.02	0.02	BB	1.1901
40	26.191	278.68	79.39	0.02	0.02	BB	3.5103
41	26.423	404.97	94.57	0.03	0.03	BB	4.2825
42	26.661	429.43	125.40	0.03	0.03	BB	3.4246
		1600295.40	1.12e+06	100.00	100.00		

Warning -- Signal level out-of-range in peak
Missing Component Report

Component	Expected Retention (Calibration File)

All components were found

8/11/2017 10:32:52 AM Result: C:\Documents and Settings\FES\Desktop\Result\2017\Leong Weng Fai\75 C.rst

Chromatogram

Software Version : 6.3.1.0504
Sample Name :
Data Acquisition Time : 8/11/2017 9:35:37 AM

Date : 8/11/2017 10:32:52 AM
Sample Number :

Raw Data File : C:\GC\Data\1-20170811-093544.raw